Fall 12-15-2017

# Novel therapeutic approaches for Juvenile Neuronal Ceroid Lipofuscinosis (CLN3)

Megan Elizabeth Bosch
*University of Nebraska Medical Center*

# Novel therapeutic approaches for Juvenile Neuronal Ceroid Lipofuscinosis (CLN3)

**By**

**Megan E. Bosch**

**A DISSERTATION**

**Presented to the Faculty of**

**The Graduate College of the University of Nebraska Medical Center**

**In partial fulfillment of the requirements for the degree of**

**Doctor of Philosophy**

**Department of Pharmacology and Experimental Neuroscience**

**Under the supervision of Professor Tammy Kielian, Ph.D.**

**University of Nebraska Medical Center**

**Omaha, NE**

**September 2017**

**Table of contents:**

**Acknowledgements**

First and foremost, I would like to my mentor Dr. Tammy Kielian for seeing my potential and accepting me into her laboratory. Dr. Kielian has provided me with support and guidance for the last 5 years. Dr. Kielian has taught me how to think critically, question everything, how to become a confident scientist, and much more. These are invaluable lessons that I will carry with for the entirety of my career in science. Dr. Kielian is an amazing role model and I couldn't have imagined a more successful graduate study. Thank you.

To my supervisory committee, Dr. Howard Gendelman, Dr. Howard Fox, Dr. Joythi Arikkath and Dr. Lee Mosley, who have been an instrumental part in the success of my projects and contributed critical and invaluable suggestions.

None of this work would have been possible without the members of Dr. Kielian's laboratory. Thank you to Amy Aldrich who has been an amazing and patient lab mentor and taught me many laboratory techniques and skills, including cell culture, qRT-PCR, confocal microscopy, mouse studies. Thank you Amy, for answering my never ending questions about experimental designs, analysis, and all protocols. I would not have been able to get through graduate school without you. Thank you to Maria Burkovetskaya and Nikolay Karpuk for teaching me the complex layouts of the electrophysiology microscopes and live cell imaging. Thank you to Rachel Fallet, for caring for the breeding colony, answering mouse-related questions, and assisting with breeding protocols for transgenic mice. None of these studies would have been possible without all of your diligent mouse work. I would also like to thank all members of the lab Corteny Heim, Jessica Odvody, and Kelsey Yamada. Thank you for support, guidance, and making the lab enjoyable. I would like to thank former members of the lab who helped get my project started, Juan Xiong, Debbie Vidlak, Casey Gries, Rama Kakulavarapu

and Amanda Angle. I would like to also acknowledge the proteomics core facility for the use of the Seahorse Bioscience Assay.

Finally, I would like to thank my friends and family for their never ending love and support. To my parents and sister who have listened to all of scientific rambles and given me nothing but encouragements, thank you for always supporting me and reminding me to never give up. If you are going to be a bear, be a grizzly bear. To Nicholas DeKorver, thank you for being my rock throughout graduate school, for helping me figure out failed experiments, supporting me through late night time points, and being by my side for all the ups and downs. I could not have done it without you.

**Abbreviations:**

| | |
|---|---|
| **AAV** | Adeno-Associated Virus |
| **ACSF** | Artificial cerebral spinal fluid |
| **AD** | Alzheimer's disease |
| **BBB** | Blood-brain barrier |
| **C6** | C6 ceramide |
| **$Ca^{2+}$** | Calcium |
| **cGMP** | Cyclic guanosine monophosphate |
| **$Cln3^{-/-}$** | CLN 3 knockout mouse |
| **$Cln3^{\Delta ex7/8}$** | CLN 3 Knock-in mouse |
| **CNS** | Central nervous system |
| **COPD** | Chronic obstructive pulmonary disease |
| **CREB** | cAMP-responsive element binding protein |
| **DAMPs** | Danger-associated molecular patterns |
| **dsDNA** | double stranded DNA |
| **EAAT 1** | Excitatory amino acid transporters 1 |
| **EAAT 2** | Excitatory amino acid transporters 2 |
| **ECAR** | Extracellular acidification rate |
| **FOV** | Field of view |
| **GD** | Gaucher disease4 |
| **GFAP** | Glial fibrillary acidic protein |
| **GFP** | Green fluorescent protein |
| **HC** | Hemichannel |
| **HPC** | Hippocampus |

| | |
|---|---|
| **IL-15** | Interleukin-15 |
| **IL-1α** | Interleukin-1-alpha |
| **IL-1β** | Interleukin-1-beta |
| **IL-9** | Interleukin-9 |
| **INCL** | Infantile Neuronal Ceroid Lipofuscinosis |
| **JNCL** | Juvenile Neuronal Ceroid Lipofuscinosis |
| **LINCL** | Late Infantile Neuronal Ceroid Lipofuscinosis |
| **LMP** | Lysosomal membrane permeability |
| **LSD** | Lysosomal storage disease |
| **MeCP2** | Methyl-CpG-binding protein 2 |
| **MPS II** | Mucopolysaccharidosis type II |
| **NCL** | Neuronal Ceroid Lipofuscinosis |
| **NL** | Neuronal Lysate |
| **NPC** | Niemann-Pick type C |
| **OCR** | Oxygen consumption rate |
| **PAMPs** | Pathogen-associated molecular patterns |
| **PD** | Parkinson's Disease |
| **PDE** | Cyclic nucleotide phosphodiesterases |
| **PF** | PF-06266047 |
| **PFA** | Paraformaldehyde |
| **PPT-1** | Palmitoyl-Protein Thioesterase 1 |
| **rAAV** | Recombinant AAV |
| **ROI** | Regions of interest |
| **ROS** | Reactive oxygen species |
| **S1BF** | Somatosensory barrel field cortex |

| | |
|---|---|
| **S1P** | Sphinosine-1-phosphate |
| **scAAV** | self-complementary Adeno-Associated Virus |
| **SMase** | Sphingomyelinase |
| **SOD-1** | Superoxide dismutatse-1 |
| **ssDNA** | Single-stranded DNA |
| **TH** | Thalamus |
| **TPP-1** | Tripeptidyle peptidase 1 |
| **UPR** | Unfolded protein response |
| **VC** | Visual cortex |
| **WT** | Wild type |

## List of Figures and Tables

**University of Nebraska Medical Center**

**Omaha, Nebraska**

**September, 2017**

**Novel therapeutic approaches for Juvenile Neuronal Ceroid Lipofuscinosis**

**Megan E. Bosch, Ph.D.**

**University of Nebraska Medical Center, 2015**

**Advisor: Tammy Kielian, Ph.D.**

**Abstract**

Juvenile Neuronal Ceroid Lipofuscinosis (JNCL) is a lysosomal storage disease caused by autosomal recessive mutations in *CLN3*. Neuronal loss is thought to occur via glutamate excitotoxicity; however, little is known about neuron-astrocyte glutamate regulation in JNCL. We discovered that $Cln3^{\Delta ex7/8}$ astrocytes have significantly lower basal spontaneous $Ca^{2+}$ oscillations and decreased responses to glutamate, indicating a disrupted signaling network. $Cln3^{\Delta ex7/8}$ astrocytes also displayed significantly lower basal mitochondrial respiration and ATP production, suggesting impaired metabolic functions. Concurrent with diminished astrocyte metabolism and $Ca^{2+}$ signaling, $Cln3^{\Delta ex7/8}$ neurons were hyper-responsive to glutamate stimulation. These studies suggest that CLN3 loss disrupts neuronal synaptic activity causing increased glutamate release, which astrocytes are unequipped to regulate due to reductions in $Ca^{2+}$ signaling and energy metabolism. Therefore, a therapeutic capable of targeting several molecular deficits associated with JNCL would be an ideal. Cyclic AMP (cAMP) is a second messenger with pleiotropic effects, including regulating neuroinflammation, glutamate transporter expression, and neuron survival. We investigated whether three distinct phosphodiesterase-4 (PDE4) inhibitors could mitigate disease pathology in the $Cln3^{\Delta ex7/8}$ mouse model. cAMP levels were significantly reduced in the $Cln3^{\Delta ex7/8}$ brain, which were restored by PF-06266047. PDE4 inhibitors significantly improved motor function, attenuated glial activation and lysosomal pathology, and restored glutamate transporter expression with no evidence of toxicity. These studies revealed neuroprotective effects of PDE4 inhibitors in $Cln3^{\Delta ex7/8}$ mice and support their therapeutic potential. However, PDE4 inhibitors do not provide a long-term treatment for JNCL because the CLN3 mutation is still present. Therefore, we explored a gene delivery approach for JNCL utilizing two self-complementary AAV9 (scAAV9) constructs with the MeCP2 and β-actin

promoters to drive low versus high transgene expression and to test efficacy in the $Cln3^{\Delta ex7/8}$ model. Only the scAAV9/MeCP2-hCLN3 construct corrected motor deficits and attenuated glia activation and lysosomal pathology, possibly resulting from preferential viral promoter usage by neurons. This is the first demonstration of a systemic delivery route to restore CLN3 *in vivo* using scAAV9 and highlights the importance of promoter selection for disease modification. Collectively, these projects provide novel insights into CLN3 pathology and identify two promising modes of therapeutic advancement for this fatal lysosomal storage disease.

# Chapter 1: Introduction

**Lysosomal Storage Diseases**

Since the discovery of the lysosome nearly 60 years ago by Christian de Duve [1], the field of lysosomal storage diseases (LSDs) has expanded significantly. LSDs currently encompass approximately 70 genetically distinct diseases, with a collective incidence of 1:5000 live births annually [2]. LSDs account for roughly 14% of all inherited metabolic diseases [3, 4], among which the majority are autosomal recessive with the exception of mucopolysaccharidosis type II (MPS II) being inherited as an X-linked recessive trait [3]. A common denominator across all LSDs is lysosomal dysfunction originating from the loss of function or expression of lysosomal enzymes or other proteins that are vital for lysosomal homeostasis [5]. While the function of mutated molecules in some LSDs is well-characterized, in others, such as Niemann-Pick type C (NPC) and Juvenile Neuronal Ceroid Lipofuscinosis (JNCL; CLN3 disease), the normal function of mutated proteins is unknown [2, 6, 7]. Nevertheless, studies using mouse models and cells from affected patients, as well as lower species when available (i.e. yeast, Drosophila), have provided valuable information concerning the downstream sequelae of LSDs where the putative function of mutated molecules remains to be identified [8-13].

Lysosomes are membrane-bound organelles found in all eukaryotic cells, whose primary function is to degrade and recycle lipids, proteins, macromolecules, and intracellular organelles required for cellular homeostasis [14]. There are three main degradation pathways that converge in the lysosome[15]. Endocytosis and phagocytosis result in the internalization of extracellular components into endocytic vesicles, which then fuse to create endosomes[16]. Endosomes combine with Golgi transport vesicles carrying hydrolases to form late endosomes, which eventually mature into lysosomes as they continue to develop and acquire degradative enzymes. Autophagy degrades intracellular components, such as damaged, diseased, or senescent organelles by

transporting material to mature lysosomes via macroautophagy pathways. Lysosomes harbor over 60 different enzymes which include proteases, lipases, nucleases, glycosidase, and phospholipases that are responsible for lipid and protein degradation and recycling [5]. Lysosomal enzymes function at a pH < 5 that is maintained by vacuolar ATPases, which transport protons from the cytoplasm into the lumen [17, 18]. Other essential lysosomal components are integral membrane proteins, such as LAMP-1 and LAMP-2, which regulate lysosomal movement, exocytosis, and maintain lysosomal membrane integrity [18-20]. Recently it was discovered that the lysosome plays a role in multiple cellular pathways other than degradation [18, 21]. For example, lysosomes have a central role in responding and controlling cellular reactions to nutrients. During cellular starvation, lysosomes cluster with autophagosomes in the perinuclear space for rapid degradation and recycling of proteins and amino acids to produce new molecules to maintain cellular functions [21]. Due to their substantial enzyme burden and low pH, it is vital that lysosomal membrane integrity is maintained because release of lysosomal contents would induce cell death [1, 22]. The lysosome is also capable of inducing programmed cell death via lysosomal membrane permeability (LMP) [23, 24]. LMP releases proteases, such as cathepsins, into the cytoplasm, which can activate multiple apoptotic pathways as well as the inflammasome [25, 26]. Disruptions in lysosomal function, such as loss of degradative enzymes or membrane proteins, can lead to the accumulation of undigested macromolecules, which is a hallmark feature of LSDs [27].

Lysosomal inclusions are a hallmark of LSDs, where the composition of inclusions can vary widely depending on the type of mutation to include a heterogeneous combination of sphingolipids, phospholipids, or galactosylceramide as well as proteins [28]. In general, most LSDs are typified by inclusions in both the central nervous system (CNS) and periphery, since affected proteins are generally universally expressed in the

lysosomes of all cells. Nevertheless, it is evident that the CNS is extremely vulnerable to impaired lysosomal function and, as such, numerous LSDs are associated with neurological sequalae. LSDs are often characterized into four subgroups based on the composition of lipid accumulation, namely, mucopolysaccharidoses, glycolipidoses, mucolipidoses, and glycoproteinoses [5, 29]. These glycolipids and glycoproteins comprise the main structural components of cell membranes and influence cellular trafficking, second messenger signaling, and cell-cell communication [30, 31]. Therefore, perturbations in membrane lipid recycling or breakdown consequently lead to disruptions in myelin production, molecular transport systems, apoptosis, and immune system activation [5]. While inclusions are a prominent biomarker and reflect lysosomal function, there has been no compelling evidence to suggest that inclusions directly cause neuronal death in JNCL. Inclusions form in multiple types of neurons in different brain regions; however, neurodegeneration is primarily seen in thalamocortical regions at later stages of the disease process (i.e 9-12 months in $Cln3^{\Delta ex7/8}$ mice [32, 33].

**Neuroinflammation in Lysosomal Storage Diseases: A common thread**

Neuroinflammation is typically elicited as a protective response following CNS injury, infection, or disease; however, heightened or chronic inflammation can exert detrimental effects on neural cells [34-36]. Inflammatory events are initiated in the CNS upon sensing danger-associated molecular patterns (DAMPs) or pathogen-associated molecular patterns (PAMPs) by resident microglia and astrocytes, often leading to the mobilization of peripheral leukocytes into the CNS [37]. The goal is a swift response to contain the insult, which is rapidly downregulated to avoid unnecessary bystander damage [35]. This process is facilitated by several factors, including inflammatory cytokines and chemokines, trophic factors, phagocytosis, and regulated forms of cell

death (i.e. apoptosis or pyroptosis) [35, 38, 39]. However, persistent inflammation can elicit additional damage, further perpetuating the inflammatory cycle and CNS pathology.

Neuroinflammation has been reported in several LSDs, although the intensity of inflammatory changes and the molecular pathways responsible for triggering neuroinflammation in each likely differ. Although LSDs are caused by distinct genetic mutations they share some common downstream attributes, the foremost being lysosomal storage material accumulation. While the biochemical composition of storage material differs between various LSDs, emerging evidence suggests that it can either activate or perpetuate neuroinflammation, which can contribute to neuronal death [27]. Indeed, recent studies report that an imbalance between the synthesis and degradation of sphingolipid intermediates plays a prominent role in eliciting neuroinflammatory outcomes [40]. For example, tumor necrosis factor α (TNF-α) can activate sphingomyelinase (SMase), a key enzyme responsible for ceramide production, which leads to elevated ceramide levels that have been reported in CLN3 disease [41, 42]. It is well appreciated that high ceramide concentrations can also perpetuate inflammatory cascades such as NF-κB activation, trigger inflammasome activation, and disrupt normal cellular functions [40, 41]. Ceramide accumulation correlates with decreases in sphinosine-1-phosphate (S1P), thereby inducing apoptotic pathways and glial activation [40]. The S1P antagonist FTY720 has been shown to attenuate glial activation and neuroinflammatory processes, which leads to reduced relapse rates in multiple sclerosis [43, 44] and a recent report has demonstrated beneficial effects of FTY720 in a mouse model of Sandhoff disease [45]. Glucosylceramide accumulation in Gaucher disease (GD), resulting from glucocerebrosidase deficiency, has been shown to augment cytokine production in microglia [46]. Likewise, glucocerebrosidase loss in a mouse neuropathic model of GD causes microglial activation as early as postnatal day 12 [47]. The loss of lysosomal function coupled with lipid inclusion formation disrupts lysosomal

membrane integrity, resulting in increased permeability and translocation of lysosomal contents into the cytosol [48]. For example, defective lysosomes release hydrolases, metabolites, and cathepsins into the cytoplasm that can be sensed as intracellular DAMPs [29]. Cathepsins, in particular cathepsin B, have been shown to trigger NLRP3 inflammasome activation that contributes to neuroinflammation as well as induces neuronal apoptosis [49]. Additional intracellular changes that have been reported in various LSDs also have the ability to trigger and/or propagate neuroinflammation. For example, several LSDs display elevated intracellular calcium $(Ca^{2+})_i$ levels [50, 51] and disruption of $Ca^{2+}$ homeostasis can induce multiple inflammatory processes in many CNS cell types [52]. In the case of microglia, elevated $Ca^{2+}{}_i$ can induce inflammasome activity, cytokine release, and NF-κB activation. In neurons, increased $Ca^{2+}{}_i$ disrupts synchronized synaptic activity, and dysregulated neuronal firing can augment glutamate and ATP release as well as other "danger" signals that, in turn, trigger $Ca^{2+}{}_i$ elevations in surrounding glia [53], effectively perpetuating the response. In addition, storage material accumulation in LSDs disrupts normal ER function and causes ER stress, eliciting an unfolded protein response (UPR), a physiological reaction that halts protein synthesis in an effort to correct disrupted protein folding. However, a persistent UPR induces apoptosis by activating various signaling cascades, which can have catastrophic effects on the CNS [54-56]. Besides inducing cell death, ER stress can also trigger intracellular proinflammatory processes [57]. For example, $Ca^{2+}{}_i$ release leads to NF-κB activation and subsequent cytokine, chemokine, and ROS production, which can exacerbate neuropathology [57, 58]. Additionally, ER stress in astrocytes can trigger the activation of surrounding microglia, leading to increased IL-6 production [59]. In the context of CLN3 disease, cytokine/chemokine production and caspase-1 activation has been shown to be exaggerated in $Cln3^{\Delta ex7/8}$ microglia; however, the impact of neuroinflammation during early disease is uncertain, since attempts to detect traditional pro-inflammatory

mediators during acute CLN3 pathology in the mouse model have been negative. However, our group has found that aberrant caspase-1 is a critical driver of early disease pathology (Kielian laboratory, unpublished observations), suggesting that caspase-1 may act independently of its traditional role in pro-IL-β processing to cleave other proteins implicated in lysosomal biology and cargo trafficking. Neuroinflammation is an overarching theme in several LSDs that may propagate neurodegeneration.

**Neuronal Ceroid Lipofuscinosis (NCL):**

NCLs are a diverse group of autosomal recessively inherited LSDs caused by a mutation in one of 14 different ceroid lipofuscinosis (CLN) genes [7]. To date, 403 mutations have been associated with the known NCL forms. NCLs have been estimated to collectively occur in 1 out of every 100,000 live births per year [60-65]. There are four age-dependent classifications of NCL that correlate with specific genetic mutations; namely, infantile (INCL), late infantile (LINCL), juvenile (JNCL), and adult onset [66]. The four subtypes generally present with similar symptoms that include visual deterioration, neurocognitive and physical decline, seizures, and premature death, although the sequence of symptom appearance differs between forms [8, 67-69]. The early onset NCLs, including infantile and late infantile, are the most aggressive in terms of the short interval from diagnosis to death and are generally typified by more prominent neuroinflammatory responses [70]. The various NCL-related mutations result in either a loss in lysosomal enzymes, lysosomal transmembrane proteins, or synaptic vesicle-associated proteins [7]. Although the function of some NCL-related genes are known (i.e. CLN1 and CLN2 encode for the lysosomal enzymes PPT-1 and TPP-1, respectively), others remain elusive (i.e. CLN3, CLN5, CLN6). Mutations in each of the CLN proteins lead to the accumulation of lysosomal storage material whose biochemical composition varies according to each disease type. For example, storage material can

contain mitochondrial ATP synthase subunit c, sphingolipids, and lipofuscin, the latter of which is responsible for the autofluorescent properties of storage material [71, 72]. To date there is no cure for any of the NCL forms, only treatments to manage clinical symptoms.

**Juvenile Neuronal Ceroid Lipofuscinosis (CLN3 disease)**

Juvenile Neuronal Ceroid Lipofuscinosis (JNCL), also known as juvenile Batten disease (CLN3), is the most common form of all the NCLs with an estimated incident of 2-4 in every 100,000 live births a year [60-62]. Symptom onset presents in patients between the ages of 5-10, with rapid visual deterioration caused by aggressive retinopathy, macular degeneration, and optic atrophy [73]. Vision loss is followed by motor dysfunction, manifesting as Parkinson-like symptoms due to extrapyramidal and cerebellar disruptions that progress to quadriplegia [73, 74]. CLN3 patients have severe epileptic seizures that become increasingly refractive to treatment. Cognitive impairments appear early in the disease, with incontrollable speech patterns that progress to early onset dementia and severe dysarthria [75]. Similar to other NCL forms, disease pathology mainly affects the CNS [76]. MRI reveals the development of cortical lesions in the cerebral cortex along with cortical and hippocampal atrophy [77, 78]. However, unlike early onset NCLs, CLN3 disease pathology is protracted, resulting in premature death by the late teens -early twenties [79].

JNCL is caused by autosomal recessive mutations in *CLN3*. There are currently 49 mutations that have been discovered in the *CLN3* gene, the most common (~85%) being a 1.2 kb deletion spanning exons 7 and 8 [60, 73]. This deletion causes a frame shift mutation, resulting in a premature stop codon and a truncated form of the protein. The truncated CLN3 protein is hypothesized to undergo rapid decay, resulting in the loss

of lysosomal function [80, 81]. Lysosomal disruption results in the progressive accumulation of storage material primarily composed of autofluorescent ceroid lipopigments and mitochondrial ATP synthase subunit C [82]. The fingerprint-like inclusion deposits can be visualized by electron microscopy as early as the first trimester during development [83, 84]. Unlike other forms of NCL, which have a loss of lysosomal enzymes, the CLN3 protein, or battenin, is a 438-amino acid transmembrane protein primarily localized to the lysosomal membrane with minor expression reported in the endosome [85-87]. Both the CLN3 gene and protein are ubiquitously expressed in all cell types; however, the mutation has been found to primarily disrupt cells of neuronal lineage [8, 71, 72, 88]. The exact function of CLN3 is unknown; however, to date it has been implicated in multiple cellular processes including, lysosomal pH maintenance, cell proliferation, apoptosis, autophagy, intracellular trafficking, endocytosis, amino acid transport, mitochondrial function, and $Ca^{2+}_{i}$ regulation [86, 89-92]. The lack of high-quality CLN3-specific antibodies has made it challenging to determine the precise function and membrane localization of CLN3 and therefore, researchers have relied on overexpression or knockout models to speculate on the role of CLN3 in cellular function and disease implications.

**Current CLN3 disease models**

To gain a better understanding of the function of CLN3, researchers have developed multiple models to investigate the role of CLN3 in JNCL disease pathology and progression. One of the earliest models created was utilizing the yeast strain *Saccharomyces cerevisiae*. Yeast are often ideal for studying molecular pathways as they are similar to mammalian systems. The yeast genome is easily manipulated and

has a short growth cycle, allowing the study of complex molecular systems, such as gene function and regulation, protein function and interaction networks, and drug discovery using high-throughput library screens [93]. Following whole genome sequencing of *Saccharomyces cerevisiae*, BTN1 was discovered as a human Cln3 homologue. BTN1 is a non-essential protein that is 59% similar and 39% identical to Cln3 [94, 95]. It has been reported that BTN1 deletion disrupts pH homeostasis, leading to the formation of large vacuoles with increased intraluminal pH, similar to the lysosomal disruption observed in CLN3 disease [96]. Btn1 also plays a significant role in phospholipid distribution in the cell membrane, regulation of Golgi apparatus number, morphology, and location, as well as cellular metabolism [9, 94, 95, 97-99]. These studies suggest a similar function for mammalian Cln3 and a more complex role beyond lysosomal function, including intracellular trafficking and amino acid metabolism [97, 98]. While the yeast model is useful for studying molecular pathways, it lacks the complex system of higher vertebrates that provide greater insights into disease pathology.

There are currently two murine models utilized in the JNCL field, namely Cln3 knockout ($Cln3^{-/-}$) and Cln3 knock-in ($Cln3^{\Delta ex7/8}$) [100, 101]. The models were created on either a C57BL/6 or 12S6/SvEv genetic background, both displaying some phenotypes and pathology similar to human patients, such as accumulation lysosomal storage material, glial activation, and neuron dysfunction, however the 2 backgrounds are slightly different [27, 100-102]. For example, there are significant behavioral differences between C57BL/6 or 12S6/SvEv $Cln3^{-/-}$ and $Cln3^{\Delta ex7/8}$ animals. A comprehensive study by Kovacs and Pearce 2014 found that mice on the C57BL/6 background were significantly more explorative compared 12S6/SvEv mice, which exhibited anxiety-like behavior. It was also discovered that JNCL mice on the12S6/SvEv background had more severe motor impairment compared to C57BL6 [103]. At the cellular level, Finn et

al (2010) found that neurons cultured from $Cln3^{-/-}$ mice on the C57BL/6 background express significantly more NMDA receptor (NR2B), which is likely why these neurons are significantly more sensitive to NMDA-mediated excitotoxicity [67]. Therefore, it is imperative that the genetic background be taken into account when deciding on the most appropriate JNCL mouse model to use for studies. The first mouse model developed used targeted disruption genetic techniques to remove the Cln3 start codon and first six exons that were replaced with a *neo* cassette. $Cln3^{-/-}$ mice have been extensively characterized and recapitulate many disease attributes found in humans [32, 103-105]. Namely, these animals exhibit progressive accumulation of autofluorescent storage material, glial activation, neuronal loss, and visual deficits, although the latter two do not manifest until relatively late in the disease process (i.e. 12-18 months of age) [32]. While $Cln3^{-/-}$ mice are a good model for studying Cln3 function and its role in disease pathology, they are unable to fully recapitulate the human disease due to the fact that patients do not typically present with a complete disruption of the *CLN3* gene. On the other hand, the $Cln3^{\Delta ex7/8}$ mouse model was engineered to harbor the same mutation as roughly 85% of JNCL cases, which is a 1.02kb deletion spanning exon 7 and 8 [60]. These mice were generated by deleting exons 7 and 8 of the endogenous *CLN3* gene by homologous recombination, which was replaced with exons 7 and 8 harboring the 1.02kb *CLN3* mutation to create a “knock-in” mutation [100]. $Cln3^{\Delta ex7/8}$ animals display early accumulation of lysosomal storage material along with glial activation, motor deficits, disrupted neuronal activity, and a protracted disease time line similar to what is seen in CLN3 patients [33, 100, 102, 103, 106]. However, similar to the $Cln3^{-/-}$ model, neuronal death is not evident until late stage disease (i.e. 12-18 months). The $Cln3^{\Delta ex7/8}$ mouse model has been especially valuable in the discovery and development of novel therapeutics for CLN3 disease.

## Cell-Specific Disease Pathology in CLN3 disease

### Microglia

Microglia are the principal resident immune cells in the CNS parenchyma, accounting for approximately 10% of cells in the brain. Under non-pathological conditions, microglia are quiescent and in a constant state of surveillance for stress signals i.e. danger-associated molecular patterns (DAMPs) or pathogen-associated molecular patterns (PAMPs) [39, 107]. Along with ensuring cellular protection by phagocytosing cellular debris or preventing insult to surrounding neurons, microglia are also involved in neurodevelopment via synaptic pruning and providing trophic support [108, 109]. When microglia sense DAMPs or PAMPs released from damaged or dying neurons, reactive astrocytes, or infectious material [110] via Toll-like receptors and other pattern recognition receptors [35, 111], they become activated. Once activated microglia change both chemically and morphologically by becoming ramified in shape, undergo rapid proliferation, and begin to release growth factors, chemokines, and cytokines [112, 113]. This initial immune response is intended to be neuroprotective, as microglia increase phagocytosis to remove cell debris or pathogens as well as secrete neurotrophic factors, such as brain-derived growth factor, glia-derived growth factor, and nerve growth factor to promote neuronal health [114]. Microglia are a major source of chemokines and cytokines that serve to recruit and activate peripheral immune cells, respectively, at affected sites [112]. In addition, these mediators can act in an autocrine/paracrine manner to activate neighboring microglia, astrocytes, neurons, or oligodendrocytes [115, 116]. While intended to be neuroprotective, microglial activation is often referred to as a double-edged sword [114]. For example, when inflammation

becomes chronic, it often switches from being protective to detrimental as microglia continue to release more chemokines, cytokines, amino acids, and reactive oxygen species (ROS), which then perpetuate inflammatory mediator release from surrounding glial cells, alter target cell function, or induce cell death [117]. Microglial activation is a hallmark of virtually all neurodegenerative diseases and is known to play a major role in disease pathology and progression [113, 118, 119].

It has been suggested that activated microglia may contribute to disease progression in JNCL. Activated microglia are evident in the brains of CLN3 patients' post-mortem and JNCL murine models in regions that coincide with eventual neurodegeneration [32, 33, 120]. These findings suggest that microglia are responding to DAMPs released prior to neurodegeneration; however, the identity of these DAMPs and what cell type(s) are releasing these danger signals remains unknown. There is also evidence of increased levels of the pro-inflammatory cytokine IL-1β in JNCL post-mortem brains; however, this likely reflects secondary inflammation from cellular death at end-stage disease, since work from our laboratory has not been able to detect significant inflammatory mediator expression in the $Cln3^{\Delta ex7/8}$ brain during the first 6 months of life (Kielian lab unpublished observations). IL-1β is an important regulator of inflammation in the CNS that activates inflammatory pathways in surrounding glia that can create a toxic extracellular milieu if not tightly regulated [121, 122]. Previous work from our laboratory found that primary microglia from $Cln3^{\Delta ex7/8}$ mice exist in a primed proinflammatory state [123]. Namely, when exposed to neuronal lysate and C6 ceramide to mimic DAMPs associated with disease, numerous proinflammatory cytokines, including interleukin-1-beta (IL-1β), TNF-α, interleukin-1-alpha (IL-1α), interleukin-9 (IL-9), and interleukin-15 (IL-15) were significantly elevated in $Cln3^{\Delta ex7/8}$ compared to wild type (WT) microglia [123]. IL-1β and TNF-α were also shown to augment interleukin-6 production by $Cln3^{\Delta ex7/8}$ microglia, and as such the elevated levels of both IL-1β and

TNF-α induced by DAMPs could be expected to effectively perpetuate the neuroinflammatory circuit [123]. In terms of mechanism, elevated IL-1β production by $Cln3^{\Delta ex7/8}$ microglia was partially regulated by increased caspase-1/inflammasome activation, where caspase-1 is the primary enzyme required for processing pro-IL-1β to its active form, whereupon it can be secreted [123]. This study also demonstrated intrinsic defects in $Cln3^{\Delta ex7/8}$ neurons, as they were more susceptible to the cytotoxic effects of conditioned medium from $Cln3^{\Delta ex7/8}$ microglia. It is unclear whether diseased microglia also produce exaggerated inflammatory mediators *in vivo,* since we have been unable to detect significant pro-inflammatory mediator production in the $Cln3^{\Delta ex7/8}$ brain. However, it is possible that microglial cytokine release does occur but is undetectable in brain homogenates due to dilution effects of other CNS cell types. We have identified aberrant caspase-1 activity as a critical driver of CLN3 pathology, in that motor deficits and glial activation are significantly attenuated in $Cln3^{\Delta ex7/8}$/caspase-1 KO mice (Kielian laboratory, unpublished observations). It is possible that caspase-1 effects are independent of its ability to process pro-IL-1β, as the enzyme has been reported to cleave over 500 other proteins, many of which impinge on lysosomal function and endosomal trafficking that have been identified as pathological mechanisms in JNCL. Collectively, these findings suggest that microglial pathology in the context of CLN3 disease could set the stage for eventual neurodegeneration typical of JNCL.

**Astrocytes**

Astrocytes are the most abundant cell type in the brain and are responsible for maintaining homeostatic functions in the brain by providing neurotrophic support, synchronizing neurotransmitter metabolism and release, and regulating the extracellular

milieu [124-126]. The brain is the most energy-demanding organ in the body, yet at the same time does not maintain robust energy reserves, thus requiring a tightly regulated and uninterrupted nutrient supply. Energy balance is critical for the preservation of ion gradients, neurotransmitter production, and neurometabolism [127, 128]. Astrocytes are the primary cell that provides neurons with nutrient support required for their normal functions[129]. Astrocytes are morphologically structured to monitor the extracellular milieu and respond according to cellular requirements to ensure homeostatic functions. Astrocytic endfeet surround the intracerebral blood vessels that express glucose transporters and aquaporins to shuttle nutrients and regulate osmotic balance, respectively, across the blood-brain barrier [130, 131]. Glucose is the primary carbon source for the generation of key metabolites, including lactate, pyruvate, glutamate, and glutamine [132]. Astrocytes take up glucose, which is then utilized by glycolytic pathways to generate lactate. Lactate is released into the extracellular space where it is actively internalized by neurons via membrane-associated lactate shuttles. It has been found that neurons are capable of oxidizing both glucose and lactate for energy; however, neurons preferentially utilize lactate as an oxidative substrate because the cells are able to produce higher amounts of ATP via oxidative respiration as opposed to glycolysis [129, 133].

Along with monitoring and supplying metabolites to the brain, astrocytes regulate neuronal function. Astrocytes project fine processes to ensheath synapses to regulate synaptic firing, control neurotransmitter concentrations, and synapse development. A single astrocyte process is able to encompass and regulate 300-600 neuronal dendrites that may contain thousands of synapses [134, 135]. Astrocytes respond to neuronal activity through a cadre of membrane-associated receptors for neurotransmitters, cytokines, and growth factors at the tripartite synapse [129]. Astrocytes relay information

from neurons to surrounding astrocytes via $Ca^{2+}$ signaling through gap junctions, hemichannels, and other receptors creating a second level signaling network in the brain. This network is critical for maintaining neuronal homeostasis and neuronal signaling networks.

One of the most well studied and important astrocyte homeostatic functions is the transport and recycling of glutamate, the primary neurotransmitter in the CNS [136-138]. Once released from neuronal synapses, glutamate is quickly removed from the synaptic cleft via sodium-dependent glutamate transporters present on astrocyte processes at the tripartite synapse. Excitatory amino acid transporters 1 and 2 (EAAT 1 and EAAT 2) are high-affinity transporters driven by sodium and potassium gradients [139]. Transporter activity is an energy-demanding process, as three ATP are required for the removal of one glutamate molecule [140, 141]. Once in the astrocyte, glutamate is metabolized via one of two pathways based on the needs of the surrounding cells and extracellular glutamate concentrations [142]. First, glutamate can enter the TCA cycle to be converted to α-ketoglutarate, which can then be utilized to produce nutrients or energy metabolites such as lactate that is released back into the extracellular milieu for neurons [136]. Second, glutamate can be converted to glutamine by the enzyme glutamine synthetase. Glutamine is then released from astrocytes, whereupon it can be internalized by neurons through SAT transporters [143, 144]. Neurons then convert glutamine back into glutamate to be packaged into synaptic vesicles for neurotransmission. Astrocytes are the primary cell responsible for recycling and restoring glutamate in the brain [129]. Astrocytes not only regulate glutamate trafficking but are also capable of producing glutamate *de novo* if needed via glucose metabolism [145]. If any step in the glutamate-glutamine cycle is disrupted, this causes glutamate accumulation in the synaptic cleft, which often induces neuroexcitotoxicity and subsequent neurodegeneration. Glutamate

dysfunction has been reported in a multitude of neurodegenerative diseases, including PD, AD, epilepsy, and JNCL [104, 146-148].

Besides these critical homeostatic functions, astrocytes also participate in neuroinflammatory responses through their robust secretion of various chemokines [149, 150]. Upon activation, astrocytes undergo a morphological transformation typified by increased intermediate filament expression (i.e. glial fibrillary acidic protein (GFAP) and vimentin) and reactive astrocytes have been implicated in the pathogenesis of various neurodegenerative diseases [146-148]. For example, astrocytes with mutations in superoxide dismutatse-1 (SOD-1), a mutation responsible for some forms of amyotrophic lateral sclerosis, release soluble toxins that specifically kill motor neurons through Bax-dependent mechanisms [151]. Reactive astrocytes can also release lipocalin 2, a gelatinase-associated lipocalin, which is upregulated in frontotemporal lobe dementia patients and selectively toxic to neurons [152]. In addition, astrocyte activation often compromises glutamate homeostatic pathways, such as glutamate uptake and recycling mediated by glutamate transporters and glutamine synthetase, respectively [39, 147]. Astrogliosis has even been found to change the expression and function of neuronal proteins [153]. In the case of a glial-induced seizure model, activated astrocytes disrupted NKCC1 and KCC2 chloride channels in neurons, which impaired GABAergic inhibition and increased extracellular glutamate levels [154]. Reactive astrocytes have been detected during the acute phase of disease in animal models of AD, PD, and several LSDs, likely setting the stage for neuronal dysfunction and neurodegeneration [36, 39, 47, 155]. In response to insult or injury, reactive astrocytes have been shown to provide a bordering function to isolate areas of damage by forming a “glial scar” that prevents dying cells from impacting healthy tissue. Neuroinflammation also elicits astrocyte hemichannel opening concomitant with reduced gap junction

activity, which together can significantly disrupt neurotransmitter regulation [156, 157]. However, chronic neuroinflammation can also impair astrocyte neurotrophic support, making neurons more vulnerable to cytotoxic events [36].

Along with reactive microglia, astrocytosis has been observed in the brain of CLN3 patients' post-mortem in addition to CLN3 mouse models [32, 33, 102, 120]. Activated astrocytes have been found in multiple brain regions early in disease progression. These same areas are eventually associated with modest signs of neurodegeneration in CLN3 mouse models, namely the thalamus and somatosensory barrel field cortex [32, 33]. Early gliosis is likely an indicator of neuronal distress; however, this remains to be definitively demonstrated. Work from our group supports early neuronal dysfunction in the $Cln3^{\Delta ex7/8}$ mouse model, where synaptic activity was significantly heightened in the $Cln3^{\Delta ex7/8}$ brain from 1-4 months of age compared to WT animals [158]. The functional implications of reactive glia in CLN3 disease progression remains unclear and can be envisioned to be either a protective response to cellular stress or detrimental, leading to the loss of critical CNS homeostatic functions. Previously our lab has reported that astrocytes display increased hemichannel activity coupled with decreased expression of gap junction proteins [159]. Increased hemichannel activity can cause the release of a multitude of small hydrophilic molecules from the cytoplasm, including $Ca^{2+}$, ATP, and glutamate [160]. All three of these molecules are capable of influencing neuronal activity. Astrocytes rely on hemichannels and gap junctions to communicate with surrounding cells and to respond to the extracellular milieu. Aberrant hemichannel activity in the context of CLN3 mutation suggests a disruption or loss of astrocyte communication networks and thus the inability to regulate neuronal functions in JNCL. Coupled with the disruption of astrocyte signaling networks, our laboratory discovered that JNCL astrocytes have reduced

expression of glutamate transporter EAAT 1 and glutamine synthetase in multiple brain regions [159]. Without these critical proteins, JNCL astrocytes are ill-equipped to remove excess glutamate from the synapse or regulate neuron synaptic activity, thus potentially setting the stage for the vicious cycle of neuroexcitotoxicity characteristic of CLN3 disease.

**Neurons**

Neurons are highly specialized cells within the CNS that are responsible for regulating virtually all human functions and comprise roughly 10% of the cells in the brain [161]. There are multiple types of neurons, each with highly specific functions based on morphology, location within the brain, and connection to neuronal circuits [162]. Neurons influence brain activity through complex neuronal signaling networks. Neurons extend axons and dendrites to form synapses that are utilized to interpret and respond to external signals via electrical signaling. These signals are propagated primarily through excitatory (glutamate) and inhibitory (GABA) neurotransmitters released from the pre-synaptic neuron into the synaptic cleft [163]. These neurotransmitters bind to receptors (i.e. NMDA, AMPA, or metabotropic receptors; mGluR1-8 for glutamate and $GABA_A$ and $GABA_B$ for GABA) on the post-synaptic neuronal membrane and the message is transmitted [136]. The development of neuronal signaling circuits, their maintenance, and processing are tightly regulated and highly vulnerable to damage. Therefore, it is imperative to maintain neuronal homeostasis to hold neurodegenerative processes at bay.

Similar to several other LSDs, CLN3 disease mainly exhibits neuropathological manifestations [6, 7, 47, 164, 165]. While the CLN3 mutation is present in all cell types throughout the body, neurons are the most dramatically affected. Lysosomal inclusions begin to accumulate early in neurons, where our laboratory and others have observed

neuronal inclusions as early as postnatal day 30 in $Cln3^{\Delta ex7/8}$ mice, which precedes neurodegeneration [158, 159]. Even though lysosomal dysfunction appears early in the disease, neuronal loss does not become apparent in murine models until approximately 12-18 months [32, 33]. Likewise, neurological symptoms in humans do not present until around 10-15 years of age [73]. This implies the existence of compensatory mechanisms to maintain homeostasis until a pathological threshold is reached. Since lysosomal inclusions occur early in the disease process, this is a disconnect from neuronal death that is delayed in comparison and suggests that neuronal loss does not result from lysosomal inclusions. In addition, some neurons harbor large lysosomal inclusion burdens, yet are not lost during the disease process. Another interesting finding is that neurodegeneration in JNCL is localized to thalamocortical, cerebral cortex, and cerebellum regions for reasons that remain unclear [32, 33]. One popular view point is that neurodegeneration results, in part, from glutamate excitotoxicity. Elevated levels of glutamate have been found in the cortex and cerebellum of $Cln3^{-/-}$ mice [104]. In addition, inhibitory neurons are more impacted than excitatory neurons, which has been attributed to increased GAD65 auto-antibody production [166]. GAD65 is a glutamic acid decarboxylase that converts glutamate to GABA and the loss of inhibitory neurons leads to unregulated excitatory synaptic activity causing a rise in glutamate release [167]. As previously described, glutamate transporter and glutamine synthetase expression are significantly decreased in $Cln3^{\Delta ex7/8}$ astrocytes, which would render them ill-equipped to regulate increased levels of glutamate release [159]. In turn, elevated extracellular glutamate triggers continuous neuronal firing that further perpetuates glutamate release, which can eventually culminate in neuroexcitotoxicity. Our laboratory has recently identified supportive evidence for neuronal hyperexcitability during early CLN3 disease. Electrophysiology analysis revealed that axonal excitability was significantly enhanced in $Cln3^{\Delta ex7/8}$ neurons in the hippocampus and visual cortex at 1 month of age compared to

WT animals [158]. This represents the first evidence of early neuronal dysfunction that may lead to detrimental effects as the disease progresses. $Cln3^{\Delta ex7/8}$ axonal excitability diminished by 12 months of age and was associated with delayed signal propagation in axonal fibers [158]. This late neuronal phenotype has also been described in other forms of NCL. For example, in the $Ppt1^{-/-}$ and $Cln6^{-/-}$ mouse models of infantile Neuronal Ceroid Lipofuscinosis (INCL), changes in axonal and synaptic proteins are observed during at one month of age that precede the onset of pathology [168]. Collectively, this data indicates that neurons are the ideal and primary target for novel therapeutic interventions.

**Current JNCL Therapeutics**

Although our understanding of LSDs has significantly expanded since the discovery of the lysosome by DeDuve in the 1950s, many questions remain unanswered. There is currently no cure for any of the LSDs including JNCL, and the only available therapeutics target disease symptoms and provide palliative care for patients. Therefore, it is imperative to identify novel therapeutics to not only alleviate symptoms but also slow disease progression and extend life expectancy. The genetic mutations unique to each LSD result in distinct malfunctions of a specific lysosomal mechanism [56, 86, 169-171]. However, as previously mentioned, a common thread between all LSDs is the role of neuroinflammation in disease development and progression making the pathway an enticing target which could benefit multiple LSD [172]. One such potential drug is Mycophenolate mofetil (CellCept, which is a FDA-approved immunosuppressant used to prevent transplant rejection by inhibiting T cell and B cell expansion [173-175]. Murine studies in $Cln3^{-/-}$ mice found that CellCept reduced glial activation, decreased circulating GAD65 autoantibody, and improved motor function [176]. A phase 1/2 clinical trial was conducted on JNCL patients and found that CellCept

had some benefit in delaying vision loss (although this was a case report of a single CLN3 patient), it did not delay disease progression [177]. Many of the mutations that cause NCL affect other lysosomal enzymes, such as PPT1 and TTP1. For those NCLs that are caused by the lack of enzymatic activity, current therapeutic approaches include enzyme replacement therapy, which is costly and presents many challenges to achieve therapeutic enzyme levels in the brain because the blood-brain barrier remains intact in many instances [178].

Just as the brain is a complex system, the process of neurodegeneration in JNCL is multifactorial. Many studies have been working to identify novel therapeutic targets that could impact multiple pathways and cell types. One such target is the regulation of cyclic adenosine monophosphate (cAMP) production. cAMP is a second messenger that translates extracellular cues to affect intracellular signaling cascades [179]. cAMP production is initiated by activation of transmembrane G-protein coupled receptors that sequentially activate membrane bound adenylyl cyclases to convert ATP to cAMP [180]. cAMP then activates protein kinase A which phosphorylates several proteins [181]. cAMP has been implicated to play a role in multiple cellular pathways, including neuronal plasticity and memory, immune regulation, and maintaining neuronal homeostasis [182-184]. cAMP is able to tailor responses based on concentration levels, duration of cAMP production, and target cell type [179]. Reductions in cAMP levels have been found in multiple neurodegenerative diseases, including AD and traumatic brain injury coupled with increased microglial activation and disrupted neuronal synaptic activity [185-187]. cAMP is regulated by cyclic nucleotide phosphodiesterases (PDEs). There are 11 PDE families (PDE1-11) that are further divided based on function. For example, PDEs 5, 6, and 9 hydrolyze cyclic guanosine monophosphate (cGMP), whereas PDEs 4, 7, and 8 specifically hydrolyze cAMP. PDE4 is the most abundant isoform in the CNS [179, 188].

There are 21 genes that encode for the PDE superfamily and through splice variations approximately 100 PDE proteins are generated [179, 189]. Dysregulation or reduction in cAMP levels can have detrimental effects in the CNS, which has been demonstrated with the use of various PDE4 inhibitors to augment cAMP levels. For example, Gong et al (2017) found that rolipram, a FDA-approved PDE4 inhibitor, increased synaptic plasticity and improved learning and memory, and reduced amyloid-β aggregations in APP/PS1, an AD mouse model. Rolipram had a positive effect on learned behavior (i.e. fear conditioning) within 30 min of treatment with effects persisting well beyond treatment cessation, indicating that PDE4 inhibition can reverse disease pathology and improve cellular function [190]. Due to the success of PDE4 inhibitors in various neurodegenerative diseases, our laboratory tested the efficacy of three chemically distinct PDE4 inhibitors in $Cln3^{\Delta ex7/8}$ mouse model of JNCL. It was hypothesized that PED4 inhibitors would affect multiple disrupted pathways in JNCL, such as, glial activation, neuronal function, and glutamate regulation. All three PED4 inhibitors tested led to significant improvements in lysosomal function, increased glutamate transporter expression, reduced glia activation, and improved motor behavior in $Cln3^{\Delta ex7/8}$ mice. Additional details from this study will be discussed in Chapter 4.

**Gene therapy**

Significant progress has been made in the development and preclinical testing of gene therapy in a wide array of neurodegenerative diseases, including AD, spinal muscular atrophy, Rett syndrome, and LSDs [191-195]. Following the pioneering discovery that viruses possessed the ability to transfer genes, multiple types of viruses have been used for therapeutic studies, including retroviruses and adeno-associated viruses (AAV) each with differing benefits. Retroviruses are RNA viruses that reverse transcribe their genome into double stranded DNA (dsDNA) that is integrated into the

host cell genome [196, 197]. Retroviruses are easily manipulated to allow for a broad range of target cell specificity. This can be achieved by altering the envelop proteins on the viral surface. Because integration of the retrovirus genome into host cells is imperative for viral survival, transduction leads to stable genetic modification, which is then capable of being passed on to progeny cells in the case of stem cells [198]. Many different types of envelop proteins have been utilized for CNS transduction, including vesicular stomatitis glycoprotein, VSV-G and Mokola viral envelopes, and HIV gp41 glycoprotein, all of which provide unique and specific neuronal transduction [199]. However, the caveat of using retroviruses is there is a potential for the immune system to respond against the transgene as well as possible off-target integration that could disrupt normal genes [197].

Relatively new to the field of gene therapy yet extensively utilized, are AAV vectors that are small single-stranded DNA (ssDNA) non-enveloped viruses that can only replicate with “helper” adenoviruses due to the fact that they are replication incompetent [200]. There are currently nine known serotypes of AAV (AAV1-9), each with their own tissue-specific properties. AAV2 was the first serotype discovered with broad tissue tropism that provided the basis for future AAV vector development [201]. For example, AAV8 has high tropism for the liver and is currently undergoing clinical trials to treat hemophilia B [202]. AAV9 is capable of traversing the blood-brain barrier (BBB) following i.v. injection to target the CNS through mechanisms that are currently not fully understood [203-205]. Utilizing the 37/67-kDA laminin receptor to gain cell entry, AAV9 preferentially targets neurons and astrocytes in brain of both neonatal and adult mice [204, 206]. Recombinant AAV (rAAV) vectors do not contain viral genes nor integrate into the host genome; therefore, eliminating previous concerns of activating inflammatory pathways by RNA intermediates or disrupting normal gene functions

caused by retroviruses [207]. However, because the AAV genome is not able to integrate into the host DNA, transgenes are lost during cell division. While rAAVs appear to be ideal candidates for gene therapy, there are multiple limitations, including the rate-limiting steps of converting ssDNA into dsDNA prior to gene expression, and genome instability and expression following conversion [208]. This can be bypassed by using self-complimentary AAV (scAAV) vectors. scAAV is a ssDNA construct that contains palindromic inverted terminal repeats that cause the ssDNA to fold into a hairpin loop forming dsDNA. The repeats are the replication origins for DNA polymerase to synthesize complementary strands [209]. The scAAV dsDNA packaging significantly increases viral efficiency, speed of transduction, as well as increase stable protein expression that is capable of persisting for up to 10 years in the human brain following a single injection [210]. The only drawback to scAAV is that the viral DNA packaging capacity is reduced from 4.7 to 2.5 kb; however scAAVs are 600-fold more efficient at transduction than ssAAV vectors [209].

Many studies testing the utility of gene therapy are currently ongoing for NCLs. Infantile (CLN1) and Late Infantile (CLN2) Neuronal Ceroid Lipofuscinosis mutations lead to a loss of the soluble lysosomal-specific enzymes, PPT1 and tripeptidyle peptidase 1 (TPP1), respectively [80]. PPT1 catalyzes the cleavage of thioester bonds between fatty acids and TPP1 is a serine protease that removes tripeptides from amino termini of proteins as well having endopeptidase activity; however, the precise substrates *in vivo* have not yet been defined [211, 212]. Both PPT1 and TPP1 are secreted from cells during lysosomal exocytosis and can internalized surrounding cells via mannose-6-receptor-mediated endocytosis, allowing for cross-correction to occur. This is adventageous for CLN1 and CLN2 gene therapy because it does not require high CNS transduction efficiencies to achieve therapeutic benefit. For example, Passini et al

(2006) performed intracranial injections of an AAV2 vector harboring human CLN2 into the hippocampus, thalamus, and cerebellum of 6-week-old CLN2 KO mice and studied effects on disease progression for 6 – 13 weeks post-injection [213]. Although TPP1 enzyme activity was only increased proximal to the injection site, significant reductions in lysosomal inclusions were observed in the ipsilateral hemisphere [213]. Similarly, Haskell et al (2003) discovered that following a single intracranial injection of AAV5-CLN2 there were very few $TPP1^{+}$ cells; however, over a 10 day to 16-week period TPP1 activity gradually increased, suggesting TPP1 cross-correction [214]. Unfortunately, JNCL cannot benefit from cross-correction, since CLN3 encodes a transmembrane protein that is not secreted [197, 215]. Therefore, only cells that are successfully transduced with a particular virus will be affected. Nevertheless, this has not deterred researchers from developing and testing gene therapy, since prior work with sheep chimeric for CLN5, another lysosomal transmembrane protein did not display overt disease symptoms, suggesting that not all cells need to be corrected to achieve clinical benefit.

Since CLN3 is a transmembrane protein whose protein expression is maintained at low but constant levels throughout life and loss of CLN3 results in primarily neurological symptoms, there are certain criteria that need to be satisfied when considering gene therapy approaches [73-76, 216]. First and most importantly, the viral vector needs to transduce cells in the CNS, which has been well documented for AAV2, AAVrh.10, and AAV9 [217]. Secondly, transgene expression must remain stable for a long period of time because multiple injections are neither necessarily practical nor feasible for clinical trials because of the generation of anti-AAV antibodies [218]. It is also likely important that CLN3 protein levels mimic endogenous expression, since over-expression could lead to toxicity as has been reported in the yeast model of CLN3 and

too low of expression may have no effect. Utilizing AAVrh.10 containing human CLN3, Sondhi et al (2012) injected $3x10^3$ viral genomes directly into the hippocampus, cerebellum, and striatum of neonatal $Cln3^{\Delta ex7/8}$ mice[219]. Sixteen to eighteen months post-injection, $Cln3^{\Delta ex7/8}$ mice displayed hCLN3 expression in these brain regions along with significant reductions in lysosomal inclusions, suggesting improved lysosomal function [219]. However, hCLN3 expression was only found in close proximity to the injection site and did not disseminate. The virus was also only able to reduce astrocytosis with no effect on microglial activation or preventing neurodegeneration. These results indicate that it is possible to utilize gene therapy to replace a lysosomal transmembrane protein; however, the experiment fell short in reversing or slowing JNCL disease progression [219]. Recently our laboratory developed a novel JNCL gene therapy approach utilizing scAAV9 harboring hCLN3 driven by two distinct promoters (chicken β-actin and mouse MeCP2) that have different cell specificity and expression levels to determine the most appropriate level of CLN3 required for homeostasis, as well as, determine if neurons or astrocytes would benefit more from CLN3 expression. One month-old $Cln3^{\Delta ex7/8}$ mice were given a single i.v. injection of each promoter construct to replicate onset of JNCL disease symptoms and the most therapeutically relevant route of injection. The scAAV9-MeCP2-hCLN3 construct was able to significantly improve lysosomal pathology, glial activation, and motor behavior in $Cln3^{\Delta ex7/8}$ mice, which will be further discussed in Chapter 5.

## Overview of Dissertation

This dissertation describes two major focus areas in our laboratory; namely, elucidating underling mechanisms that cause JNCL pathology (role of astrocyte

glutamate regulation, mitochondrial dysfunction, and $Ca^{2+}$ signaling activity) and the development of novel therapeutics to slow disease progression and improve the lives of children afflicted with JNCL. Prior work from our laboratory identified reactive astrocytes in $Cln3^{\Delta ex7/8}$ mice at postnatal day 90 coupled with reduced expression of the glutamate transporter GLAST and glutamine synthetase, key regulators in the glutamate-glutamine pathway. $Cln3^{\Delta ex7/8}$ astrocytes also exhibited aberrant hemichannel activity and reductions in hemichannel protein expression. These results indicate a disruption in astrocyte homeostasis and a potential loss of neuronal support. Currently there is very little known about the role of astrocytes in JNCL. My research examined changes in mitochondrial function and $Ca^{2+}$ signaling in $Cln3^{\Delta ex7/8}$ astrocytes, two pathways that can contribute to neuronal excitotoxicity in JNCL.

There is currently no cure for JNCL making it imperative to find novel therapeutics to improve and prolong patient survival. Previous studies of several mouse neurodegenerative disease models have found positive results with PDE4 inhibitors. PDE4 inhibitors were considered to be an ideal drug candidate for JNCL due to their ability to affect the pathological cellular triad in the diseased CNS, namely neuronal, astrocyte, and microglial dysfunction. Originally PED4 inhibitors were envisioned to impact neuroinflammation in JNCL to promote neuroprotection. However, after further investigation, our results suggest that the primary mode of PED4 inhibitor action is on neuronal activity and neuroprotection that consequently leads to reduced glial activation and enhanced glutamate transporter expression.

While PDE4 inhibitors were able to reduce disease pathology and improve motor function, this approach does not correct the root of the disease, which is the loss of CLN3 protein. Utilizing scAAV9 gene therapy, our laboratory was the first to successfully transduce the CNS of $Cln3^{\Delta ex7/8}$ mice with hCLN3 following a single i.v. injection. This

study answered multiple important questions concerning gene therapy for JNCL, namely, 1) what is the efficacy, tropism, and longevity of scAAV9 following a single intravenous injection; 2) what is the ideal expression level of CLN3 for gene therapy; and 3) are there benefits to targeting specific cell types during CNS gene therapy. Our study found that a single i.v. dose of scAAV9-MeCP2-hCLN3 delivered to one month-old $Cln3^{\Delta ex7/8}$ mice was able to transduce cells throughout the brain, spinal cord, and eye. It was also determined that low CLN3 protein expression levels were more efficacious in reversing disease pathology then higher expression. Finally, our study found that mice transduced with hCLN3 controlled by a neuron-specific promoter (i.e. MeCP2) had significantly reduced glial activation, less lysosomal pathology, and improved motor coordination. Collectively, these results indicate that neurons in JNCL exert a greater impact on disease progression then previously hypothesized neuroinflammation induced by early glial activation.

# Chapter 2: Materials and Methods

**1) Mice.**

The studies described in this dissertation were conducted in strict accordance with the recommendations in the Guide for the Care and Use of Laboratory Animals of the National Institutes of Health. The protocol was approved by the Institutional Animal Care and Use Committee of the University of Nebraska Medical Center (Approval ID: 11-074-08-EP). Male $Cln3^{\Delta ex7/8}$ "knock-in" mice (C57BL/6 background) were used throughout these studies, which harbor the same 1.02 kb deletion in *CLN3* that occurs in approximately 85% of mutated CLN3 alleles[100]. Age-matched male C57BL/6 mice were used as WT controls.

**2) Astrocyte and neuron cultures.**

Primary WT and $Cln3^{\Delta ex7/8}$ astrocytes were prepared as previously described (Esen et al 2007). Briefly, whole brains were dissected from pups euthanized with an overdose of inhaled isoflurane at postnatal day 2-3. Following removal of the cerebellum, the cortex was disassociated with trypsin and plated in 75$mm^2$ flasks (one brain per flask). Cells were grown in DMEM (4.5 g/L glucose; Hyclone) supplemented with 10% FBS (Atlanta Biological), 200µM L-glutamine (Corning), oxaloacetic acid/sodium pyruvate/insulin (OPI; Sigma), 1X penicillin/streptomycin/fungizone (Corning), and 100µM L-leucine methyl ester (L-LME; Sigma) to induce microglial apoptosis and prevent their expansion. Upon reaching confluence (approximately 7-10 days *in vitro*; DIV), astrocytes were passaged every 3-4 days and were not used for experiments past three passages (DIV 30-40). To ensure the removal of residual loosely adherent microglia, flasks were shaken at 200 rpm for 12 h prior to plating.

Primary cultures of WT and $Cln3^{\Delta ex7/8}$ neurons were prepared as previously described [123]. Briefly, whole cortices were dissected from E16 embryos and following

trypsin disassociation, cells were plated on polyethyleneimine (PEI)-coated 10mm$^2$ dishes at $10^6$ cells/dish. Medium was changed 4 h after plating to remove non-adherent cells. Neurons were grown in Neurobasal medium (Life Technologies) supplemented with L-glutamine, penicillin/streptomycin/fungizone (Corning), and B-27 supplement (Life). Cultures were treated with 1 μM AraC to prevent glial expansion beginning on DIV 3 and continuing until use in experiments. Every three days, half of the spent culture medium was replaced with fresh medium and cultures were not utilized until after DIV 10.

**3) Seahorse mitochondrial stress test and glycolysis assays.**

Primary WT and Cln3$^{\Delta ex7/8}$ astrocytes were plated at 2x$10^4$ cells per well in 96-well plates. Cells were incubated for 12 h prior to treatment with combinations of TNF-α and IL-1β (10ng/ml each) or 5μM C6 ceramide and neuronal lysate (1:5 dilution) for 24 h. Neuronal lysate was prepared from primary mouse E16 neurons after multiple freeze-thaw cycles as previously described [123]. Prior to the start of metabolic assays, culture medium was replaced with sodium bicarbonate- and serum-free medium. Mitochondrial stress and glycolysis protocols were performed according to the manufacturer's instructions (Seahorse Biosciences). For mitochondrial stress tests, astrocyte oxygen consumption rate (OCR) was measured following exposure to sequential injections of oligomycin (1μM), FCCP (2μM), and rotenone (1μM). To measure astrocyte glycolytic activity, cells were incubated in sodium bicarbonate-, serum-, and glucose-free medium for 1 h prior to initiating the assay to reduce astrocyte intracellular glucose stores. Next, glucose (2.5M), oligomycin (1μM), and 2-deoxy-D-glucose (100μM) were sequentially injected into the wells and extracellular acidification rate (ECAR) was measured. LDH release was measured in each well following Seahorse assays to confirm lack of cell toxicity.

**4) Mitochondrial quantification.**

Primary WT and Cln3$^{\Delta ex7/8}$ astrocytes were plated on 18mm 0.25mg/mL poly-L-lysine coated glass coverslips (2x10$^4$ cells per coverslip) and incubated for 24 h prior to staining with Mitotracker Red CMXRos (1μM; ThermoFisher) to visualize mitochondria. Cell Mask Green (ThermoFisher) was added to demarcate the cytoplasm. Immediately following staining, astrocytes were washed extensively with culture medium and fixed with 4% paraformaldehyde at 37°C for 10 min. Coverslips were mounted using Prolong Gold Anti-fade mounting reagent (Life Technologies) and sealed using nail polish. Z-stack images of single astrocytes were acquired using a Zeiss LSM710 confocal microscope. Mitochondria were quantified using the spot function application in Imaris (Bitplane; Zurich, Switzerland) and three-dimensional reconstructions of mitochondrial staining in astrocytes were generated.

**5) Calcium signaling.**

Primary WT and Cln3$^{\Delta ex7/8}$ neurons and astrocytes were prepared as described above and plated on non-coated 18mm glass coverslips. Cells were loaded with the $Ca^{2+}$ indicator dye Fluo4-AM (1μM) for 30 min. Prior to staining, cells were washed and continuously perfused with artificial cerebral spinal fluid (ACSF) during the imaging period using AxioVision software (Zeiss; Jena, Germany). For neurons, live cell imaging was performed for 1 min to acquire baseline fluorescence signals, whereupon cells were stimulated with 25nM glutamate and images were captured every 5 sec for 10 min. For neurons, three dishes per experimental group were imaged (7-10 neurons per dish) and the experiment was replicated three times. For astrocytes, spontaneous $Ca^{2+}$ oscillations with or without cytokine exposure (TNF-α and IL-1β; 10ng/ml each) for 24 h were measured over a 5 min period with images taken every 5 sec for baseline

measurements. Astrocytes were then stimulated with 10mM glutamate and intracellular $Ca^{2+}$ signaling associated with the cell soma was quantitated by changes in mean fluorescent intensity after normalization to baseline values. Three dishes per experimental group were imaged (20 astrocytes per dish) and the experiment was replicated 3-4 times.

**6) Glutamate uptake assay.**

Primary WT and $Cln3^{\Delta ex7/8}$ astrocytes were seeded at $2x10^4$ cells per well in 96-well plates. Cells were incubated for 12 h prior to stimulation with TNF-α and IL-1β (both at 10ng/ml), C6 ceramide (5μM), or neuronal lysate (1:5 dilution) alone or in combination. To examine glutamate uptake efficiency, astrocytes were treated with 1mM glutamic acid in phenol red-free medium, whereupon supernatants were collected 30 min and 2 h later. Glutamate concentrations were immediately analyzed using an Amplex Red Glutamic Acid Assay kit according to manufacturer's instructions (ThermoFisher) with values normalized to the respective 1mM glutamate control at each time point.

**7) PDE4 inhibitor treatment.**

The PDE4 inhibitor rolipram (Sigma-Aldrich, St. Louis, MO) was reconstituted in DMSO and working stocks for s.c. injections were made weekly in sterile PBS. Based on studies of rolipram pharmacokinetics (PK)[220], doses of 0.5 and 5 mg/kg/day were selected for proof-of-principle studies in $Cln3^{\Delta ex7/8}$ mice. A dose of 0.5 mg/kg was calculated to yield a concentration of around 68 nM in the brain 1 h after administration with a half-life of 1-3 h. By extension, 5 mg/kg was expected to increase CNS doses 10-fold (i.e. ~ 680 mM). The FDA approved PDE4 inhibitor roflumilast (Daliresp$^{TM}$) was provided by AstraZeneca (Wilmington, DE) and was tested at oral doses of 2.5, 5, and 10 mg/kg/day in $Cln3^{\Delta ex7/8}$ mice. A roflumilast stock solution was prepared by dissolving

in PEG400 (Sigma-Aldrich, St. Louis, MO) and working stocks for oral gavage were made weekly by diluting in Methocel E15 (Dow Chemical Inc., Midland, MI). Based on the PK properties of roflumilast following oral delivery[221, 222], the highest dose of 10 mg/kg would lead to a concentration around 50 nM in the brain 1 h after treatment with a half-life of 1-4 h, although it's active metabolite, roflumilast-N-oxide, extends drug action to 8 h. Of note, the half-life of roflumilast is much longer in humans (18 h), making it amenable to once daily dosing[221, 222]. The PDE4 inhibitor PF-06266047 (ABI-4) was provided by Pfizer (Boston, MA) and evaluated at oral doses of 0.5 and 1 mg/kg/day in $Cln3^{\Delta ex7/8}$ mice. A working solution of PF-06266047 for oral gavage was prepared weekly by directly dissolving in Methocel A4M (Dow Chemical Inc., Midland, MI). Based on the PK properties of PF-06266047, the highest dose of 1 mg/kg would lead to a concentration of around 400 nM (total) in the brain 1 h after administration with a half-life of 7.5 h[223]. Importantly, because therapeutic levels of PF-06266047 would persist in the brain for nearly 24 h with 1 mg/kg dosing, a lower dose of 0.5 mg/kg was also examined, which equated to an approximate concentration of 200 nM (total) in the brain 1 h after treatment. In terms of selectively, rolipram, roflumilast, and PF-06266047 are specific inhibitors of all PDE4 isoforms (PDE4A-D) in rodents and do not affect the function of any other PDE isoenzymes[221, 222]. In addition, PF-06266047 had no activity at 10 μM in greater than 100 off-targets (which exceeds the highest dose examined in our study by ~ 100-fold; Patent Number, US 20140235612). Several concentrations of each PDE4 inhibitor were examined to identify the minimal effective dose that could be considered for potential clinical use. Since roflumilast is currently available in oral tablet form and several preclinical studies with other PDE4 inhibitors have utilized oral delivery[24, 25], roflumilast and PF-06266047 were adminstered via oral gavage to most closely model the mode of therapeutic delivery in CLN3 patients.

Experiments were performed using the National Institute of Neurological Disorders and Stroke (NINDS) recommended guidelines to ensure the rigor of these preclinical studies[224]. Briefly, age-matched male $Cln3^{\Delta ex7/8}$ and C57BL/6 WT mice were randomized into treatment groups (WT vehicle, $Cln3^{\Delta ex7/8}$ vehicle, WT PDE4 inhibitor, and $Cln3^{\Delta ex7/8}$ PDE4 inhibitor (n=8/group) and assigned numbered ear tags to ensure that all participating research personnel were blinded to mouse genotype and treatment group. The number of mice utilized for each experiment was determined in pilot studies by identifying a sufficient group size that demonstrated statistical significance for accelerating rotarod activity. The minimal group size required for statistical power (0.85; alpha = 0.05) was n = 8, which also provided sufficient statistical power for histological assessments. PDE4 inhibitor and vehicle stocks were prepared and assigned generic labels, so that treatment identity was masked to the individual performing the oral gavages or s.c injections. The genotype and treatment status of individual animals remained unknown until data analysis was completed, whereupon groups were de-identified. PDE4 inhibitor treatment was initiated in either 1 or 3 month-old mice by daily oral gavage, with treatment continuing for 6-9 months. The rationale for treating 1 month-old mice is that this roughly approximates the age at which a genetic diagnosis of JNCL is usually made in children (i.e. 5-10 years), recognizing the caveats associated with human-rodent age equivalent estimates[225]. Delaying treatment until 3 months of age was performed to determine whether PDE4 inhibitors can impact advanced disease, since a positive diagnosis of CLN3 disease in children is often delayed. Body weights were recorded on a weekly basis after drug treatment commenced until completion of the study, since PDE4 inhibitors have been associated with weight loss[222].

**8) Accelerating rotarod.**

Motor activity of mice (n=5-8/group) was monitored with an AccuRotor 4-Channel Rotarod (Omnitech Electronics, Inc., Columbus, OH) using a 3 cm diameter rod [226]. Mice were subjected to testing over 4 consecutive days with a training period in the AM and testing period in the PM that were separated by 2 h. All trials were conducted during the same time of day for consistency. During the training period (one trial in the AM), mice were placed on the rotarod that was set to a constant speed of 4 rpm for 5 min. For the testing period, the apparatus was set to accelerate from 0 to 40 rpm over 5 min. The rotation speed of 40 rpm was maintained after the 5 min acceleration phase and the latency to fall was digitally recorded by the instrument. Each mouse was subjected to three afternoon trials daily with at least 20 min rest between each run.

**9) Blood chemistry analysis.**

To assess the safety profile of chronic PDE4 inhibitor dosing in juvenile mice, blood chemistry analysis was performed at 2-3 month intervals throughout the study. Blood was collected from the facial vein into heparinized capillary tubes and transferred to Vetscan® Comprehensive Diagnostic Panel rotors (Abaxis, Union City, CA), which measured alanine aminotransferase (ALT), albumin (ALB), alkaline phosphatase (ALP), amylase (AMY) total calcium ($Ca^{2+}$), creatinine (CRE), globulin (GLOB), glucose (GLU), phosphorus (PHOS), potassium ($K^{+}$), sodium ($Na^{2+}$), total bilirubin (TBIL), total protein (TP), and urea nitrogen (BUN).

**10) Histology and quantitation of ocular inclusions.**

As another assessment of safety/toxicity of PDE4 inhibitors in juvenile mice, organs were collected following sacrifice for histopathological assessment by a board-certified pathologist with expertise in mouse toxicology studies (Samuel M. Cohen). The following tissues were fixed in 10% formalin and sent to AML Laboratories (Baltimore, MD) for

sectioning and H&E staining: kidney, stomach, liver, lung, spleen, heart, cervical lymph nodes, testes, thymus, trachea, muscle, spinal cord, larynx, pancreas, adrenal gland, aorta, bladder, colon, esophagus, small intestine, and femur/bone marrow.

To evaluate ocular inclusions, eyes were dissected under a microscope to remove the cornea and lens. Dissected eye cups were washed in PBS and embedded in acrylamide, whereupon cryostat sections (8 µm) were prepared to include the optic nerve. The most central optic nerve section was chosen for each eye, where a series of sequentially overlapping 10x images were taken covering the entire section using fluorescence microscopy (TRITC filter). Inclusions from each retinal layer were counted in a masked fashion using ImageJ software.

**11) cAMP quantitation.**

Various brain regions that are known to be affected in in $Cln3^{\Delta ex7/8}$ mice [i.e. somatosensory barrel field cortex (S1BF), visual cortex (VC), hippocampus (HPC), and thalamus (TH)] were dissected from vibratome sections of WT and $Cln3^{\Delta ex7/8}$ mice at 7 and 12 months of age (n=5-10 per group), whereupon cAMP levels were quantified using a cAMP ELISA kit (Enzo, Farmingdale, NY). cAMP concentrations were normalized to the amount of total protein collected to account for differences in tissue size. In some experiments where only tissue sections were available, cAMP levels were assessed by immunofluorescence staining as described below.

**12) Immunofluorescence and confocal microscopy of PDE4 or vehicle treated mice.**

Coronal brain sections were prepared from vehicle or PDE4 inhibitor treated WT and $Cln3^{\Delta ex7/8}$ mice at the end of the 6 month dosing period as previously described with minor modifications[227]. Briefly, animals were deeply anesthetized using sodium

pentobarbital and transcardially perfused with saline followed by 4% paraformaldehyde (PFA). The brain was removed, post-fixed in 4% PFA overnight and cryoprotected with 30% sucrose overnight prior to embedding in optimal cutting temperature medium. Free-floating cryostat sections (30 µm) were incubated overnight at 4°C with antibodies specific for cAMP (1:200, Santa Cruz, Dallas, TX), GFAP (1:500, Dako, Carpinteria, CA), GLAST (1:200), LAMP-1 (1:250), or CD68 (1:200, all from Abcam, Cambridge, MA) followed by appropriate biotin-streptavidin conjugated secondary antibodies (Jackson Immunoresearch, West Grove, PA) and detection with either streptavidin-AlexaFluor 592 or -AlexaFluor 488 (Invitrogen, Carlsbad, CA). TrueBlack (Biotium, Hayward, CA) was used to quench autofluorescent inclusions in $Cln3^{\Delta ex7/8}$ tissues. Immunofluorescence staining was visualized using a Carl Zeiss LSM 710 META confocal microscope with a 40x oil immersion objective in a FOV 450×450 µm (200x magnification) or 225×225 µm FOV (400x magnification). Tile images were acquired to visualize the entire S1BF (810 µm×1080 µm) or TH (810 µm×810 µm) of each section (two tissue slices per brain region per mouse). Tile images for GLAST quantitation were acquired at 270 µm×270 µm for greater resolution. For image quantification, 200 µm×200 µm non-overlapping regions of interest (ROI) were positioned throughout the S1BF (total of 9 ROIs) and TH (total of 6 ROIs) using AxioVision software (Zeiss), whereupon total values from all 6-9 ROIs were averaged for each of the two sections per mouse. Individual slice values per mouse were analyzed using SPSS to evaluate statistical significance using a mixed linear model approach. Results are reported as the mean intensity staining values (GFAP and GLAST) or area (CD68 and LAMP-1) determined by a custom software program incorporating the Visual Basic function of AxioVision (developed by Dr. Nikolay Karpuk, University of Nebraska Medical Center). To quantify cAMP expression levels in the brain, 6 non-overlapping 40x images in the TH, HPC, and VC from 5 mice per group

were acquired. Images were processed as described above and results are reported as the mean staining intensity values.

**13) AAV Vector Production and Purification.**

scAAV genomes were engineered to encode green fluorescent protein (GFP) or human CLN3 cDNA (NM_000086.2) under the control of the chicken-β-actin/cytomegalovirus hybrid promoter or the mouse minimal MeCP2 promoter [228]. Viral packaging was performed by SAB Technology (Philadelphia, PA). Briefly, viruses were packaged by standard triple transfection of helper, packaging (AAV2/9), and ITR-containing plasmids into HEK293 cells. Vectors were purified by cesium chloride gradient centrifugation and titers were determined by silver staining.

**14) *In vivo* administration of scAAV9 virus.**

One month-old male WT and $CLN3^{\Delta ex7/8}$ mice (n=5-8/group) were randomized into vehicle or virus treatment groups and received a single i.v. injection of $2x10^{12}$ vg scAAV9/MeCP2-hCLN3, scAAV9/β-actin-hCLN3, scAAV9/MeCP2-GFP, or scAAV9/β-actin-GFP or vehicle (PBS) via the retro-orbital sinus under isoflurane anesthesia. Body weights were recorded at weekly intervals throughout the study and blood chemistry analysis was conducted every 2 months post-injection.

**15) Immunofluorescence staining and confocal microscopy of scAAV9 treated mice.**

Representative coronal brain sections were prepared from $CLN3^{\Delta ex7/8}$ mice receiving i.v. injections of scAAV9 constructs as well as WT and $CLN3^{\Delta ex7/8}$ vehicle treated animals at 5 months post-injection as previously described with minor modifications [159]. Briefly, animals were deeply anesthetized using sodium pentobarbital and transcardially

perfused with saline followed by 4% paraformaldehyde (PFA). The brain was removed, post-fixed in 4% PFA overnight and cryoprotected with 30% sucrose overnight prior to embedding in optimal cutting temperature (OCT) medium. Free-floating cryostat sections (30 µm; two tissue slices per brain region per mouse) were prepared and slices containing the desired brain regions (S1BF and TH) were permeabilized by incubation in 0.1 M PBS containing 0.3% Triton-X (2X, 5 min each). Tissues were then blocked with 10% donkey serum for 1 h at room temperature and incubated overnight at 4°C with primary antibodies, including a polyclonal rabbit anti-mitochondrial ATP synthase subunit C (kindly provided by Dr. Susan Cotman, Harvard Medical School, Boston, MA), Iba-1 (1:200, BioCare Medical, Concord, CA), NeuN (1:500, Abcam, San Francisco, CA), CD68 (1:200, Abcam), LAMP-1 (1:250, Abcam), or GFP (1:500, Abcam, incubated with tissues for 72 h). After 3 washes with 1X PBS, brain sections were incubated with an appropriate biotin-streptavidin conjugated secondary antibody and DAPI for nuclear identification. Autofluorescent inclusions in CLN3$^{\Delta ex7/8}$ tissues were quenched with a 70% solution of Sudan Black for 10 min [159] or TrueBlack according to the manufacturer's recommendations (Biotium, Hayward, CA). Immunofluorescence was visualized using a Carl Zeiss LSM 710 META confocal microscope with a 40X oil immersion objective in a FOV 450×450 µm (200× magnification) or 225×225 µm FOV (400× magnification). Tile images were acquired to visualize the entire S1BF (810 µm×1080 µm) or TH (810 µm×810 µm) for each section. For image quantification, 200 µm×200 µm non-overlapping regions of interest (ROI) were positioned throughout the S1BF (total of 9 ROIs) and TH (total of 6 ROIs) using AxioVision software (Zeiss), whereupon total values from all 6-9 ROIs were averaged for each slice. Individual slice averages per mouse were analyzed using SPSS to evaluate statistical significance using a mixed linear model approach. Results are reported as the mean intensity staining

values (GFAP), area (CD68 and LAMP-1), or region of interest count (SCMAS) as determined using AxioVision software [159].

To quantify transgene expression in various CNS cell types, co-localization of transgene-positive cells ($GFP^+$) with $NeuN^+$ neurons and $GFAP^+$ astrocytes was determined using the Imaris program (Bitplane; Zurich, Germany). The Imaris auto-threshold co-localization function was used to determine non-random signal co-localization in the red and green channels [229]. Next, settings were determined on a per image basis and quantitative spot analysis [230] was performed to determine the number of $GFP^+$, $GFAP^+$, and $NeuN^+$ cells. Results are reported as the percentage of $GFP^+NeuN^+$ cells or $GFP^+GFAP^+$ cells.

**16) Western Blot.**

Coronal sections (1,200 µm thick) were prepared from acute brain slices using a vibratome while bathed in ice-cold ACSF, whereupon the S1BF, STR, VC, TH, CB, and HPC were dissected to collect total protein extracts. Tissues were homogenized in cell lysis buffer [50 mM Tris-HCl, pH 7.5; 150 mM sodium chloride; 0.5% Triton X-100; 1 mM sodium orthovanadate; 10 mM sodium fluoride; 0.5 mM phenylmethanesulfonyl fluoride and supplemented with complete protease inhibitor (Roche, South San Francisco, CA) and phosphatase inhibitor (Thermo Scientific, Waltham, MA) tablets]. Twenty µg of total protein was run on 10% PAGE gels, whereupon Western blotting was performed as previously described [159]. Blots were probed with anti-GFP (1:500, Abcam) and developed using chemiluminescence. Blots were stripped and re-probed with an antibody against β-actin (Sigma, St. Louis, MO) to confirm uniformity in gel loading. Blots were quantitated by densitometry analysis using an Alpha Innotech imager (Protein Simple, San Jose, CA) with signals normalized to β-actin.

**17) Real-time quantitative PCR.**

Mice were perfused with PBS and brain regions dissected from vibratome sections as described above. RNA was isolated using the Trizol reagent and treated with DNase I (Invitrogen, Carlsbad, CA) prior to cDNA conversion using an iScript cDNA synthesis kit (Bio-Rad, Hercules, CA). cDNA was used for real-time PCR with Applied Biosystems Gene Expression Master Mix and an Assays on Demand primer/probe set specific for exons 7-8 of human CLN3 (Hs01029238) and the housekeeping gene GAPDH. Relative expression of AAV9/β-actin-hCLN3 was then calculated for each region relative to AAV9/MeCP2-hCLN3 after GAPDH normalization.

**18) Statistics.**

For Seahorse mitochondrial and glycolysis assays, results were evaluated using an analysis of variance [231] [231] and multiple group Tukey-Krammer post-hoc to compare between groups. A Student's t-test was used to analyze mitochondrial number. Quantification of $Ca^{2+}$ oscillations was assessed using a mixed linear model, where variables included, group, genotype, coverslip, and number of oscillations per cell. Statistical significance between groups was analyzed in SPSS (IBM SPSS Statistic, Armonk). All assays for therapeutic studies were blinded throughout the entirety of data collection and analysis. For body weight comparisons, weights were averaged for mice in each treatment group and were analyzed by repeated measures ANOVA followed by a *post-hoc* Tukey test. Quantification of CD68, GFAP, LAMP-1, and GLAST immunofluorescence staining was assessed using a mixed linear model, where the variables included group, animal, slice, and staining area or intensity. Statistical significance between groups for each brain region was analyzed in SPSS (IBM SPSS Statistic, Armonk). For accelerating rotarod analysis were analyzed by a mixed linear

model in SPSS. Quantification of cAMP was assessed by one-way ANOVA in GraphPad Prism (La Jolla, CA).

# Chapter 3: Astrocytes in Juvenile Neuronal Ceroid Lipofuscinosis (CLN3) display metabolic and calcium signaling abnormalities

**Abstract**

Juvenile Neuronal Ceroid Lipofuscinosis (JNCL) is a lysosomal storage disease caused by autosomal recessive mutations in *CLN3*. Children with JNCL experience progressive visual, cognitive, and motor deterioration with a decreased life expectancy (late teens-early 20s). Neuronal loss is thought to occur, in part, via glutamate excitotoxicity; however, little is known about astrocyte glutamate regulation in JNCL. Spontaneous $Ca^{2+}$ waves were reduced in murine $Cln3^{\Delta ex7/8}$ astrocytes, which was also observed following glutamate or cytokine exposure. Astrocyte glutamate transport is an energy-demanding process and disruptions in metabolic pathways could influence glutamate homeostasis in $Cln3^{\Delta ex7/8}$ astrocytes. Indeed, basal mitochondrial respiration and ATP production were significantly reduced in $Cln3^{\Delta ex7/8}$ astrocytes. These changes were not attributable to reduced mitochondria, since $Cln3^{\Delta ex7/8}$ astrocytes displayed significant increases in mitochondrial numbers. Interestingly, despite these functional deficits in $Cln3^{\Delta ex7/8}$ astrocytes, glutamate transporter expression and glutamate uptake were not dramatically affected. Concurrent with impaired astrocyte metabolism and $Ca^{2+}$ signaling, murine $Cln3^{\Delta ex7/8}$ neurons were hyper-responsive to glutamate, as reflected by heightened and prolonged $Ca^{2+}$ signals. These findings identify intrinsic metabolic and $Ca^{2+}$ signaling defects in $Cln3^{\Delta ex7/8}$ astrocytes that may contribute to neuronal dysfunction in CLN3 disease.

## Introduction

Juvenile Neuronal Ceroid Lipofuscinosis (JNCL), or CLN3 disease, is a pediatric lysosomal storage disorder afflicting an estimated 1 in every 100,000 live births [60-62]. Children appear healthy until the onset of disease symptoms between the ages of 5-10 that initiates as vision loss, followed by seizures, dementia, and motor and cognitive decline, with premature death by the late teens to-early 20s [60, 74, 232]. JNCL is caused by autosomal recessive mutations in *CLN3* [60, 233]. Most common is a 1.02kb deletion that occurs in approximately 85% of mutated *CLN3* alleles, which is thought to encode a truncated protein that is minimally expressed and/or rapidly degraded [60] [234]. While its function still remains unknown, CLN3 has been implicated in multiple cellular processes, including lysosomal acidification, amino acid transport, mitochondrial function, and intracellular $Ca^{2+}$ regulation [86, 89-92].

CLN3 pathology is characterized by the accumulation of lysosomal inclusions in all cell types, with neurons most dramatically affected [71, 72]. Current evidence suggests that inclusions are not a direct cause of neuron death, since many inclusion-positive neurons are not lost during the disease [88, 100]. In terms of alternative possibilities, previous studies have reported a disruption in glial function and potential loss of neuron homeostatic support that might contribute to neuron dysfunction in JNCL. In particular, astrocytes have increased hemichannel (HC) opening during early disease that can serve as a conduit for ATP, $Ca^{2+}$, and glutamate release [159, 235]. In addition, $Cln3^{\Delta ex7/8}$ microglia exist in a primed pro-inflammatory state, producing exaggerated levels of several cytokines, such as IL-1β and TNF-α, than can potentiate astrocyte HC opening and augment glutamate release, disrupting cellular homeostasis [123, 160]. These data are supported by the finding that glutamate levels are elevated in the brains of both JNCL patients as well as CLN3 mouse models [104, 236-238]. However, the underlying mechanisms responsible for elevated glutamate in the JNCL brain remain to

be identified, but collectively the available evidence suggests a disruption in vital astrocyte homeostatic functions is a contributing factor.

Astrocytes are the primary cell type responsible for regulating extracellular glutamate levels to maintain neuronal homeostasis [138]. Astrocyte projections surround the tripartite synapse and remove glutamate primarily through the $Na^{2+}$-dependent glutamate symporters GLAST and GLT-1 [139]. Glutamate transporter action is an energy-demanding process, which requires the $Na^{+}/K^{+}$ ATPase to produce large quantities of ATP [239]. Disruption in any step of the glutamate uptake pathway can result in increased synaptic glutamate concentrations that are capable of inducing neuron excitotoxicity [240, 241]. In addition to CLN3 disease, alterations in glutamate homeostasis have been reported in several neurodegenerative disorders, including Alzheimer's disease, Parkinson's disease, and other lysosomal storage disorders, such as Niemann-Pick type C [146-148, 242]. Besides maintaining CNS metabolic homeostasis, astrocytes control neurotransmitter release and neuronal signaling, in part, by regulating $Ca^{2+}$ levels at the synapse [243-245]. Astrocytes interpret neuronal signaling patterns and communicate to surrounding cells via $Ca^{2+}$ waves, which act as a glial signaling system for the propagation of both paracrine and distant signals in the CNS [246, 247]. Strong evidence has emerged suggesting that perturbations in astrocyte signaling $Ca^{2+}$ contribute to neuronal hyperactivity, loss of astrocyte homeostatic support, and disruption of the extracellular milieu [248, 249].

Here we present evidence of intrinsic abnormalities in $Cln3^{\Delta ex7/8}$ astrocytes that may account for, in part, neuroexcitotoxicity in the CLN3 brain. Specifically, $Cln3^{\Delta ex7/8}$ astrocytes displayed reduced $Ca^{2+}$ waves, impaired mitochondrial activity, and ATP production. However, despite these intrinsic defects, glutamate transporter expression and glutamate uptake were not significantly different between $Cln3^{\Delta ex7/8}$ and WT astrocytes. $Cln3^{\Delta ex7/8}$ neurons were hyper-responsive to glutamate, exhibiting elevated

and prolonged $Ca^{2+}$ signals. Collectively, these findings reveal mechanisms that could impair astrocyte-neuron glutamate crosstalk and contribute to neuronal excitotoxicity during CLN3 disease progression.

## Results

**CLN3 mutation causes perturbations in astrocyte $Ca^{2+}$ oscillations.** Astrocytes utilize $Ca^{2+}$ signaling to communicate with surrounding cells as well as regulate synaptic firing. Glutamate released from neurons activates astrocyte glutamate transporters and triggers an increase in astrocytic intracellular $Ca^{+2}$ [250, 251]. Elevated intracellular $Ca^{2+}$ in astrocytes can activate multiple glutamate regulatory pathways, including trafficking of GLAST transporters to the membrane, mobilizing mitochondria to increase energy production, and increased $Na^{+}$-$Ca^{2+}$ exchange pump activity to reduce $K^{+}$ levels and neuronal firing [246, 252-254]. Unchecked neuronal activity from impaired astrocyte regulation can increase glutamate concentrations, further potentiating glutamate dysregulation. To determine whether $Ca^{2+}$ transients are perturbed in $Cln3^{\Delta ex7/8}$ astrocytes, live-cell $Ca^{2+}$ imaging was performed. $Cln3^{\Delta ex7/8}$ astrocytes displayed decreased spontaneous $Ca^{2+}$ oscillations under resting conditions, which was also observed when cells were exposed to proinflammatory cytokines that have previously been shown to be over-produced by $Cln3^{\Delta ex7/8}$ microglia (Figure 1) [123]. Following the assessment of basal spontaneous $Ca^{2+}$ activity, astrocytes were exposed to 10mM glutamate to model extracellular neuronal signaling. Glutamate treatment increased intracellular $Ca^{2+}$ in both WT and $Cln3^{\Delta ex7/8}$ astrocytes compared to baseline; however, levels were still significantly reduced in $Cln3^{\Delta ex7/8}$ cells (Figure 1). A single astrocyte is capable of simultaneously regulating multiple synapses, while at the same time one neuron may have its synapses enveloped by multiple astrocytes. Therefore, the reduction in $Cln3^{\Delta ex7/8}$ astrocyte $Ca^{2+}$ signaling may not only have intrinsic effects or regulate local neuronal activity, but could also disrupt larger signaling networks.

**Figure. 3.1**

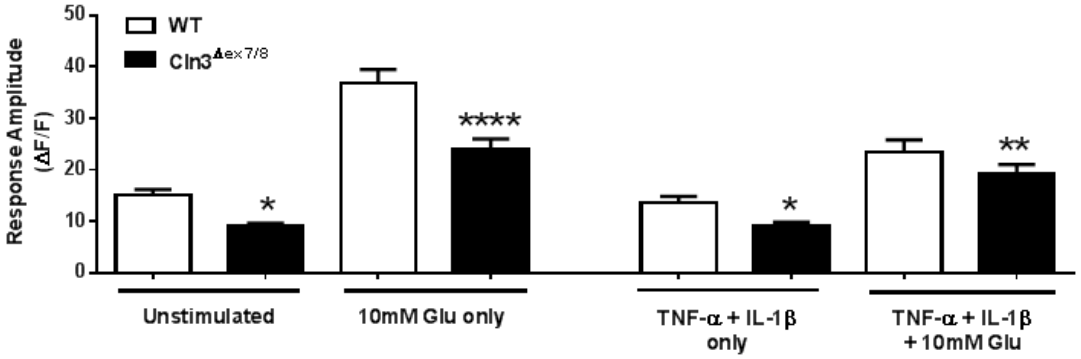


**CLN3 mutation alters astrocyte $Ca^{+}$ responses.** Primary WT and $Cln3^{\Delta ex7/8}$ astrocytes were unstimulated or treated with TNF-α and IL-1β (10ng/mL each) for 24 h and loaded with the $Ca^{2+}$ indicator dye Fluo4-AM. Following a 5 min period for baseline readings, cells were exposed to 10mM glutamate (Glu) and the amplitude of the first $Ca^{2+}$ response was calculated (*, $p < 0.05$; **, $p < 0.01$; ****, $p < 0.0001$).

**Mitochondrial respiration is impaired in Cln3$^{\Delta ex7/8}$ astrocytes.** During periods of robust neuronal activity, astrocyte energy demands increase to maintain homeostatic functions [239]. Although neurons possess the highest metabolic requirements in the CNS, astrocytes account for approximately 20% of the energy usage in the brain during consciousness [255]. Astrocytes must maintain mitochondrial and glycolytic function to regulate neurotransmitter and ion homeostasis and synaptic activity. Previous studies support mitochondrial dysfunction in JNCL, including increased mitochondrial oxidative stress molecules, mitochondrial membrane depolarization, and alterations in mitochondrial morphology [89, 91, 256-258]. However, most of these studies were conducted with an immortalized Cln3$^{\Delta ex7/8}$ cerebellar cell line and none have examined mitochondrial activity in real-time in astrocytes. Here we utilized Seahorse bioassays to determine whether Cln3$^{\Delta ex7/8}$ astrocytes display defects in mitochondrial respiration. Under resting conditions, both basal respiration and ATP production were significantly reduced in Cln3$^{\Delta ex7/8}$ astrocytes (Figure 2). Mitochondrial defects in Cln3$^{\Delta ex7/8}$ astrocytes were also evident when cells were exposed to JNCL danger signals (ceramide + neuronal lysate) or proinflammatory cytokines (TNF-α + IL-1β; Figure 2). These mitochondrial defects could be attributed, in part, to dampened intracellular $Ca^{2+}$ in Cln3$^{\Delta ex7/8}$ astrocytes, since mitochondrial respiration and ATP production are $Ca^{2+}$-dependent and the failure to raise intracellular $Ca^{2+}$ in Cln3$^{\Delta ex7/8}$ cells would be expected to interfere with mitochondrial function. Importantly, total protein concentrations were equivalent between WT and Cln3$^{\Delta ex7/8}$ astrocytes pre/post assay, indicating lack of toxicity.

**Figure 3.2**

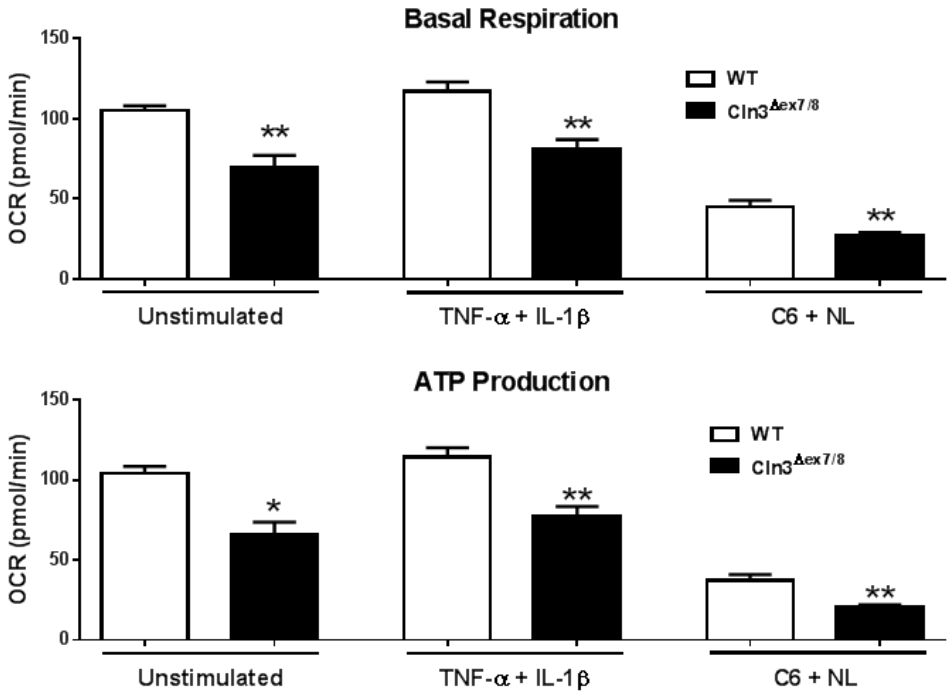


**Mitochondrial respiration is impaired in Cln3$^{\Delta ex7/8}$ astrocytes.** Primary WT and Cln3$^{\Delta ex7/8}$ astrocytes were unstimulated or treated with TNF-α and IL-1β (10ng/mL each) or C6 ceramide (5μM) and neuronal lysate (NL) for 24 h, whereupon OX PHOS activity was examined using Seahorse Bioscience assays. (A) Basal mitochondrial respiration and (B) ATP production was measured based on oxygen consumption rate (OCR). Significant differences in mitochondrial function between WT and CLN3$^{\Delta ex7/8}$ astrocytes are denoted by asterisks (*, $p < 0.05$; **, $p < 0.01$).

To determine whether defective mitochondrial activity in Cln3$^{\Delta ex7/8}$ astrocytes was due to alterations in mitochondrial number, cells were stained with the mitochondrial-selective dye MitoTracker Red CMXRos. Cln3$^{\Delta ex7/8}$ astrocytes displayed significantly more mitochondria per cell compared to WT (Figure 3), indicating that impaired mitochondrial respiration in Cln3$^{\Delta ex7/8}$ astrocytes is not due to reduced mitochondrial biomass, but more likely senescent mitochondria due to mitophagy defects, which has been found to occur in JNCL models [89, 259, 260]. Without sufficient ATP generation in the face of high neuronal activity, Cln3$^{\Delta ex7/8}$ astrocytes may become overwhelmed and unable to regulate the CNS extracellular milieu.

In instances of increased neuronal activity or distress, astrocytes augment glycolysis to produce more ATP. Since mitochondrial metabolism and ATP production were reduced in Cln3$^{\Delta ex7/8}$ astrocytes, we next examined whether cells shift to a more glycolytic profile to compensate. No significant differences in glycolytic rates were observed between Cln3$^{\Delta ex7/8}$ and WT astrocytes (Figure 4). This indicates that Cln3$^{\Delta ex7/8}$ astrocytes do not compensate for the reduction in mitochondrial ATP production by augmenting glycolytic pathways.

**Figure 3.3**

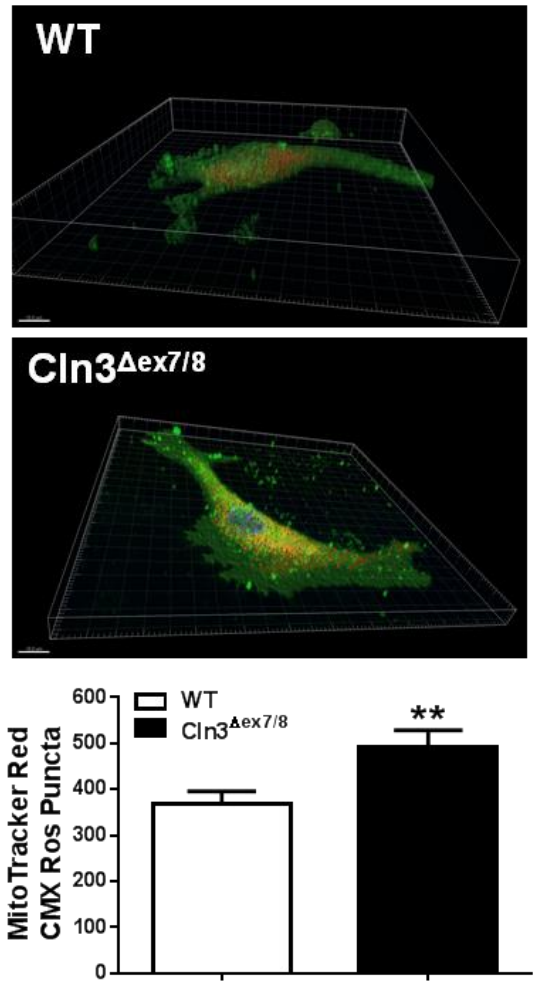


**Cln3$^{\Delta ex7/8}$ astrocytes display increased mitochondrial abundance.** Primary WT and Cln3$^{\Delta ex7/8}$ astrocytes were stained with MitoTracker Red CMX ROS to quantify mitochondria. Mitochondrial numbers were calculated using a spot analysis program with Imaris Scientific 3D/4D Image Processing & Analysis Software (**, $p < 0.01$).

**Figure 3.4**

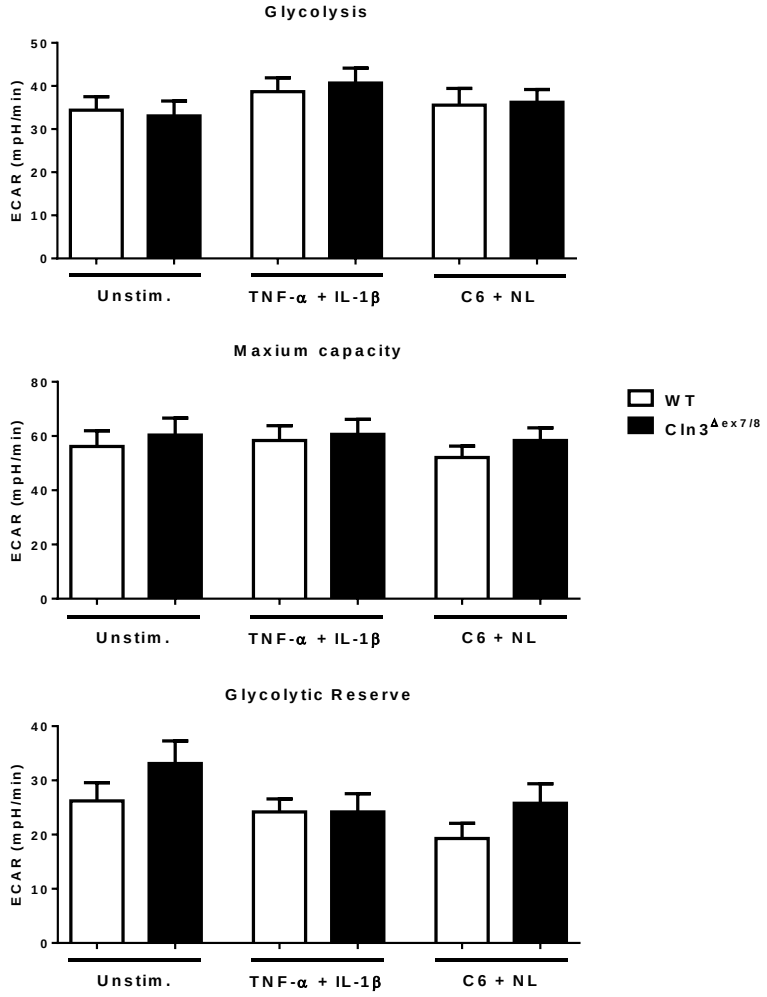


**CLN3 mutation does not affect astrocyte glycolytic activity.** Primary WT and $Cln3^{\Delta ex7/8}$ astrocytes were unstimulated or treated with TNF-α and IL-1β (10ng/mL each) or C6 ceramide (5μM) and neuronal lysate (NL) for 24 h, whereupon glycolytic activity was examined using Seahorse Bioscience assays. (A) Fmitsis, (B) Maximum capacity, and (C) Glycolytic reserve was measured based on extracellular acidification rate (ECAR).

**Glutamate transporter expression and uptake are not significantly altered in Cln3$^{\Delta ex7/8}$ astrocytes.** The excitatory neurotransmitter glutamate is tightly regulated in the CNS and the pathways responsible for maintaining glutamate homeostasis are highly conserved [261, 262]. Disruptions in glutamate regulation have been implicated in CLN3 disease, where glutamate levels are elevated in CLN3 mouse models and treatment with NMDA or AMPA receptor antagonists improved motor function [104, 146, 236, 237, 242, 263]. To explore the possibility of intrinsic alterations in glutamate transport in Cln3$^{\Delta ex7/8}$ astrocytes, we first examined glutamate transporter expression by Western blot. No significant differences in either GLT-1 or GLAST expression were detected between WT and Cln3$^{\Delta ex7/8}$ astrocytes under resting conditions or following cytokine (TNF-α + IL-1β) or glutamate treatment (data not shown). To determine whether glutamate uptake was affected in Cln3$^{\Delta ex7/8}$ astrocytes, cells were assessed for their ability to remove excess glutamate from the extracellular milieu using an Amplex Red glutamic acid assay. Following a 24 h treatment with danger signals (ceramide + neuronal lysate) or cytokines (TNF-α + IL-1β), astrocytes were exposed to a bolus of glutamic acid (1mM), whereupon the amount of glutamate remaining in the supernatant at 30 min and 2 h was measured. Extracellular glutamate levels were similar between Cln3$^{\Delta ex7/8}$ and WT astrocytes in all treatment conditions (Figure 5). Collectively, the decreases in $Ca^{2+}$ signaling and ATP production in Cln3$^{\Delta ex7/8}$ astrocytes do not significantly impact intrinsic glutamate regulatory pathways, instead suggesting possible defects in cell-cell communication with neurons.

**Figure 3.5**

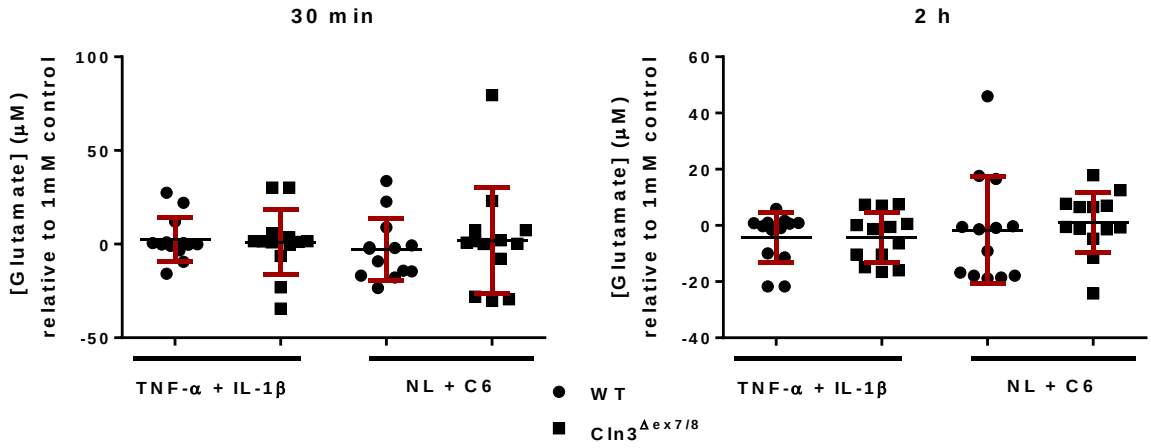


**Glutamate uptake is not altered in Cln3$^{\Delta ex7/8}$ astrocytes.** Primary WT and Cln3$^{\Delta ex7/8}$ astrocytes were treated with TNF-α and IL-1β (10ng/mL each) or C6 ceramide (5μM) and neuronal lysate (NL) for 24 h. Cells were then exposed to 1mM glutamate, whereupon supernatants were collected 30 min and 2 h later to evaluate residual extracellular glutamate concentrations. Results were normalized to the 1mM glutamate control.

**Cln3$^{\Delta ex7/8}$ neurons are hyperexcitable to extracellular glutamate.** Neurons are the principle cell type lost in CLN3 disease and this is thought to result, in part, from glutamate excitotoxicity [33, 71, 72, 104, 166]. Hyper-excitable or uninhibited excitatory neurons are a primary cause of seizures, which is a hallmark of disease in CLN3 patients [264]. To investigate the sensitivity of Cln3$^{\Delta ex7/8}$ neurons to physiological glutamate concentrations at the synaptic cleft (i.e. ~25nM), live-cell $Ca^{2+}$ imaging was performed [265-267]. Glutamate application evoked a significant increase in intracellular $Ca^{2+}$ in Cln3$^{\Delta ex7/8}$ neurons, reflecting their hyper-sensitivity to glutamate (Figure 6). After a 1 min stimulation period, glutamate washout was performed, which returned intracellular $Ca^{2+}$ levels to baseline in WT but not Cln3$^{\Delta ex7/8}$ neurons, which is often used as an indication of impending excitotoxicity [268-270]. Collectively, these studies suggest the existence of autonomous and non-cell autonomous mechanisms that may lead to glutamate dysregulation in CLN3 disease via impaired neuron and astrocyte activity. By extension, since Cln3$^{\Delta ex7/8}$ neurons are hyper-responsive to glutamate this could perpetuate glutamate release, which would ultimately lead to excitotoxicity and neuron death that is reminiscent of CLN3 disease.

**Figure 3.6**

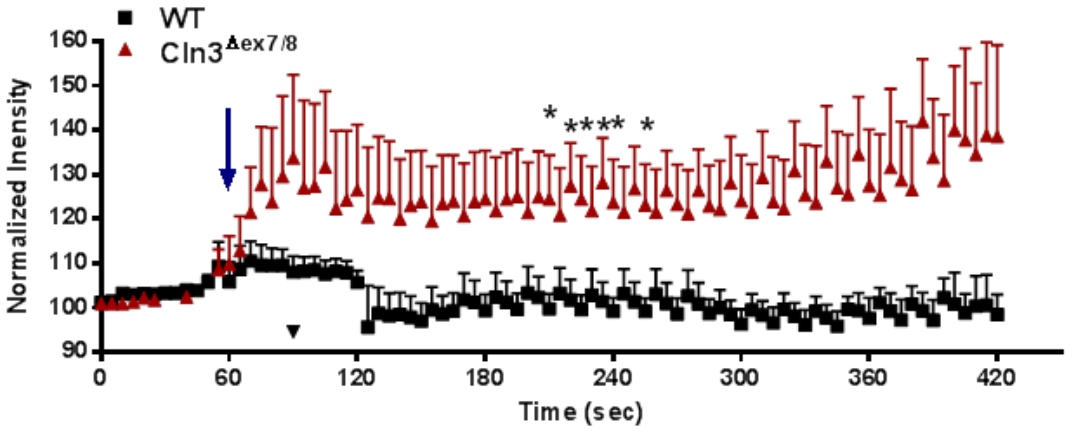


**$Ca^{2+}$ signaling is disrupted in $Cln3^{\Delta ex7/8}$ neurons.** Primary WT and $Cln3^{\Delta ex7/8}$ neurons were loaded with Fluor4-AM. Following a 5 min period for baseline recordings, neurons were treated with 25nM L-glutamic acid and evaluated for a 420 sec period. Measurements were obtained using AxioVision software and are reported as the mean fluorescent intensity normalized to baseline values (*, $p < 0.05$). The arrow depicts the point of L-glutamic acid addition.

## Discussion

Although CLN3 mutations were identified as the cause of JNCL in 1995, the precise function of CLN3 remains unknown [60, 86]. To date, CLN3 has been implicated in multiple processes critical for maintaining cellular homeostasis as well as dampening microglial proinflammatory activity [86, 89-92, 123]. Earlier studies have focused on the accumulation of lysosomal storage material within neurons, a hallmark of disease pathology and progression [60, 71, 72]. However, there is little evidence directly implicating lysosomal inclusions as the cause of neuronal death [54, 67]. For this reason, we chose to investigate other pathways that could contribute to neurodegeneration that is a hallmark of CLN3 disease.

One such pathway is glutamate regulation, which has been implicated as one mode of neurotoxicity in JNCL. However little is known about the mechanisms contributing to aberrant glutamate regulation in JNCL or the role of astrocytes in this process. It is likely that astrocyte activity influences neuronal survival in JNCL based on previous studies reporting that activated astrocytes coincide with brain regions where neurons are eventually lost in CLN3 mouse models [32, 33]. Likewise, it has been shown that increased astrocyte hemichannel activity and reduced expression of the glutamate transporter GLAST and glutamine synthetase are apparent in the $Cln3^{\Delta ex7/8}$ brain, which supports the concept of disrupted astrocyte glutamate regulation and homeostatic functions in JNCL [159]. Here we present a potential mechanistic model to account for increased extracellular glutamate in the JNCL brain, primarily centered on astrocyte-neuron crosstalk because intrinsic astrocyte glutamate pathways are not dramatically affected (Figure 7).

**Figure 3. 7**

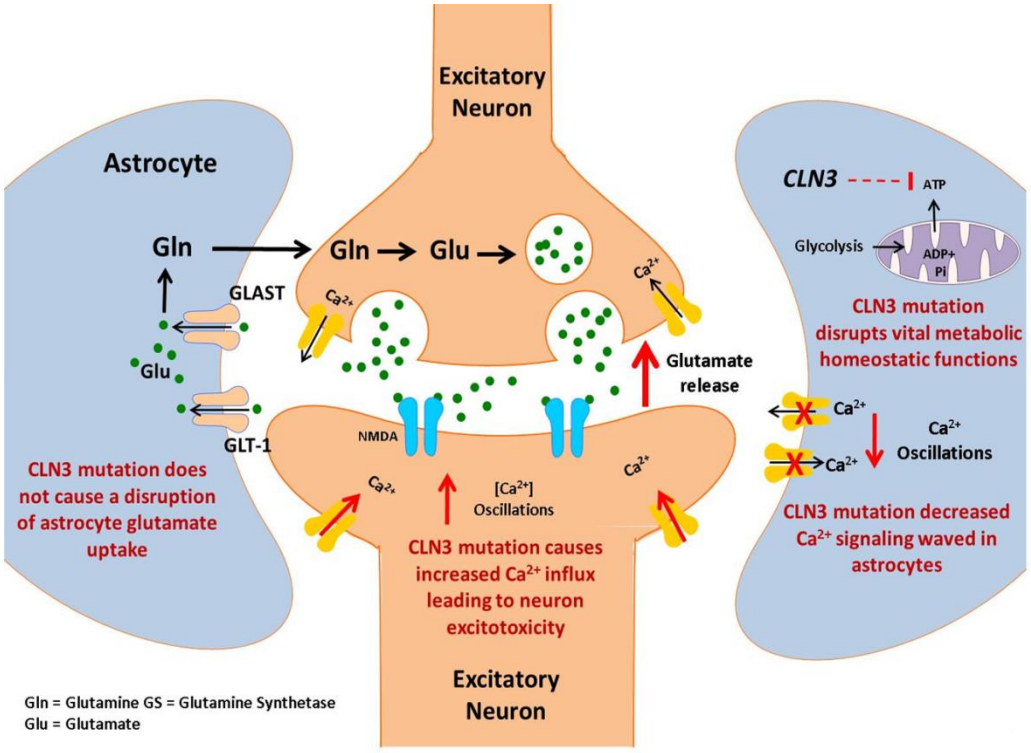


**Proposed mechanism for aberrant astrocyte-neuron crosstalk during CLN3 disease.** Glutamate uptake by astrocytes is an energy-demanding process and ATP production was significantly decreased in $Cln3^{\Delta ex7/8}$ astrocytes, which coincided with impaired $Ca^{2+}$ signaling. $Cln3^{\Delta ex7/8}$ neurons were hyper-sensitive to physiological concentrations of glutamate, which elicited heightened and prolonged $Ca^{2+}$ signals that with time may contribute to neuronal dysfunction and/or death. Gln, glutamine; Glu, glutamate; GLAST, *glutamate*-aspartate transporter; GLT-1, glutamate transporter 1.

An interesting attribute of CLN3 disease that distinguishes it from other forms of Batten is the protracted nature of disease progression (occurs over a period of 10-15 years) and the fact that disease symptoms do not typically manifest until around 5-10 years of age [164, 271]. This suggests the existence of compensatory mechanisms to maintain CNS homeostasis until a disease threshold is achieved. Although the mechanisms responsible for this prolonged disease course are unknown, one possibility may be progressive glutamate accumulation that initially leads to excessive neuronal activity and ultimately cell death. This is also an attractive possibility from a clinical perspective, since seizures are often an early hallmark of CLN3 disease, which may be attributed to glutamate hyperactivity, followed by neuronal death that could be due to glutamate excitotoxicity [239, 272, 273]. We found that $Cln3^{\Delta ex7/8}$ neurons were hyper-reactive in response to physiological glutamate concentrations at the synaptic cleft [268-270]. By extension, not only do $Cln3^{\Delta ex7/8}$ neurons require less glutamate to be activated, but increased activation would augment glutamate release, perpetuating the pathological circuit. $Cln3^{\Delta ex7/8}$ neurons also maintained higher levels of intracellular $Ca^{2+}$ following glutamate exposure, indicative of a longer activation state [274]. In addition, whereas intracellular $Ca^{2+}$ levels in WT neurons returned to baseline within 1 min of stimulation, $Cln3^{\Delta ex7/8}$ neurons maintained exaggerated intracellular $Ca^{2+}$ levels, which has been shown to precede excitotoxicity [248, 249]. It was recently reported that neuronal activity was exaggerated in the $Cln3^{\Delta ex7/8}$ hippocampus and cortex using electrophysiological recordings of acute brain slices, supporting the heightened neuronal responses presented here [158].

Glutamate regulation is critical for maintaining optimal neuron-astrocyte signaling networks [137, 244]. This is an extremely energy-demanding process, requiring a constant supply of ATP that becomes even more pronounced during times of heightened

neuronal activity [239], as suggested by our findings of hyper-reactive $Cln3^{\Delta ex7/8}$ neurons. Previous reports have described several mitochondrial abnormalities in CLN3 cells, including morphological changes, increased oxidative stress molecules, and elevated membrane potentials [89, 91, 256-258]. However, most of these studies have been performed using immortalized cell lines and none have assessed mitochondrial function in astrocytes. Using Seahorse metabolic assays, mitochondrial basal respiration and ATP production were significantly lower in $Cln3^{\Delta ex7/8}$ astrocytes, even at the resting state. Mitochondrial function was also impaired when $Cln3^{\Delta ex7/8}$ astrocytes were exposed to JNCL-relevant stimuli. Importantly, these changes were independent of mitochondrial numbers, since $Cln3^{\Delta ex7/8}$ astrocytes harbored significantly more mitochondria on a per cell basis. This likely results from disruptions in autophagy and lysosomal degradation mechanisms that have been described in CLN3 disease [89, 231]. This is the first report to demonstrate disruptions in astrocyte mitochondrial function in the context of CLN3 mutation.

Astrocytes utilize $Ca^{2+}$ signaling to communicate with surrounding astrocytes and neurons, sense extracellular cues, and regulate synaptic activity [243-245, 275]. Here we show that $Cln3^{\Delta ex7/8}$ astrocytes have lower spontaneous $Ca^{2+}$ oscillations under resting conditions and following exposure to danger signals/proinflammatory cytokines. $Ca^{2+}$ transients were also significantly reduced in $Cln3^{\Delta ex7/8}$ astrocytes in response to extracellular glutamate. By extension, if $Cln3^{\Delta ex7/8}$ astrocytes are less responsive to extracellular signals and are unable to properly regulate synaptic activity, $Cln3^{\Delta ex7/8}$ neurons will continue to fire and release more glutamate, resulting in the pathological propagation of a dysfunctional glutamate circuit in CLN3 disease.

In summary, our study supports the following model to account for neuronal hyper-excitability in the context of CLN3 mutation (Figure 7). First, CLN3 loss leads to cell autonomous changes in neurons, resulting in hyper-sensitivity to low glutamate

concentrations. Excessive excitatory activity in $Cln3^{\Delta ex7/8}$ neurons triggers heightened glutamate release into the synaptic cleft and the surrounding extracellular milieu. Persistent elevations in extracellular glutamate are known to further induce pre-existing neuroinflammatory pathways that trigger the release of cytotoxic mediators, inhibit cellular homeostatic functions, and induce apoptosis [276-278]. Mitochondrial basal respiration, ATP production, and spontaneous $Ca^{2+}$ oscillations were significantly reduced in $Cln3^{\Delta ex7/8}$ astrocytes, which can have a major impact on cell signaling and synaptic activity. Without proper astrocytic regulation, synaptic firing can escalate in $Cln3^{\Delta ex7/8}$ neurons, which augments glutamate release and perpetuates the pathological cycle. Ultimately, this could be one mechanism to account for eventual neuronal loss associated with CLN3 disease.

## Chapter 4: Efficacy of phosphodiesterase-4 inhibitors in juvenile Batten disease (CLN3)

Published in Annals of Neurology 80(6):909-923, 2016

**ABSTRACT**

Juvenile Neuronal Ceroid Lipofuscinosis (JNCL), or juvenile Batten disease, is a pediatric lysosomal storage disease caused by autosomal recessive mutations in *CLN3*, typified by blindness, seizures, progressive cognitive and motor decline, and premature death. Currently, there is no treatment for JNCL that slows disease progression, which highlights the need to explore novel strategies to extend the survival and quality-of-life of afflicted children. Cyclic AMP (cAMP) is a second messenger with pleiotropic effects, including regulating neuroinflammation and neuronal survival. Here we investigated whether three phosphodiesterase-4 (PDE4) inhibitors (rolipram, roflumilast, and PF-06266047) could mitigate behavioral deficits and cell-specific pathology in the $Cln3^{\Delta ex7/8}$ mouse model of JNCL. In a randomized, blinded study, wild type (WT) and $Cln3^{\Delta ex7/8}$ mice received PDE4 inhibitors daily beginning at 1 or 3 months of age and continuing for 6-9 months, with motor deficits assessed by accelerating rotarod testing. The effect of PDE4 inhibitors on cAMP levels, astrocyte and microglial activation (GFAP and CD68, respectively), lysosomal pathology (LAMP-1), and astrocyte glutamate transporter expression (GLAST) were also examined in WT and $Cln3^{\Delta ex7/8}$ animals. cAMP levels were significantly reduced in the $Cln3^{\Delta ex7/8}$ brain, which were restored by PF-06266047. PDE4 inhibitors significantly improved motor function in $Cln3^{\Delta ex7/8}$ mice, attenuated glial activation and lysosomal pathology, and restored glutamate transporter expression to levels observed in WT animals with no evidence of toxicity as revealed by blood chemistry analysis. These studies reveal neuroprotective effects for PDE4 inhibitors in $Cln3^{\Delta ex7/8}$ mice and support their therapeutic potential in JNCL patients.

## INTRODUCTION

Juvenile Neuronal Ceroid Lipofuscinosis (JNCL or CLN3 disease) is an autosomal recessive lysosomal storage disease resulting from *CLN3* mutations, with an estimated incidence of 1 in 100,000 live births [60, 233]. Children with JNCL appear healthy at birth, with progressive vision loss typically being the first sign of disease that presents around 4-7 years of age. Later, affected children develop motor dysfunction that manifests as Parkinson-like symptoms, along with seizures and cognitive deterioration, with a life expectancy of late teens to 20s [62]. MRI findings include cortical and cerebellar atrophy with abnormally high signal intensity in the white matter, reflecting moderate demyelination [279, 280]. The protracted nature of the disease coupled with the current lack of effective therapeutics, highlights the need to identify novel approaches to improve the longevity and quality-of-life for these patients.

In JNCL mouse models, reactive glia are apparent within 1-3 months of age and coincide with areas of eventual neuron loss, which is significantly delayed in comparison (i.e. 12-18 months) [33, 227]. Current evidence supports non-cell autonomous influences of diseased glia in JNCL pathogenesis in addition to intrinsic neuronal deficits. For example, $Cln3^{\Delta ex7/8}$ microglia are primed to produce exaggerated levels of several inflammatory mediators in response to danger signals encountered in the JNCL brain [123]. Likewise, molecules critical for astrocyte glutamate regulation are dramatically reduced in $Cln3^{\Delta ex7/8}$ mice, including GLAST and glutamine synthetase [227]. These findings support the neurotransmitter imbalance described in CLN3 mouse models, namely excessive glutamate and reduced GABA, which has been implicated in neurotoxicity [104, 236, 281].

Cyclic AMP (cAMP) is a second messenger that can regulate a variety of signaling events involved in learning and memory and synaptic plasticity [182, 183]. Reductions in cAMP can have broad effects, ranging from a generalized negative impact on neuronal

homeostasis, promotion of microglial proinflammatory activity, and reduced glutamate transporter expression in astrocytes [282-284]. cAMP levels are regulated by a balance between synthesis and degradation, mediated by adenylyl cyclase and phosphodiesterases (PDEs), respectively. There are a total of 11 PDE enzyme families, with PDE4 most prominently expressed in the CNS [285]. PDE4 inhibitors have shown beneficial effects in a wide range of neurodegenerative disorders, by limiting neuronal apoptosis and neuroinflammation as well as augmenting glutamate transporter expression [185, 186, 282, 286]. Based on our previous findings demonstrating reductions in GLAST expression in $Cln3^{\Delta ex7/8}$ astrocytes [227], exaggerated proinflammatory mediator production in $Cln3^{\Delta ex7/8}$ microglia [123], and intrinsic neuron pathology as shown by other groups [33, 91], we surmised that PDE4 inhibitors would represent an excellent means to target this triad of cellular dysfunction.

Here we show that cAMP levels are significantly reduced in several brain regions of $Cln3^{\Delta ex7/8}$ mice where neuropathology occurs. Treatment of $Cln3^{\Delta ex7/8}$ animals with three distinct PDE4 inhibitors (rolipram, roflumilast, or PF-06266047) significantly improved motor function over a 6 month period. PDE4 inhibitors also reduced glial activation and lysosomal pathology as well as restored impaired glutamate transporter expression in $Cln3^{\Delta ex7/8}$ mice to WT levels. Importantly, the beneficial effects of PDE4 inhibitors were still observed when treatment was delayed until 3 months of age, suggesting that they are capable of improving more advanced disease. This is the first study demonstrating that PDE4 inhibitors are effective at reducing motor deficits and pathological attributes of JNCL, supporting their potential therapeutic utility.

## RESULTS

**Brain cAMP levels are significantly reduced in Cln3$^{\Delta ex7/8}$ mice.** Reductions in cAMP-mediated signaling have been shown to impact neurobehavioral and cognitive function in normal aging, as well as in neurodegenerative diseases [182, 183]. In addition, decreased cAMP levels are associated with proinflammatory responses and reductions in glutamate transporter expression [282, 283], which agrees with our prior findings of increased inflammatory mediator production by Cln3$^{\Delta ex7/8}$ microglia and decreased GLAST expression in the Cln3$^{\Delta ex7/8}$ brain[123, 227]. To determine whether these changes may be linked to alterations in cAMP, cAMP levels were quantitated by ELISA in brain regions where neuropathology occurs in Cln3$^{\Delta ex7/8}$ mice [33]. cAMP was significantly reduced in the thalamus (TH) of Cln3$^{\Delta ex7/8}$ mice at 7 months, whereas the hippocampus (HPC) and visual cortex (VC) showed a similar trend but did not reach statistical significance (Fig 1, upper panel). At 12 months, significant reductions in cAMP were observed in the TH, HPC, and VC of Cln3$^{\Delta ex7/8}$ mice compared to WT animals (Fig 1, lower panel). Immunofluorescence staining for cAMP confirmed the reductions in 7 month-old mice (data not shown). cAMP levels were similar in the somatosensory barrel field cortex (S1BF) of WT and Cln3$^{\Delta ex7/8}$ mice at both ages examined (Fig 1), emphasizing the region-specific neuropathology that is observed in JNCL.

**Figure 4.1**

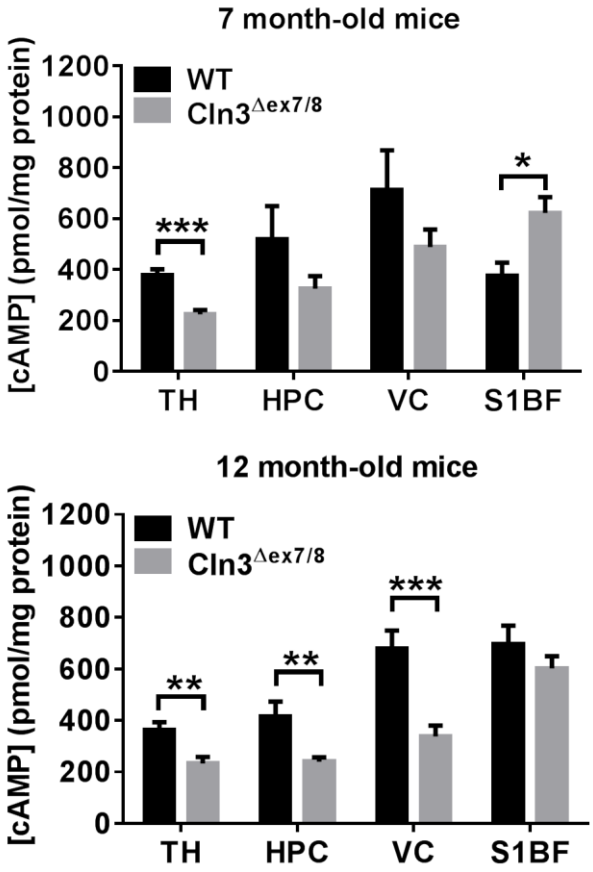


**cAMP levels are decreased in vulnerable brain regions of Cln3$^{\Delta ex7/8}$ mice.** Cln3$^{\Delta ex7/8}$ and WT mice (n=5-10/group) were sacrificed at 7 (top panel) or 12 months of age (bottom panel), whereupon cAMP levels were quantified in the thalamus (TH), hippocampus (HPC), visual cortex (VC), and somatosensory barrel field cortex (S1BF) by ELISA and normalized to total protein to account for differences in tissue size. Results are combined from 2 independent experiments and significant differences between WT and Cln3$^{\Delta ex7/8}$ mice are denoted by asterisks (*, $p < 0.05$).

**PDE4 inhibitors reverse motor deficits in Cln3$^{\Delta ex7/8}$ mice.** As previously mentioned, PDE4 inhibitors improve cognitive and motor function in various acute and chronic neurodegenerative diseases, including traumatic brain injury, spinal cord injury, Alzheimer disease, and Parkinson disease [185, 186, 190, 286-288]. In our hands, Cln3$^{\Delta ex7/8}$ mice display significant impairments in motor function, as evident by reduced latency to fall on the accelerating rotarod (Fig 2) [289], which has been attributed, in part, to excessive glutamatergic input [104, 263, 290, 291]. We utilized this rotarod deficit to determine whether three distinct PDE4 inhibitors, including an early generation (rolipram) [292], second generation (roflumilast) [221], and third generation (PF-06266047) inhibitor could improve motor function in Cln3$^{\Delta ex7/8}$ mice over a 6 month treatment period. Administration of each PDE4 inhibitor was initiated in WT and Cln3$^{\Delta ex7/8}$ mice at 1 month of age and motor activity was assessed by repeat testing at monthly intervals throughout the study.

We began our analysis with the first generation PDE4 inhibitor rolipram as proof-of-principle, since the compound has demonstrated beneficial effects in a wide range of neurological disorders but was halted from further clinical development because of its adverse side effects [185, 186, 190, 286-288]. Rolipram exhibited a dose-dependent effect on motor behavior in Cln3$^{\Delta ex7/8}$ mice, where the highest concentration examined (5 mg/kg/day) significantly improved motor function within the first month of treatment, which extended out to 4 months (Fig 2A). This benefit was negated with a lower drug concentration (0.5 mg/kg/day). Interestingly, WT mice receiving 5 mg/kg/day rolipram displayed increased rotarod performance as compared to vehicle treated WT animals at 2-6 months (Fig 2A). A recent study demonstrated that long-term rolipram treatment in WT mice enhanced mGluR-mediated long-term depression (LTD) [293], which could account for our findings in WT animals although this remains speculative. As mentioned

above, rolipram was not used for subsequent mechanistic studies in the Cln3$^{\Delta ex7/8}$ model, since it is not a clinically viable agent because of its adverse side effects.

Roflumilast (Daliresp$^{TM}$) is an FDA approved PDE4 inhibitor used to reduce the risk of exacerbations in patients with chronic obstructive pulmonary disease (COPD) [222]. Since roflumilast is FDA approved, this offered the possibility of repurposing the compound for JNCL, should efficacy be demonstrated. Cln3$^{\Delta ex7/8}$ mice were treated with three different concentrations of roflumilast (2.5, 5, and 10 mg/kg) via daily oral gavage, with effects on motor function evaluated at monthly intervals. Only the highest doses of roflumilast tested (5 and 10 mg/kg/day) led to significant improvements in rotarod activity, whereas the lower concentration (2.5 mg/kg/day) was not effective (Fig 2B and data not shown). The group of WT and Cln3$^{\Delta ex7/8}$ vehicle treated mice used to assess 5 mg/kg/day roflumilast did not differ from each other dramatically in accelerating rotarod performance, which was unusual (Fig 2B). Nevertheless, treatment of Cln3$^{\Delta ex7/8}$ animals with 5 mg/kg/day roflumilast did significantly improve motor performance compared to vehicle treated Cln3$^{\Delta ex7/8}$ mice. Compared to rolipram, the beneficial effects of roflumilast on motor activity were not observed until 3 months of treatment, which may be explained by the lower blood-brain barrier permeability of roflumilast [221, 222].

The final compound examined was a third generation PDE4 inhibitor PF-06266047 (Patent Number, US 20140235612). A Phase 1 clinical trial has recently been completed to assess the safety and tolerability of PF-06266047 in healthy human subjects (ClinicalTrials.gov Identifier: NCT02539550). Unlike roflumilast, PF-06266047 has superior blood-brain barrier permeability and better rodent PK, which translated into lower dosages for our *in vivo* studies. Cln3$^{\Delta ex7/8}$ and WT mice received 0.5 or 1 mg/kg of PF-06266047 via daily oral gavage beginning at 1 month of age, with monthly rotarod assessments performed. Cln3$^{\Delta ex7/8}$ mice treated with the lowest dose of PF-06266047 (0.5 mg/kg/day) displayed significant improvements in rotarod activity as early as one

month post-treatment, which was not observed with the higher dose (Fig 2C and data not shown). One possible explanation for this dosage-dependent effect is that the PK profile of PF-06266047 indicated that therapeutic levels would be maintained for ~24 h at the 1 mg/kg dose. Reducing the dose by a factor of 2 would inhibit enzyme activity for approximately 12 h, which was considered more desirable to allow for some PDE4 activity that is likely needed to maintain homeostatic functions. Therefore, we interpreted the inability of the higher dose to provide benefit because it completely prevented PDE4 action throughout a 24 h period. Based on this, PF-06266047 was examined at 0.5 mg/kg/day for all subsequent studies. We also demonstrated that this dose of PF-06266047 restored cAMP in the TH, VC, and HPC of $Cln3^{\Delta ex7/8}$ mice to levels seen in WT animals (Fig 3).

**Figure 4.2**

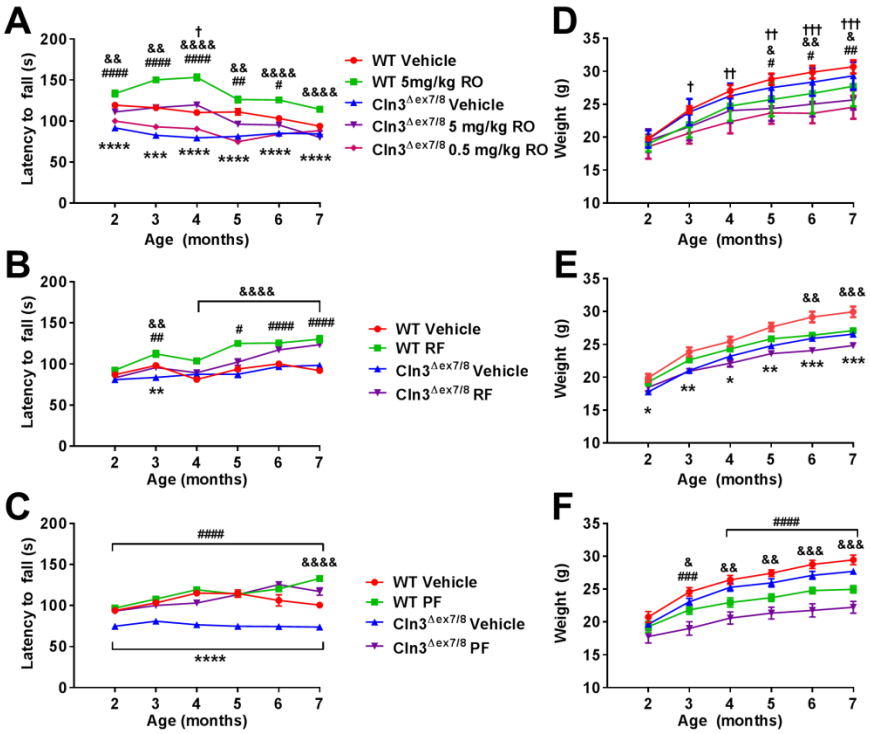


**PDE4 inhibitors improve motor function in Cln3$^{\Delta ex7/8}$ mice.** Cln3$^{\Delta ex7/8}$ and WT mice (n=8/group) received vehicle or (A and D) rolipram (RO; 0.5 or 5 mg/kg), (B and E) roflumilast (RF; 5 mg/kg), or (C and F) PF-06266047 (PF; 0.5 mg/kg) beginning at 1 month of age, after which motor activity was assessed by accelerating rotarod testing at monthly intervals. Across all comparisons, significant differences between vehicle treated WT and Cln3$^{\Delta ex7/8}$ animals are denoted by asterisks (*). (A) Significant differences between Cln3$^{\Delta ex7/8}$ vehicle treated vs. Cln3$^{\Delta ex7/8}$ 5 mg/kg/day rolipram are indicated by #, Cln3$^{\Delta ex7/8}$ vehicle treated vs. Cln3$^{\Delta ex7/8}$ 0.5 mg/kg/day rolipram are denoted by †, and WT vehicle vs. WT 5 mg/kg/day rolipram are indicated by &. (B) Cln3$^{\Delta ex7/8}$ vehicle vs. Cln3$^{\Delta ex7/8}$ roflumilast treated mice are indicated by #, and WT vehicle vs. WT roflumilast are indicated by &. (C) Cln3$^{\Delta ex7/8}$ vehicle vs. Cln3$^{\Delta ex7/8}$ PF-06266047 treated mice are indicated by #, and WT vehicle vs. WT PF-06266047 treated mice are indicated by &. (D-F) Weights of Cln3$^{\Delta ex7/8}$ and WT mice during PDE4 inhibitor treatment. (D) Significant differences between Cln3$^{\Delta ex7/8}$ vehicle treated vs. Cln3$^{\Delta ex7/8}$ 5 mg/kg/day rolipram are indicated by #, Cln3$^{\Delta ex7/8}$ vehicle treated vs. Cln3$^{\Delta ex7/8}$ 0.5 mg/kg/day rolipram are denoted by †, and WT vehicle vs. WT 5mg/kg/day rolipram are indicated by &. (E) Significant differences between WT vehicle and WT roflumilast are indicated by &. (F) Significant differences between Cln3$^{\Delta ex7/8}$ vehicle vs. Cln3$^{\Delta ex7/8}$ PF-06266047 treated mice are indicated by #, and WT vehicle vs. WT PF-06266047 treated mice are indicated by &. For all comparisons, *, #, &, † reflect $p < 0.05$; **, ##, &&, †† denote $p < 0.01$; ***, ###, &&&, ††† reflect $p < 0.001$; and ****, ####, &&&& represent $p < 0.0001$.

**Figure 4.3**

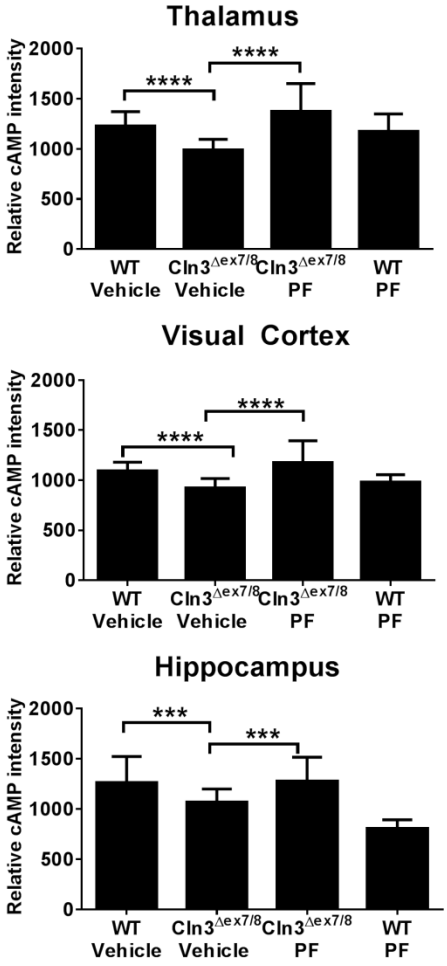


**PF-06266047 restores cAMP levels in Cln3$^{\Delta ex7/8}$ mice.** Cln3$^{\Delta ex7/8}$ and WT mice received PF-06266047 (PF; 0.5 mg/kg) or vehicle via daily oral gavage beginning at 1 month of age, whereupon animals were sacrificed 6 months later for cAMP quantitation by immunofluorescence staining in the thalamus (TH), visual cortex (VC), and hippocampus (HPC) (n=5/group). Significant differences between groups are denoted by asterisks (***, $p < 0.001$; ****, $p < 0.0001$).

To the best of our knowledge, chronic PDE4 inhibitor administration has not been examined in any juvenile species. When considering the possible utility of PDE4 inhibitors in JNCL patients, safety/toxicity assessments are needed. To this end, weekly weight measurements and blood chemistry profiles (every 2-3 months) were conducted on WT and $Cln3^{\Delta ex7/8}$ mice receiving the various PDE4 inhibitors over the 6 month treatment period, with histopathology on multiple organs at the time of sacrifice. Both WT and $Cln3^{\Delta ex7/8}$ mice that received PDE4 inhibitors weighed less than their vehicle-treated counterparts; however, the rate of weight gain was similar between the groups (Fig 2D-F). Blood chemistry analysis did not reveal any significant abnormalities in liver, kidney, or pancreatic function throughout the 6 month treatment period (data not shown), indicating that the compounds do not induce overt toxicity when chronically administered to juvenile animals. In addition, histopathological assessments of numerous organs did not reveal any evidence of toxicity as assessed by a board-certified pathologist (SMC; data not shown).

**PDE4 inhibitors attenuate disease-associated pathology in $Cln3^{\Delta ex7/8}$ mice.**

Prior work from our laboratory and others has identified early microglial and astrocyte activation in $Cln3^{\Delta ex7/8}$ mice that precedes and predicts regions of eventual neuronal loss [33, 227]. Additionally, $Cln3^{\Delta ex7/8}$ astrocytes show reduced expression of the glutamate transporter GLAST and glutamine synthetase, indicating altered glutamate recycling capacity, which supports the neurotransmitter imbalance associated with JNCL [104, 227, 236, 281]. We have also reported that $Cln3^{\Delta ex7/8}$ microglia are primed towards a proinflammatory phenotype when exposed to danger signals present in the $Cln3^{\Delta ex7/8}$ brain [123]. Given these findings and prior reports documenting the utility of PDE4 inhibitors to dampen microglial proinflammatory activity and enhance glutamate transporter expression in astrocytes [283, 294], we examined whether PDE4 inhibitors

affected glial activation and glutamate transporter expression in $Cln3^{\Delta ex7/8}$ mice. We limited our analysis to roflumilast and PF-06266047 for these studies, since both agents demonstrated beneficial effects on motor function in $Cln3^{\Delta ex7/8}$ animals and are viable therapeutics to consider for use in JNCL patients (Fig 2B-C).

$Cln3^{\Delta ex7/8}$ and WT mice were sacrificed after the 6 month PDE4 inhibitor treatment period, whereupon effects on microglial and astrocyte activation were examined by immunofluorescence staining for CD68 and GFAP, respectively. CD68 reactivity was significantly elevated in the S1BF and TH of $Cln3^{\Delta ex7/8}$ animals, which was attenuated following roflumilast treatment (Fig 4A and B). PF-06266047 also led to significant reductions in microglial activation (Fig 4C and D). GFAP immunoreactivity was significantly enhanced in the S1BF and TH of $Cln3^{\Delta ex7/8}$ mice as compared to WT controls (Fig 5), in agreement with previous observations from us and others [33, 227]. Roflumilast significantly reduced GFAP immunoreactivity in both brain regions of $Cln3^{\Delta ex7/8}$ mice (Fig 5A and B). Similar findings were obtained with PF-06266047, which significantly attenuated GFAP levels in the S1BF and TH of $Cln3^{\Delta ex7/8}$ animals (Fig 5C and D). Importantly, neither roflumilast nor PF-06266047 altered CD68 or GFAP expression in WT mice, supporting specific disease-modifying effects.

**Figure 4.4**

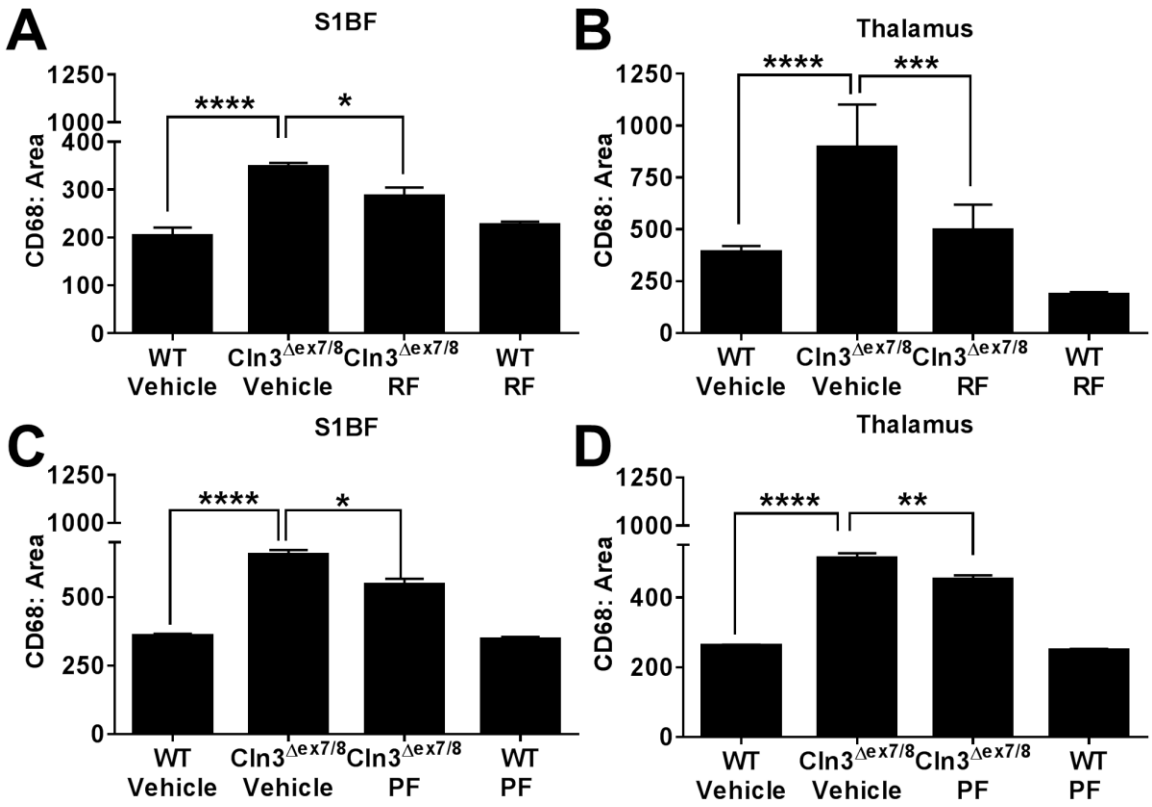


**PDE4 inhibitors attenuate microglial activation in Cln3$^{\Delta ex7/8}$ mice.** Cln3$^{\Delta ex7/8}$ and WT mice (n=4-8/group) received vehicle, 5 mg/kg roflumilast (RF; A and B), or 0.5 mg/kg PF-06266047 (PF; C and D) via daily oral gavage beginning at 1 month of age, whereupon animals were sacrificed 6 months later for quantitative assessments of microglial activation in the somatosensory barrel field cortex (S1BF) and thalamus by immunofluorescence staining for CD68. Significant differences between groups are denoted by asterisks (*, $p < 0.05$; **, $p < 0.01$; ***, $p < 0.001$; ****, $p < 0.0001$).

**Figure 4.5**

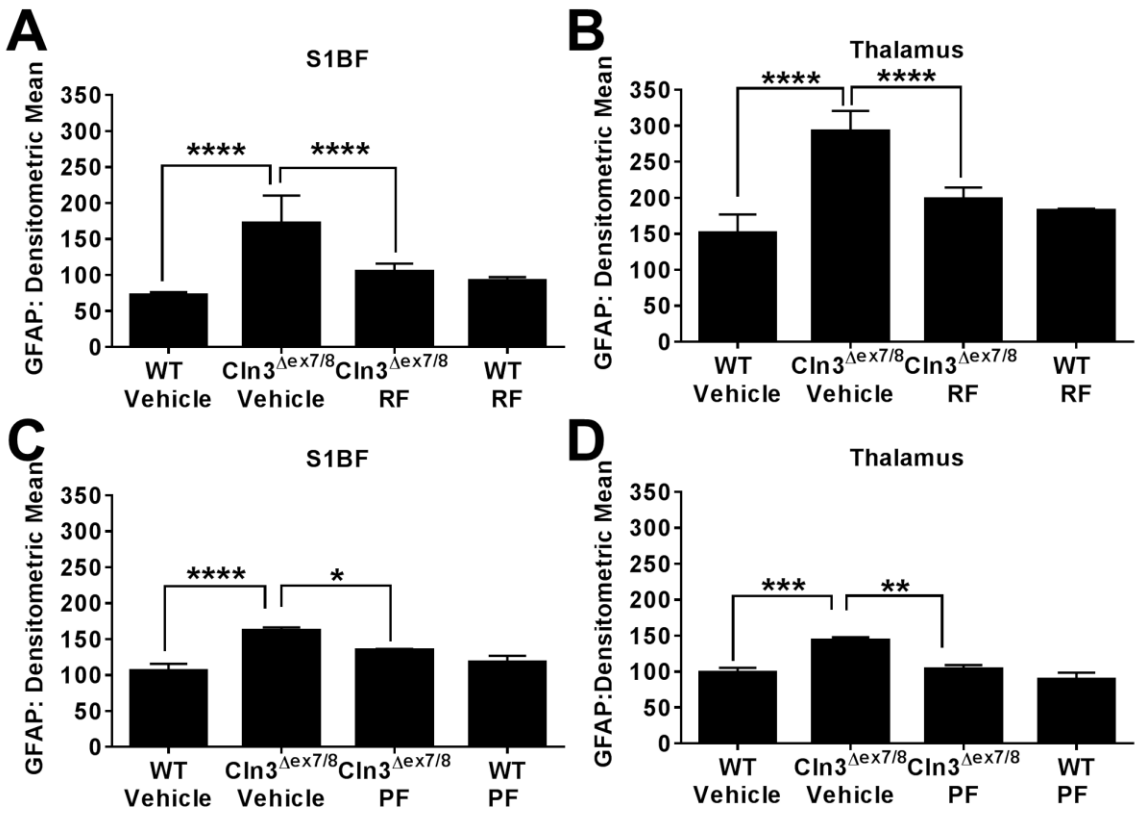


**PDE4 inhibitors reduce astrocyte activation in Cln3$^{\Delta ex7/8}$ mice.** Cln3$^{\Delta ex7/8}$ and WT mice (n=4-8/group) received vehicle, 5 mg/kg roflumilast (RF; A and B), or 0.5 mg/kg PF-06266047 (PF; C and D) via daily oral gavage beginning at 1 month of age, whereupon animals were sacrificed 6 months later for quantitative assessments of astrocyte activation in the somatosensory barrel field cortex (S1BF) and thalamus by immunofluorescence staining for GFAP. Significant differences between groups are denoted by asterisks (*, $p < 0.05$; **, $p < 0.01$; ***, $p < 0.001$; ****, $p < 0.0001$).

JNCL is characterized by progressive lysosomal dysfunction, which is most pronounced in neurons [71, 72]. LAMP-1 is widely used as a readout of lysosomal pathology and is often considered a more sensitive indicator compared to inclusion burdens [295, 296]. Therefore, we evaluated the effects of PDE4 inhibitors on lysosomal pathology by LAMP-1 immunostaining. As has been shown for other LSDs [295, 297, 298], LAMP-1 expression was increased in vehicle treated $CLN3^{\Delta ex7/8}$ mice compared to WT animals in the S1BF and TH (Fig 6). Similar to what was observed for glial activation, both roflumilast and PF-06266047 significantly reduced LAMP-1 levels (Fig 6A-B and C-D, respectively), reflecting reduced lysosomal pathology. Interestingly, neither roflumilast nor PF-06266047 had any effect on autofluorescent inclusions in either the brain or the retina (data not shown). This could be explained by the fact that drug treatment did not ensue until significant inclusion burdens had already developed at 1 month of age and although the observed reductions in LAMP-1 suggest improvements in lysosomal biology, this was not sufficient to clear established inclusion material. However, the contribution of inclusions to neuronal death remains uncertain, since many inclusion-positive neurons are not lost in the disease [54, 60, 67].

As previously mentioned, we recently reported significant reductions in the astrocytic glutamate transporter GLAST in 3 month-old $Cln3^{\Delta ex7/8}$ mice[227], which could represent one mechanism to account for excessive glutamate levels in JNCL that have been implicated in neuron excitotoxicity[104, 263, 290, 291]. This finding was extended in the current study, where significant reductions in GLAST expression were observed in the S1BF and TH of $Cln3^{\Delta ex7/8}$ mice at 7 months of age (Fig 7). Importantly, treatment of $Cln3^{\Delta ex7/8}$ animals with either roflumilast or PF-06266047 beginning at 1 month of age restored GLAST expression in both brain regions to similar levels seen in WT mice (Fig 7A-B and C-D, respectively). Recent studies attributed elevated glutamate levels to rotarod deficits in $Cln3^{\Delta ex7/8}$ mice [236, 290] and our results support a potential link

between increasing the expression of molecules critical for glutamate homeostasis with improvements in motor activity in $Cln3^{\Delta ex7/8}$ animals. Importantly, neither roflumilast nor PF-06266047 altered LAMP-1 or GLAST expression in WT mice, supporting specific disease-modifying effects. Collectively, these results demonstrate the ability of two distinct PDE4 inhibitors to reverse some pathological features of $Cln3^{\Delta ex7/8}$ mice, which when coupled with improvements in motor behavior suggest that these compounds may offer therapeutic benefit in JNCL patients.

**Figure 4.6**

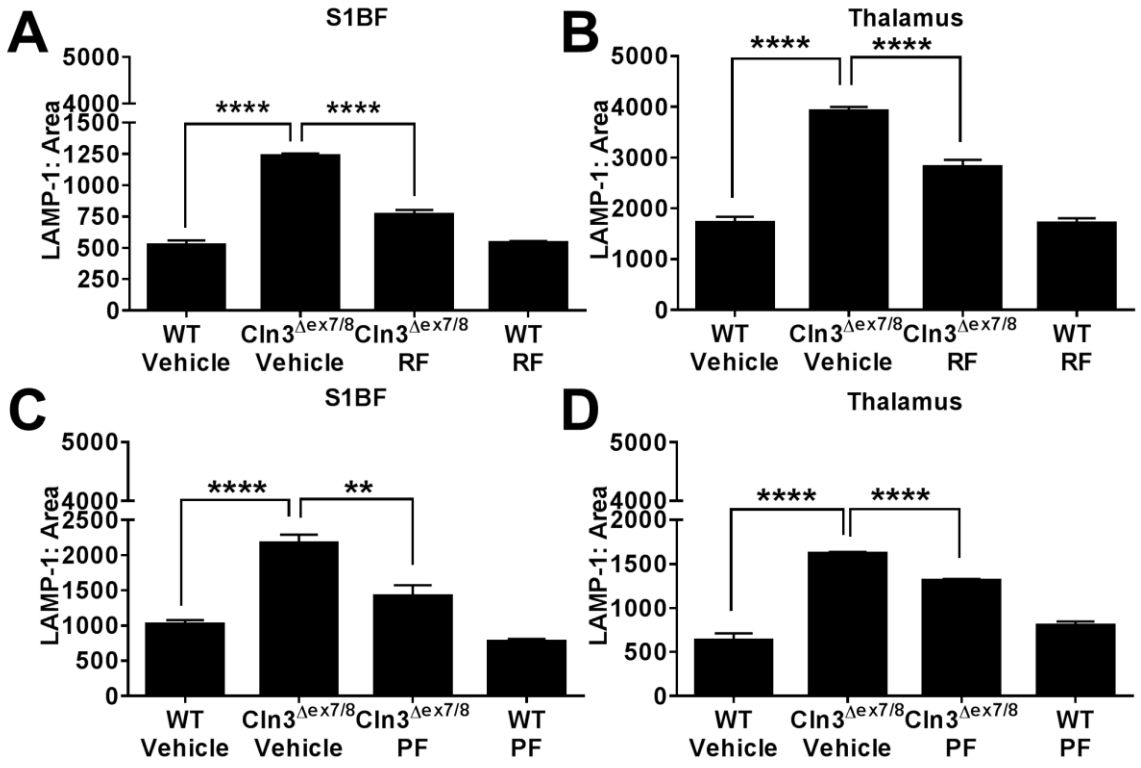


**PDE4 inhibitors attenuate lysosomal pathology in the Cln3$^{\Delta ex7/8}$ brain.** Cln3$^{\Delta ex7/8}$ and WT mice (n=4-8/group) received vehicle, 5 mg/kg roflumilast (RF; A and B), or 0.5 mg/kg PF-06266047 (PF; C and D) via daily oral gavage beginning at 1 month of age, whereupon animals were sacrificed 6 months later for quantitative assessments of LAMP-1 expression in the somatosensory barrel field cortex (S1BF) and thalamus. Significant differences between groups are denoted by asterisks (**, $p < 0.01$; ****, $p < 0.0001$).

**Figure 4.7**

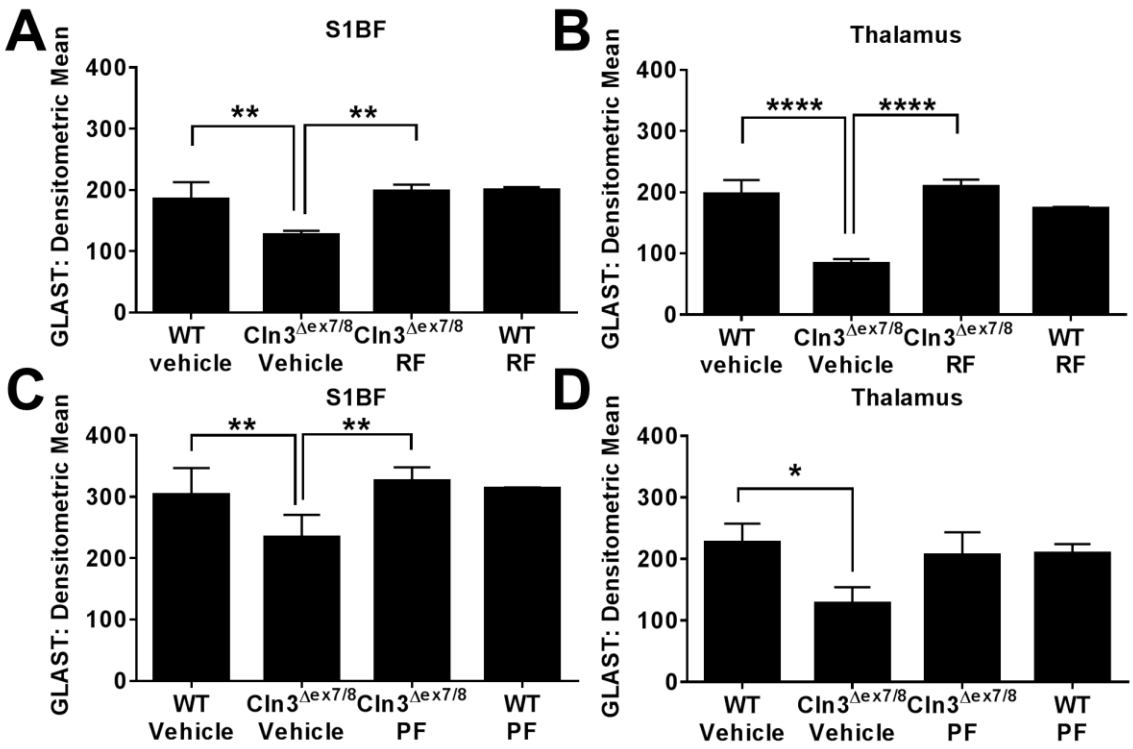


**PDE4 inhibitors restore the loss of astrocytic GLAST expression in Cln3$^{\Delta ex7/8}$ mice.** Cln3$^{\Delta ex7/8}$ and WT mice (n=4-8/group) received vehicle, 5 mg/kg roflumilast (RF; A and B), or 0.5 mg/kg PF-06266047 (PF; C and D) via daily oral gavage beginning at 1 month of age, whereupon animals were sacrificed 6 months later for quantitative assessments of GLAST expression in the somatosensory barrel field cortex (S1BF) and thalamus. Significant differences between groups are denoted by asterisks (*, $p < 0.05$; **, $p < 0.01$; ****, $p < 0.0001$).

**PDE4 inhibitors are capable of improving motor activity in Cln3$^{\Delta ex7/8}$ mice with advanced disease.** Although roflumilast and PF-06266047 were capable of improving motor activity and disease-associated features in Cln3$^{\Delta ex7/8}$ mice when treatment was initiated at 1 month of age, we next examined whether delayed administration would be efficacious. This is an important issue in terms of translational potential, since a JNCL diagnosis can often be delayed and patients would have already experienced increasing disease burden. To this end, we began PDE4 inhibitor treatment in 3 month-old animals, which display more advanced disease in terms of increased lysosomal pathology and motor deficits. Delayed treatment with both roflumilast (5 mg/kg/day) and PF-06266047 (0.5 mg/kg/day) significantly improved rotarod performance in Cln3$^{\Delta ex7/8}$ mice, with activity restored to near levels observed in WT animals (Fig 8A and B, respectively). Both WT and Cln3$^{\Delta ex7/8}$ mice receiving delayed PDE4 inhibitor treatment weighed less than their vehicle counterparts; however, weight gain occurred in all groups (Fig 8C and D). One interesting difference was observed with early vs. delayed roflumilast treatment of Cln3$^{\Delta ex7/8}$ mice, with 3 months treatment needed to demonstrate an effect when drug administration began at 1 month of age (Fig 3), whereas in animals with more advanced disease (i.e. 3 months) roflumilast improved motor function in Cln3$^{\Delta ex7/8}$ animals after only one month of treatment (Fig 8). The reason for this difference is not known; however, it could result from altered blood-brain barrier permeability with increasing disease burden at the time of treatment or PK differences in juvenile vs. adult animals. Collectively, these findings demonstrate the utility of PDE4 inhibitors to treat advanced disease, suggesting that they may offer therapeutic benefit to JNCL patients at later stages of the disease process.

**Figure 4.8**

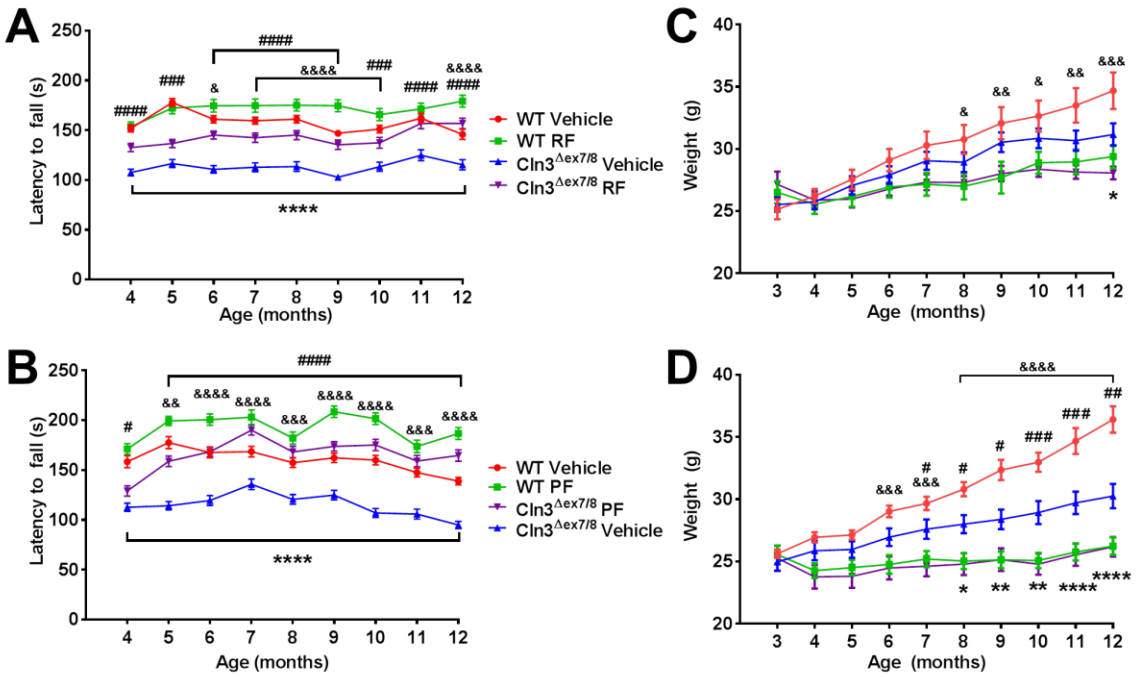


**Delayed treatment with PDE4 inhibitors improves motor function in Cln3$^{\Delta ex7/8}$ mice.** Cln3$^{\Delta ex7/8}$ and WT mice (n=8/group) received vehicle, 5 mg/kg roflumilast (RF; A and C) or 0.5 mg/kg PF-06266047 (PF; B and D) via daily oral gavage beginning at 3 months of age, after which motor activity was assessed by accelerating rotarod testing at monthly intervals. Across all comparisons, significant differences between vehicle treated WT and Cln3$^{\Delta ex7/8}$ animals are denoted by asterisks (*), Cln3$^{\Delta ex7/8}$ vehicle vs. Cln3$^{\Delta ex7/8}$ PDE4 inhibitor treated mice are indicated by hash signs (#), and WT vehicle vs. WT PDE4 inhibitor treated mice are indicated by ampersand signs (&). (C and D) Weights of Cln3$^{\Delta ex7/8}$ and WT mice receiving delayed PDE4 inhibitor treatment. Significant differences between Cln3$^{\Delta ex7/8}$ vehicle vs. Cln3$^{\Delta ex7/8}$ PDE4 inhibitor treated mice are indicated by #, and WT vehicle vs. WT PDE4 inhibitor treated mice are indicated by &. For all comparisons, *, #, & reflect $p < 0.05$; **, ##, && denote $p < 0.01$; ###, &&& reflect $p < 0.001$; and ****, ####, &&&& represent $p < 0.0001$.

**DISCUSSION**

Motor defects are a hallmark of JNCL [74], some of which are recapitulated in the $Cln3^{\Delta ex7/8}$ mouse model [289], as demonstrated by the rotarod deficits described in the current study. Prior reports using CLN3 knockout mice revealed heightened glutamate levels and reduced GABA in the cortex and cerebellum, and NMDA or AMPA receptor blockade could improve motor function in these animals, lending support to the excitotoxic theory of neuronal loss in JNCL [104, 236, 263]. Our recent work also supports this possibility, in that the expression of key molecules involved in glutamate clearance/detoxification from the synaptic cleft (GLAST and glutamine synthetase, respectively) were significantly reduced in the $Cln3^{\Delta ex7/8}$ brain [227]. In addition, we recently demonstrated transient hemichannel opening in $Cln3^{\Delta ex7/8}$ mice, which could exacerbate extracellular glutamate accumulation and promote excitotoxic neuronal death [227]. A second potential insult that may contribute to neuronal loss in JNCL is aberrant inflammatory activity that our laboratory has described in $Cln3^{\Delta ex7/8}$ microglia [123]. These potential non-cell autonomous effects of dysfunctional astrocytes and microglia in JNCL are expected to synergize with intrinsic neuronal defects to culminate in cell loss [299]. These changes led to our interest in investigating the utility of PDE4 inhibitors, since prior studies have shown their efficacy in attenuating microglial proinflammatory activity, augmenting astrocyte glutamate transporter expression, and delivering pro-survival signals to neurons [283, 284, 294]. Our findings support a key role for cAMP in dictating motor dysfunction, glial activation, and lysosomal pathology in the $Cln3^{\Delta ex7/8}$ brain, and support the feasibility of PDE4 inhibitors as potential therapeutics for the treatment of JNCL patients.

To our knowledge, this is the first report demonstrating significant cAMP reductions in the $Cln3^{\Delta ex7/8}$ brain *in vivo*. cAMP is a critical second messenger involved in regulating synaptic activity, glutamate homeostasis, and bioenergetic functions[183, 284]. cAMP

influences transcriptional events by binding to cAMP-responsive element binding protein (CREB), a ubiquitous transcription factor that controls the expression of a variety of genes, including synaptic proteins and glutamate receptors that are involved in glutamate release[284, 300]. Therefore, it is possible that generalized reductions in cAMP could affect downstream events responsible for optimal synaptic activity, behavior, and neuronal survival in JNCL. This was supported by our findings where three distinct PDE4 inhibitors (rolipram, roflumilast, and PF-06266047) were capable of restoring motor activity of $Cln3^{\Delta ex7/8}$ mice to performance levels near or equal to WT animals. Since prior work has implicated excessive glutamate stimulation as a major factor responsible for rotarod deficits in CLN3 knockout mice [236, 263] this suggests that PDE4 inhibitors may be modulating glutamatergic pathways. This was supported by our findings where chronic treatment of $Cln3^{\Delta ex7/8}$ animals with PDE4 inhibitors returned GLAST expression to levels observed in WT mice, which would be expected to help clear extracellular glutamate from the synapse and improve motor coordination. Importantly, both roflumilast and PF-06266047 were capable of improving motor activity in $Cln3^{\Delta ex7/8}$ mice when treatment was delayed until 3 months of age, revealing the ability of both compounds to benefit more advanced disease. With regard to roflumilast dosing, the group of WT and $Cln3^{\Delta ex7/8}$ vehicle treated mice used to assess 5 mg/kg/day roflumilast (Fig 2B) did not differ from each other dramatically in accelerating rotarod performance, which was unusual. Nevertheless, treatment of $Cln3^{\Delta ex7/8}$ animals with 5 mg/kg/day roflumilast did significantly improve motor performance compared to vehicle treated $Cln3^{\Delta ex7/8}$ mice and when considered in conjunction with its ability to attenuate microglial and astrocyte activation and lysosomal pathology, indicates that roflumilast exerts beneficial effects on CNS pathology at this dose. Increasing roflumilast to 10 mg/kg/day improved accelerating rotarod performance even further in $Cln3^{\Delta ex7/8}$ mice, which still reduced glial activation (data not shown); however, 10 mg/kg in mice is

nearing the maximal tolerated dose in humans of 500 µg/day [221, 222] and resulted in more weight loss in both WT and Cln3$^{\Delta ex7/8}$ animals compared to 5 mg/kg/day (data not shown). This suggests that the dose required to improve motor activity may fall slightly above that needed to attenuate glial activation and lysosomal pathology and would require regular clinical assessments of JNCL patients to identify the optimal dose to improve motor coordination while minimizing known side effects of the compound (i.e. nausea and weight loss). To date, roflumilast is only FDA approved for adult use; however, one report examined the PK properties of a single roflumilast dose in children and adolescents with stable mild to moderate asthma and found that the drug was well-tolerated with similar PK parameters to adults [301]. Chronic roflumilast dosing in children has not yet been performed but the authors speculated that this would be well-tolerated, which is supported by our findings where chronic dosing of juvenile animals was not associated with severe adverse events.

One interesting observation was that both roflumilast and PF-06266047 also increased motor performance in WT animals. The reason for this is not clear, but may be explained by compensation in cAMP signaling. For example, the neuronal network maintains an optimal range for cAMP signaling in the brain [302]. Therefore, chronic cAMP elevations in WT mice, which would occur with continued PDE4 inhibitor treatment, likely increased cAMP-mediated signaling above the optimal range. This could result in an altered set point and manifest as improved motor performance, which was observed in the current study. Although WT mice demonstrated improved accelerating rotarod activity with chronic PDE4 inhibitor administration this did not translate to changes in glial activation, glutamate transporter expression, or lysosome biology, which were identical between WT animals treated with vehicle or PDE4 inhibitors. In contrast, all three PDE4 inhibitors reduced disease-associated pathology in Cln3$^{\Delta ex7/8}$ mice across all of the neurological readouts examined in this study, which

suggests that they are disease-modifying rather than symptomatic treatment. From a therapeutic perspective, PDE4 inhibitors would not be used in healthy individuals, but the inclusion of WT animals in the current study design was for completeness and to evaluate the potential toxicity of PDE4 inhibitors in juvenile animals, which has not yet been examined over a prolonged (6 month) interval. This was an important issue to address, since treatment of JNCL patients would require chronic dosing to impact disease progression. To this end, we did not observe any significant differences in blood chemistry values or tissue histopathology after a 6 month dosing period, although animals receiving PDE4 inhibitors weighed less than vehicle controls, but still showed weight gain throughout the study.

Another feature of JNCL is neuronal loss, which is more limited in Cln3 mouse models compared to human disease [32, 33]. A prior publication reported thalamic neuron loss in $Cln3^{\Delta ex7/8}$ mice on a mixed 129Sv/Ev/CD1 background at 12 months [33]; however, this reduction was relatively modest and we have not observed any differences in neuron counts of Nissl stained sections in a 1 in 6 series using unbiased stereology between vehicle treated WT and $Cln3^{\Delta ex7/8}$ animals on a C57BL/6 background, which is known to harbor milder disease phenotypes. The fact that we could not demonstrate evidence of neuronal loss in $Cln3^{\Delta ex7/8}$ mice at this time point precluded our ability to assess the effects of PDE4 inhibitors on promoting neuronal survival. Therefore, our analysis has instead focused on other quantifiable pathological outcomes, including glial activation and lysosomal pathology. Nevertheless, at the conclusion of each dosing trial, brains were weighed and normalized to total body weight to account for weight loss resulting from chronic PDE4 inhibitor treatment. There were no significant changes in brain:body weight ratios between either vehicle treated WT and $Cln3^{\Delta ex7/8}$ mice or with any of the three PDE4 inhibitors tested, demonstrating that chronic PDE4 inhibitor dosing did not adversely affect neuron survival as measured by total brain weight.

In addition to augmenting glutamate transporter expression, it is also possible that the beneficial effects of PDE4 inhibitors in $Cln3^{\Delta ex7/8}$ mice may be mediated, in part, by dampening neuroinflammatory responses that are suggested to occur in JNCL [33, 123, 172, 227], since PDE4 inhibitors have been shown to reduce inflammation in other neurological conditions[17-19, 24-26]. The ability of PDE4 inhibitors to significantly reduce astrocyte and microglial activation in $Cln3^{\Delta ex7/8}$ mice supports this tenet. Neuroinflammation could be a risk factor in JNCL, since $Cln3^{\Delta ex7/8}$ microglia were shown to produce numerous proinflammatory cytokines (including TNF-α and IL-1β) when exposed to danger-associated molecular patterns (DAMPs) encountered during the disease process [123]. Another possibility is that $Cln3^{\Delta ex7/8}$ microglia could release DAMPs that induce reactive astrocytosis and impair glutamate homeostasis and other astrocyte functions[299]. Glial crosstalk could also occur via TNF-α and IL-1β production by $Cln3^{\Delta ex7/8}$ microglia that are known to induce astrocyte hemichannel opening[303], which we have also shown occurs in $Cln3^{\Delta ex7/8}$ mice and can lead to extracellular glutamate release [160, 227].

Although lysosomal inclusions form throughout the body in JNCL due to the ubiquitous expression of CLN3, the primary site of disease manifestation is within the CNS. However, cardiac dysfunction is also observed in children as the disease progresses [304], and it remains unknown what systemic effects PDE4 inhibitors may exert in this context. Of note, besides the CNS, PDE4 isoforms are expressed in the cardiovascular system, the reproductive organs, the gastrointestinal tract, and the immune system where PDE4 inhibition has been associated with anti-inflammatory effects [305]. Since inflammation has been linked to pathology in JNCL, it is likely that PDE4 inhibitors may dampen inflammation, which would be desirable in the CNS to limit deleterious inflammation in response to dying neurons and autoantibody formation that is characteristic of the disease [166, 306]. We did not examine potential systemic effects

of PDE4 inhibitors in the current report, since there are no peripheral biomarkers that have been identified in JNCL and the few systemic changes reported to be altered in $Cln3^{\Delta ex7/8}$ mice are modest in nature [102]. However, we did not observe any adverse effects on blood chemistry values throughout the 6 month duration of PDE4 inhibitor treatment in either $Cln3^{\Delta ex7/8}$ or WT animals. Importantly, clinical studies have not revealed any severe adverse effects of roflumilast on the cardiac, reproductive, or gastrointestinal systems [221, 222].

In summary, this study is the first to demonstrate the utility of PDE4 inhibitors to limit disease-associated attributes of JNCL. In particular, PDE4 inhibitors were found to improve motor function as well as mitigate astrocyte and microglial activation, reduce lysosomal pathology, and restore glutamate transporter expression in $Cln3^{\Delta ex7/8}$ mice. While the precise mechanisms whereby PDE4 inhibitors exert these beneficial effects are not known, targeting PDE4 represents a novel therapeutic strategy for JNCL patients.

## Chapter 5: Self-complementary AAV9 gene delivery partially corrects pathology associated with Juvenile Neuronal Ceroid Lipofuscinosis (CLN3)

Published Journal of Neuroscience 36(37):9669-82, 2016

**ABSTRACT**

Juvenile Neuronal Ceroid Lipofuscinosis (JNCL) is a fatal lysosomal storage disease caused by autosomal recessive mutations in *CLN3* for which no treatment exists. Symptoms appear between 5-10 years of age, beginning with blindness and seizures, followed by progressive cognitive and motor decline, and premature death (late teens-20s). We explored a gene delivery approach for JNCL by generating two self-complementary AAV9 (scAAV9) constructs to address CLN3 dosage effects using the methyl-CpG-binding protein 2 (MeCP2) and β-actin promoters to drive low vs. high transgene expression, respectively. This was based on the expectation that low CLN3 levels are required for cellular homeostasis due to minimal CLN3 expression postnatally, although this had not yet been demonstrated *in vivo*. One month-old $Cln3^{\Delta ex7/8}$ mice received one systemic (i.v.) injection of scAAV9/MeCP2-hCLN3 or scAAV9/β-actin-hCLN3, with GFP expressing viruses as controls. A promoter-dosage effect was observed in all brain regions examined, where hCLN3 levels were elevated 3- to 8-fold in $Cln3^{\Delta ex7/8}$ mice receiving scAAV9/β-actin-hCLN3 vs. scAAV9/MeCP2-hCLN3. However, a disconnect occurred between CLN3 levels and disease improvement, since only the scAAV9 construct driving low CLN3 expression (scAAV9/MeCP2-hCLN3) corrected motor deficits and attenuated microglial and astrocyte activation and lysosomal pathology. This may have resulted from preferential promoter usage, as transgene expression following i.v. scAAV9/MeCP2-GFP injection was primarily detected in $NeuN^+$ neurons, whereas scAAV9/β-actin-GFP drove transgene expression in $GFAP^+$ astrocytes. This is the first demonstration of a systemic delivery route to restore CLN3 *in vivo* using scAAV9 and highlights the importance of promoter selection for disease modification in juvenile animals.

## INTRODUCTION

Juvenile Neuronal Ceroid Lipofuscinosis (JNCL) is an autosomal recessive lysosomal storage disease (LSD) occurring in 1 per 100,000 live births [62]. JNCL is caused by mutations in *CLN3* that result in loss of protein expression [60]. *CLN3* encodes a transmembrane protein primarily localized to the lysosome [234]; however, its function remains unknown [86]. JNCL is characterized by lysosomal inclusions composed of mitochondrial ATP synthase subunit C and lipids [307]. Despite the fact that disease symptoms are primarily neurological, there is no clear indication that lysosomal inclusions are directly responsible for neuron loss. This is because although most neurons exhibit evidence of lysosomal storage, only certain neuron populations die [8, 71, 72, 88].

JNCL onset occurs between the ages of 5-10, presenting with rapid visual loss and seizures, progressive cognitive and motor decline [74], and premature death by the late teens-20s [232]. Neurodegeneration occurs in the cortex, cerebellum, and sub-regions of the hippocampus [77, 78]. Neuron loss has been reported in JNCL mouse models, but is relatively modest and not observed until late disease (i.e. 12-18 months), as opposed to early astrocyte and microglial activation (i.e. 1-3 months) [32, 159]. There is no cure for JNCL and current therapeutics only manage disease symptoms; therefore, we examined the feasibility of gene delivery to restore normal CLN3 function. Gene therapy has shown promise in other LSDs that involve mutations in soluble enzymes, in part, due to cross-correction of non-transduced cells [213, 308]. The therapeutic bar is higher for JNCL because CLN3 encodes a transmembrane protein, presumably requiring more transduced cells to produce a phenotypic effect [87].

Gene delivery via self-complementary adeno-associated virus 9 (scAAV9) has shown benefits in multiple neurodegenerative diseases including, spinal muscular atrophy and Rett syndrome [192-194]. AAV9 is an effective vector for CNS delivery

following systemic (i.v.) injection as it crosses the blood-brain barrier and transduces both neuronal and non-neuronal cells [204]. The scAAV9 genome is maintained as an episome in non-dividing cells, with studies reporting transgene expression for years [309, 310]. A prior study utilized a different AAV serotype (AAVrh.10/β-actin-hCLN3) in neonatal $Cln3^{\Delta ex7/8}$ mice, which required multiple intracranial injections and limited biodistribution [219]. In addition, $Cln3^{\Delta ex7/8}$ mice were treated at post-natal day 2, before disease-associated pathology manifested, and the identity of CNS transgene$^{+}$ cells or behavioral assessments were not performed [219]. Our approach advances the field by employing a systemic delivery route to enhance virus biodistribution and a unique promoter (methyl-CpG-binding protein 2; MeCP2), which preferentially drives transgene expression in neurons when administered to juvenile (i.e. 1 month-old) $Cln3^{\Delta ex7/8}$ mice, at time at which disease burden has already manifested.

Two scAAV9 constructs were generated to address CLN3 dosage effects *in vivo*; one driving low CLN3 expression with the MeCP2 promoter that showed efficacy in Rett syndrome [193], and a second driving high CLN3 levels via the chicken β-actin promoter. This approach was based on the expectation that low CLN3 levels are required for cellular homeostasis due to minimal postnatal CLN3 expression [216], although this had not yet been demonstrated *in vivo*. One month-old $Cln3^{\Delta ex7/8}$ mice received a single i.v. injection of scAAV9/β-actin-hCLN3 or scAAV9/MeCP2-hCLN3, with GFP expressing viruses as controls. Only the scAAV9 construct driving low CLN3 expression (scAAV9/MeCP2-hCLN3) was capable of reducing motor deficits, glial activation, and lysosomal pathology in the $Cln3^{\Delta ex7/8}$ brain, whereas scAAV9/β-actin-hCLN3 and GFP viruses had no benefit. Collectively, this is the first demonstration of a systemic delivery route to restore CLN3 using scAAV9 and highlights the importance of promoter selection for modifying disease.

## RESULTS

### Generation of scAAV9/CLN3 constructs to assess CLN3 gene dosage effects.

Unlike other NCL forms with deficiencies in soluble lysosomal enzymes, *CLN3* encodes a lysosomal transmembrane protein [60, 87, 234]. Therefore, although enzyme replacement therapy trials are currently underway to treat late-infantile neuronal ceroid lipofuscinosis (CLN2), where restoration of enzyme function in a larger number of cells is thought to occur by cross-correction, this is not feasible for JNCL. Another issue in the field was the expectation that low CLN3 expression is required for cellular homeostasis. This was based on earlier studies with CLN3-lacZ reporter mice, which revealed limited CLN3 expression postnatally, as well as *btn1* mutant yeast (CLN3 ortholog) where overexpression was toxic [95, 99, 216]. However, a gene dosage effect for CLN3 has not yet been directly tested *in vivo*. To address this question, we generated two scAAV9 constructs; one driving low CLN3 expression with the MeCP2 promoter and a second driving high CLN3 levels via the chicken β-actin promoter (Figure 1).

**Figure 5.1**


**Self-complimentary adeno-associated virus 9 constructs**. Each construct contains identical minimal SV40 intron (grey), human CLN3 cDNA (blue), bovine growth hormone polyadenylation signals (black) and viral inverted terminal repeats (red) to package self-complementary virus. The first construct (top) contains the high expressing chicken β-actin promoter (purple), while the second (bottom) contains the minimal essential promoter from the mouse MeCP2 gene (light blue).

**Systemic administration of scAAV9 successfully crosses the blood-brain barrier to transduce neurons and astrocytes in juvenile CLN3$^{\Delta ex7/8}$ mice.**

In these studies, one month-old Cln3$^{\Delta ex7/8}$ mice received a single i.v. injection of scAAV9/β-actin-hCLN3, scAAV9/MeCP2-hCLN3, or GFP constructs, with vehicle treated WT and Cln3$^{\Delta ex7/8}$ animals as controls. Virus administration was delayed to more accurately depict the age at which children are diagnosed with CLN3 disease (7-10 years old) based on mouse-human age equivalent estimates [225] and when disease burden had already manifested. Throughout the 5 month study period, mice were weighed weekly and serum chemistry panels were performed every other month to assess potential toxicity. No significant changes in weight gain or serum chemistry profiles were observed throughout the study nor was there any evidence of systemic inflammation as measured by the presence of serum cytokines/chemokines (data not shown). These findings demonstrate that the scAAV9 constructs did not induce toxicity or systemic inflammation, which is in agreement with prior reports using scAAV9 in both mice and non-human primates [193, 194, 311].

scAAV has a limited packaging capacity (i.e. 2.2 kb) [312], which required CLN3 and GFP to be placed in separate viral constructs. In addition, this approach allowed virus biodistribution to be identified by GFP without interfering with CLN3 protein translation and function that could occur if a CLN3-GFP fusion construct was used. To assess scAAV9 biodistribution after a single i.v. injection of CLN3$^{\Delta ex7/8}$ mice with scAAV9/β-actin-GFP or scAAV9/MeCP2-GFP, the percentage of GFP$^{+}$ cells and the specific cell types targeted was determined. Widespread GFP expression was observed with both the scAAV9/β-actin-GFP and scAAV9/MeCP2-GFP constructs, with GFP detected throughout the brain, spinal cord, and eye (Figures 2 and 3). Interestingly, the percentage of GFP$^{+}$ cells in several brain regions of Cln3$^{\Delta ex7/8}$ mice receiving

scAAV9/MeCP2-GFP was higher at 5 months post-injection compared to scAAV9/β-actin-GFP (Figure 2A). The scAAV9/MeCP2-GFP construct primarily drove GFP expression in $NeuN^+$ neurons (> 80% of $GFP^+$ cells) in the somatosensory barrel field cortex (S1BF), thalamus (TH), and visual cortex (VC) with some $GFAP^+$ astrocytes ($\leq$ 10% of $GFP^+$ cells) also observed (Figure 2B-C). In contrast, scAAV9/β-actin-GFP expression was more evident in astrocytes in the S1BF and VC (50-60% of $GFP^+$ cells) compared to the scAAV9/MeCP2-GFP construct, although a few $NeuN^+$ neurons ($\leq$ 16% of $GFP^+$ cells) were still detected with scAAV9/β-actin-GFP (Figure 2B-C). These regions were selected since they have been reported to display significant increases in early glial activation as well as reduced neuron counts at advanced stages of disease (12-18 months)[33, 159]. GFP expression was undetectable in microglia (data not shown), in agreement with previous reports showing that microglia are not permissive to AAV9-mediated transduction [204, 313]. We also found that primary microglia were recalcitrant to scAAV9 transduction *in vitro*, whereas primary astrocytes were receptive (data not shown), confirming our *in vivo* findings. Along with widespread transduction in the brain, both scAAV9/β-actin-GFP and scAAV9/MeCP2-GFP transduced the eye and spinal cord (Figure 3).

**Figure 5.2**

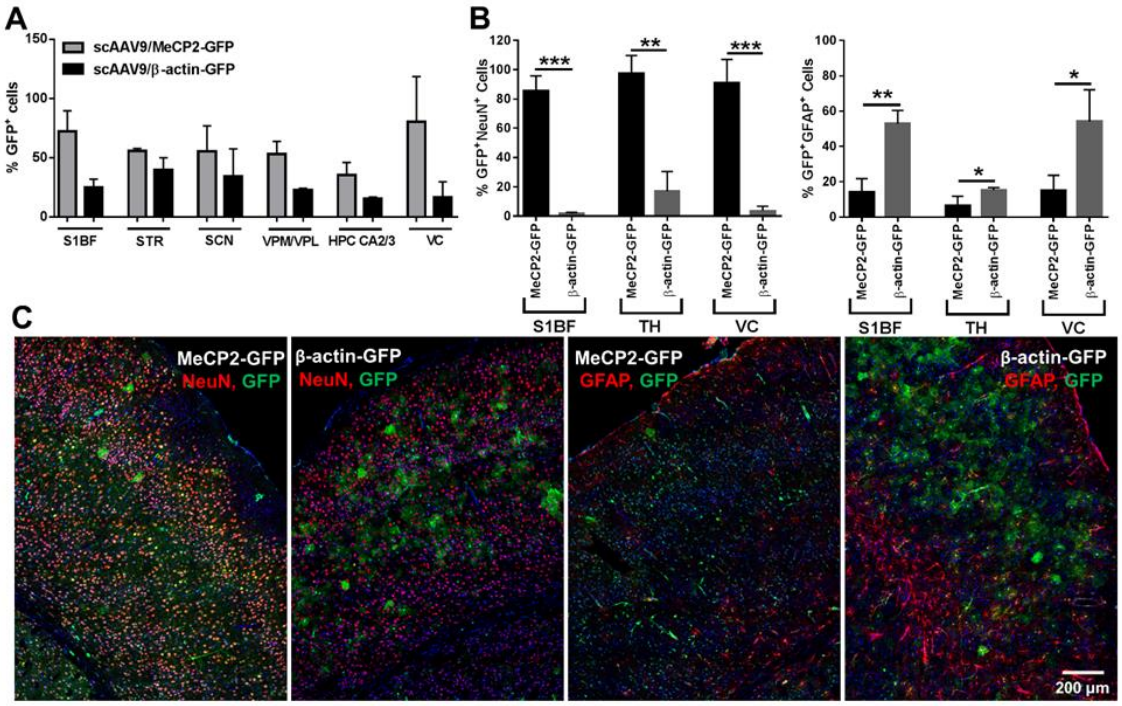


**Comparative biodistribution of scAAV9 constructs in the Cln3$^{\Delta ex7/8}$ brain following systemic delivery.** One month-old mice Cln3$^{\Delta ex7/8}$ mice (n=4-5/group) received one i.v. injection of 2x10$^{12}$ vg of scAAV9/MeCP2-GFP or scAAV9/β-actin-GFP, whereupon animals were sacrificed at 5 months post-injection for analysis of virus biodistribution. A) Quantitation of total % GFP$^+$ cells in the somatosensory barrel field cortex (S1BF), striatum (STR), suprachiasmatic nucleus (SCN), thalamus (VPM/VPL), hippocampus (CA1/CA3), and visual cortex (VC). B) Quantification of GFP$^+$ neurons (NeuN$^+$GFP$^+$) and astrocytes (GFAP$^+$GFP$^+$) in the S1BF, thalamus (TH), and VC of scAAV9/β-actin-GFP vs. scAAV9/MeCP2-GFP treated mice. C) Tiled 40X confocal images depicting preferential GFP expression in NeuN$^+$ neurons with scAAV9/MeCP2-GFP compared to scAAV9/β-actin-GFP, with both constructs targeting astrocytes. Significant differences are denoted by asterisks (*, $p < 0.05$; **, $p < 0.01$; ***, $p < 0.001$ as determined by paired *t*-test).

**Figure 5.3**

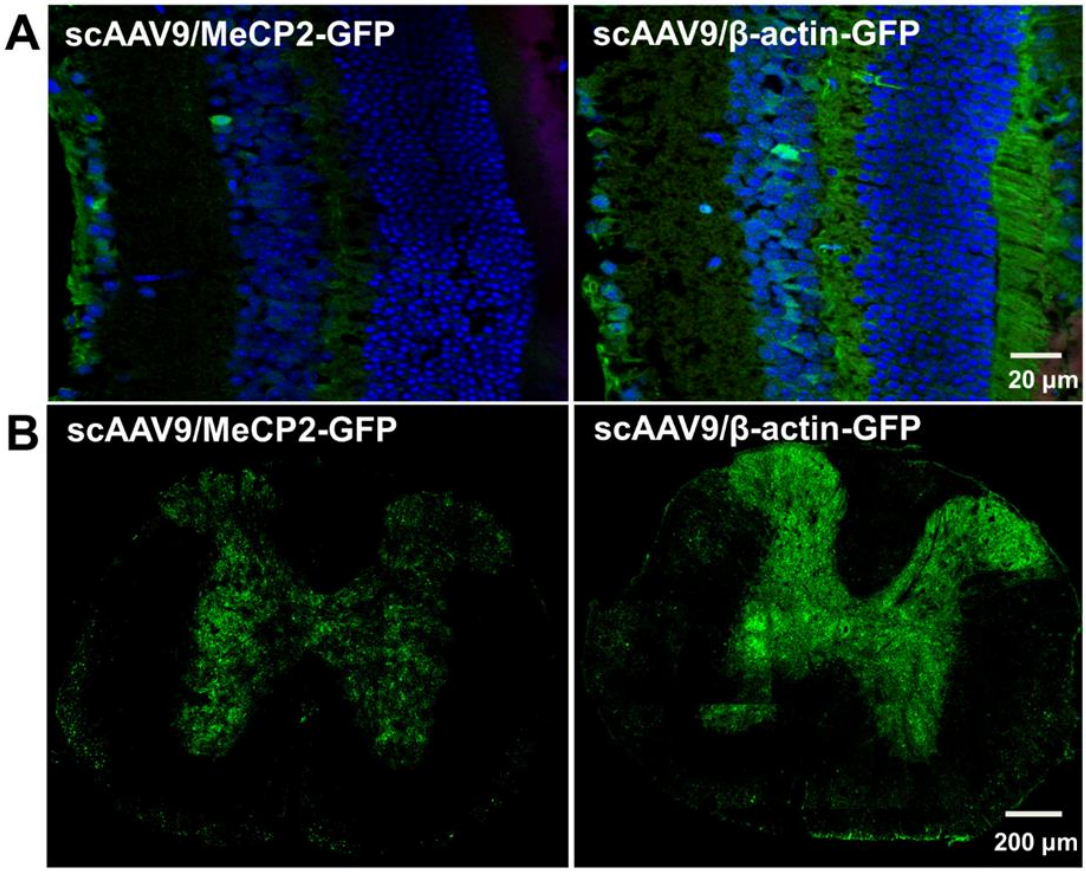


**Intravenous scAAV9 delivery successfully transduces the spinal cord and eye.** One month-old mice $Cln3^{\Delta ex7/8}$ mice (n=4-5/group) received one i.v. injection of $2x10^{12}$ vg of scAAV9/MeCP2-GFP or scAAV9/β-actin-GFP, whereupon animals were sacrificed at 13 months post-injection for analysis of virus biodistribution. Both scAAV9/β-actin-GFP and scAAV9/MeCP2-GFP transduced multiple cells with in the eye (A) and spinal cord (B).

Collectively, these results demonstrate that a single i.v. injection of scAA9 results in extensive CNS transduction and that the MeCP2 promoter preferentially drives transgene expression in neurons in one month-old mice, which does not occur with the β-actin construct. Since we were unable to directly measure hCLN3 protein expression due to the lack of specific antibodies, combined with the limiting packaging size of scAAV9 vectors precluding the generation of a hCLN3/GFP bisictronic construct, it remains possible that hCLN3 biodistribution may differ slightly from GFP. However, since both the hCLN3 and GFP constructs utilized an identical capsid (AAV9) and promoters, monitoring GFP expression as a readout for cells that would also be expressing hCLN3 represented the best available approach and represents a strategy that has been widely used in other studies [314, 315].

**The MeCP2 and β-actin promoters exhibit a gene dosage effect *in vivo*.**

A current viewpoint in the JNCL field is that postnatal CLN3 expression should be maintained at low levels to support homeostasis, whereas overexpression of CLN3 may be toxic [95, 99, 216]. This is suggested by CLN3 reporter mice and yeast studies with the CLN3 ortholog *btn1*; however, to date, there is limited *in vivo* evidence to support this tenant. To investigate whether a promoter dosage effect was evident between the β-actin and MeCP2 constructs *in vivo*, Western blot analysis, immunofluorescence staining, and quantitative RT-PCR were conducted on multiple brain regions affected in JNCL. Western blot analysis confirmed that GFP expression driven by the β-actin promoter was up to 4-fold higher compared to the MeCP2 promoter (Figure 4A-B). This difference was also apparent in brain tissues by confocal microscopy, where images were collected using the same acquisition parameters (Figure 4C). Quantitative PCR

analysis revealed a 3- to 8-fold increase in hCLN3 expression driven by the scAAV9/β-actin vs. scAAV9/MeCP2 construct at 5 months post-injection in several brain regions (Figure 4D). hCLN3 protein expression could not be assessed, since currently available antibodies exhibit non-specific reactivity in both Western blots and immunostaining of brain tissues. hCLN3 mRNA expression was still detected at 13 months post-injection, the latest time point examined (data not shown). This finding reflects episome stability, which is in agreement with other reports where AAV9-driven transgene expression has been detected for years [193, 207, 310]. These data support widespread scAAV9-mediated transgene expression throughout the CNS following a single i.v. injection and a promoter dosage effect in terms of transgene expression *in vivo*.

**Figure 5.4**

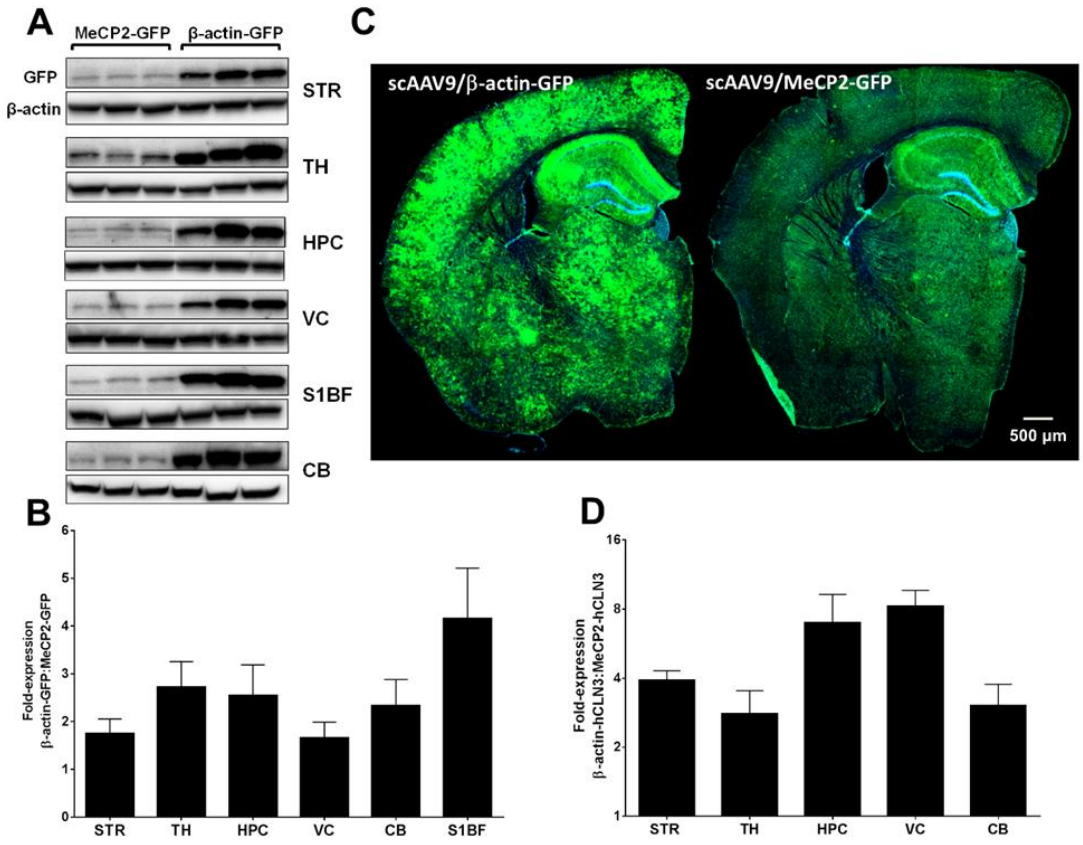


**Promoter dosage effect for transgene expression driven by the β-actin versus MeCP2 promoter.** One month-old mice $Cln3^{\Delta ex7/8}$ mice (n=4-5/group) received one i.v. injection of $2x10^{12}$ vg of scAAV9/MeCP2-hCLN3, scAAV9/β-actin-hCLN3, or GFP constructs, whereupon animals were sacrificed at 5 months post-injection for analysis of transgene expression in numerous brain regions. (A and B) Western blot of GFP expression in the striatum (STR), thalamus (TH), hippocampus (HP), visual cortex (VC), somatosensory barrel field cortex (S1BF), and cerebellum (CB) with raw (A) and quantitative (B) results expressed as fold-change. (C) Confocal images acquired with the same settings depict differences in GFP expression in the brain with animals injected with scAAV9/β-actin-GFP vs. scAAV9/MeCP2-GFP. (D) hCLN3 expression driven by the MeCP2 vs. β-actin promoters was determined by quantitative PCR following normalization to GAPDH and is presented as the fold-change in hCLN3 driven by scAAV9/β-actin relative to scAAV9/MeCP2.

**Systemic delivery of scAAV9/MeCP2-hCLN3 reverses motor deficits in Cln3$^{\Delta ex7/8}$ mice, whereas scAAV9/β-actin-hCLN3 is ineffective.**

Unlike infantile and late-infantile NCL mouse models (CLN1 and CLN2, respectively), Cln3$^{\Delta ex7/8}$ mice do not have a reduced lifespan [100]; however, animals develop robust and persistent motor deficits beginning at 2 months of age [67, 103]. To determine whether scAAV9/hCLN3 could reverse motor deficits in Cln3$^{\Delta ex7/8}$ animals, Cln3$^{\Delta ex7/8}$ mice receiving scAAV9/MeCP2-hCLN3, scAAV9/β-actin-hCLN3, or GFP control constructs were subjected to monthly accelerating rotarod testing. As expected, the latency to fall was significantly lower in vehicle-treated Cln3$^{\Delta ex7/8}$ mice compared to WT animals throughout the 5 month study period (Figure 5). Importantly, motor activity was restored to nearly WT levels only in Cln3$^{\Delta ex7/8}$ mice receiving scAAV9/MeCP2-hCLN3 as early as 1 month post-injection, whereas the scAAV9/β-actin-hCLN3 and GFP constructs had no significant effect (Figure 5). Significant improvements in rotarod performance for Cln3$^{\Delta ex7/8}$ mice receiving scAAV9/MeCP2-hCLN3 continued until 5 months post-injection, the latest interval examined. We were not able to extend behavioral assessments beyond 5 months, since half of the animals in each group were sacrificed at this interval to assess virus biodistribution and transgene expression and the remaining group size was not sufficient to produce robust results. Collectively, these findings indicate that CLN3 delivery is able to improve motor performance in a JNCL mouse model.

**Figure 5.5**

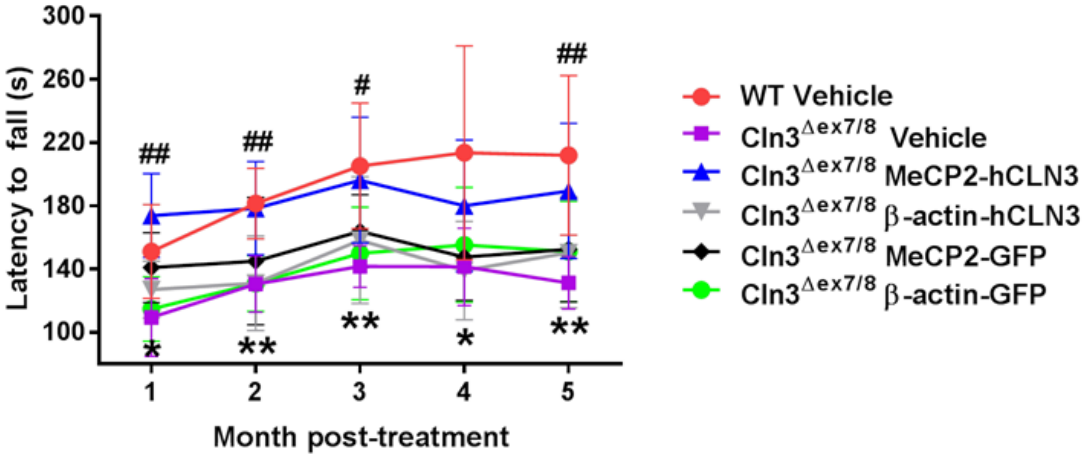


**Peripheral delivery of scAAV9/MeCP2-hCLN3 corrects motor deficits in Cln3$^{\Delta ex7/8}$ mice.** One month-old mice Cln3$^{\Delta ex7/8}$ mice (n=5-8/group) received one i.v. injection of 2x10$^{12}$ vg of scAAV9/MeCP2-hCLN3, scAAV9/β-actin-hCLN3, or GFP constructs, with vehicle treated Cln3$^{\Delta ex7/8}$ and WT animals as controls, whereupon motor coordination was assessed by monthly repeated accelerating rotarod assay, with results reported as latency to fall. Significant differences between WT vehicle and Cln3$^{\Delta ex7/8}$ vehicle treated animals are denoted by asterisks, whereas significant changes between Cln3$^{\Delta ex7/8}$ vehicle and Cln3$^{\Delta ex7/8}$ MeCP2-hCLN3 treated mice are denoted by hash signs (* or #, $p < 0.05$; ** or ##, $p < 0.01$, using a repeated measures ANOVA with Tukey post-hoc analysis).

**Systemic delivery of scAAV9/MeCP2-hCLN3 suppresses glial activation and reduces lysosomal pathology in the Cln3$^{\Delta ex7/8}$ brain.**

Reactive astrocytes and microglia are known to precede and predict regions of subsequent neuronal loss in JNCL mouse models [32, 33]. In addition, chronic microglial activation can create a toxic environment that induces and/or facilitates neurodegeneration [117]. A potential pathogenic role for microglia in JNCL is supported by our recent study demonstrating that Cln3$^{\Delta ex7/8}$ microglia are primed to be proinflammatory [123]. To determine the effects of scAAV9/hCLN3 constructs on microglial activation, brain tissues were stained for CD68 at 5 months post-injection. Microglial activation was significantly increased in vehicle treated Cln3$^{\Delta ex7/8}$ mice compared to WT animals in the TH and S1BF (Figure 6). In both brain regions, only the scAAV9/MeCP2-hCLN3 construct was able to significantly reduce microglial reactivity to near WT levels, whereas the scAAV9/β-actin-hCLN3 and GFP constructs had no significant effect (Figure 6B). Similar findings were observed with regard to astrocyte activation. Reactive astrocytes were increased in Cln3$^{\Delta ex7/8}$ mice compared to WT animals and only scAAV9/MeCP2-hCLN3 was able to reduce astrocyte activation, although this did not reach statistical significance (Figure 7). Neither the scAAV9/β-actin-hCLN3 nor GFP constructs influenced astrocyte reactivity in Cln3$^{\Delta ex7/8}$ mice (Figure 7B). The selectivity of the scAAV9/MeCP2-hCLN3 construct to attenuate glial activation agrees with its ability to improve motor function, suggesting that either low levels of CLN3 expression or preferential transgene expression in neurons afforded by the MeCP2 promoter is critical.

**Figure 5.6**

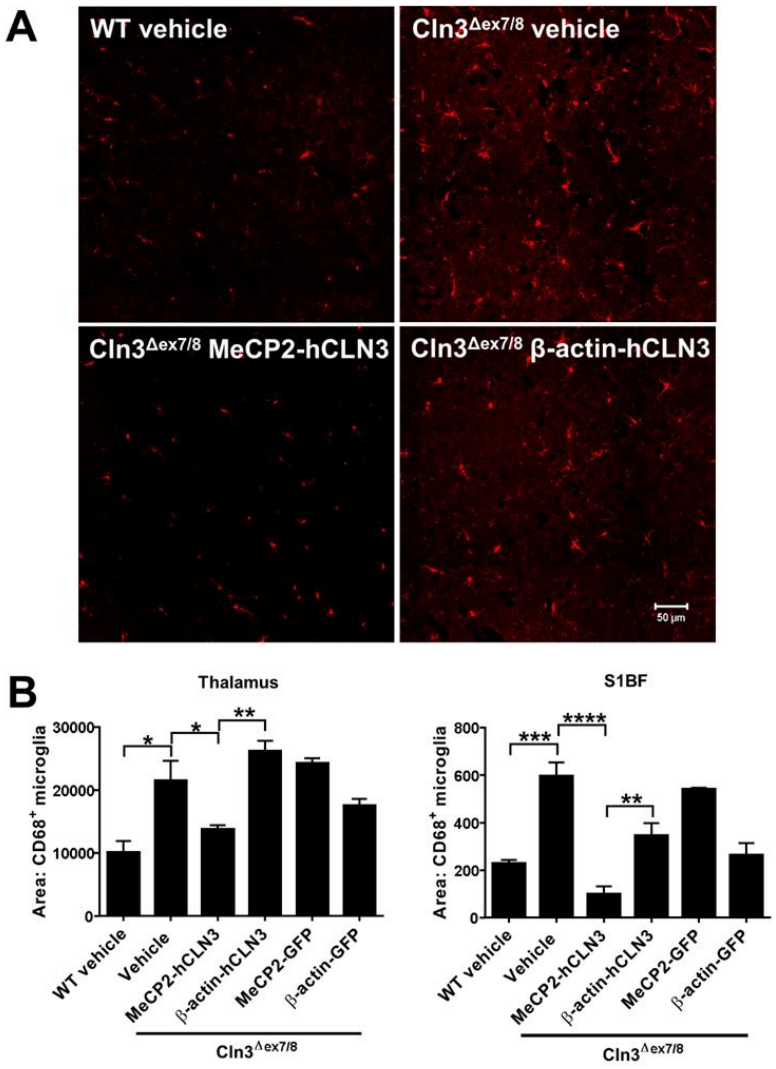


**scAAV9/MeCP2-hCLN3 reduces microglial activation in the Cln3$^{\Delta ex7/8}$ brain.** One month-old mice Cln3$^{\Delta ex7/8}$ mice (n=4-5/group) received one i.v. injection of 2x10$^{12}$ vg of scAAV9/MeCP2-hCLN3, scAAV9/β-actin-hCLN3, or GFP constructs, with vehicle treated Cln3$^{\Delta ex7/8}$ and WT animals as controls, whereupon microglial activation was evaluated by CD68 immunostaining in the thalamus and somatosensory barrel field cortex (S1BF) with representative images of the S1BF shown in (A) and quantitative analysis in (B). Significant differences are denoted by asterisks (*, $p < 0.05$; **, $p < 0.01$; ***, $p < 0.001$; ****, $p < 0.0001$ using a mixed linear model).

**Figure 5.7**

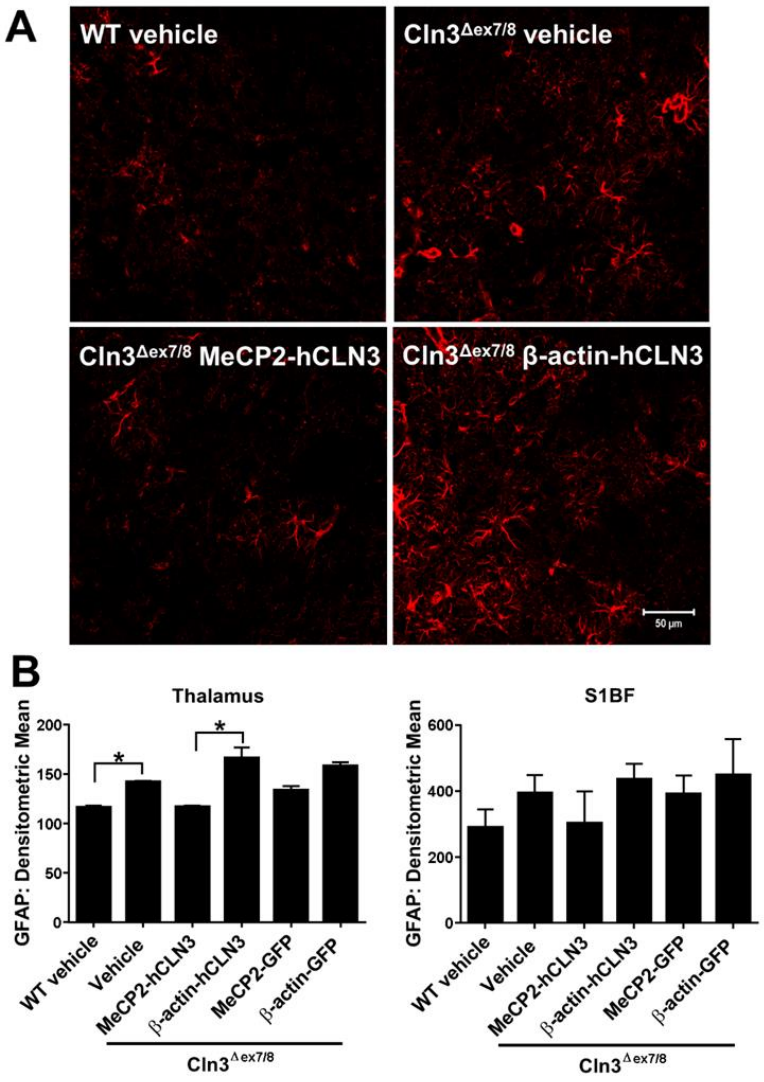


**scAAV9/MeCP2-hCLN3 reduces astrocyte activation in the Cln3$^{\Delta ex7/8}$ brain.** One month-old mice Cln3$^{\Delta ex7/8}$ mice (n=4-5/group) received one i.v. injection of 2x10$^{12}$ vg of scAAV9/MeCP2-hCLN3, scAAV9/β-actin-hCLN3, or GFP constructs, with vehicle treated Cln3$^{\Delta ex7/8}$ and WT animals as controls, whereupon astrocyte activation was evaluated by GFAP immunostaining in the thalamus and somatosensory barrel field cortex (S1BF) with representative images of the S1BF shown in (A) and quantitative analysis in (B). Significant differences are denoted by asterisks (*, $p < 0.05$ using a mixed linear model).

JNCL is characterized by the progressive accumulation of autofluorescent storage material in lysosomes, which is most pronounced in neurons [71, 72]. Inclusions are composed of a heterogeneous mixture of mitochondrial ATP synthase subunit c (SCMAS), lipofuscin, and other protein aggregates [71, 72, 75, 307, 316]. While inclusions are not considered to be a direct cause of neuronal death, since many inclusion-positive neurons are not lost in the disease, inclusions are commonly used as a biomarker of disease progression [54, 60, 67]. The extent of LAMP-1 expression is also used as another readout of lysosomal dysfunction [295, 296]. Therefore, we evaluated the effects of scAAV9/hCLN3 constructs on lysosomal pathology by immunostaining for LAMP-1 and the major storage component SCMAS. As has been shown for other LSDs [295, 297, 298], LAMP-1 expression was increased in vehicle treated $Cln3^{\Delta ex7/8}$ mice compared to WT animals in the TH and S1BF (Figure 8). Similar to what was observed for glial activation, only the scAAV9/MeCP2-hCLN3 construct was capable of reducing LAMP-1 levels in $Cln3^{\Delta ex7/8}$ animals, whereas the scAAV9/β-actin-hCLN3 or GFP constructs had no effect (Fig 8B). As expected, SCMAS was significantly higher in vehicle treated $Cln3^{\Delta ex7/8}$ mice compared to WT animals in the TH and S1BF (Figure 9). $Cln3^{\Delta ex7/8}$ mice injected with scAAV9/MeCP2-hCLN3 displayed a trend towards lower levels of SCMAS in the S1BF, which was not evident with the scAAV9/β-actin-hCLN3 or GFP constructs (Figure 9B). It should be noted that virus injections occurred at 1 month of age, a time when significant lysosomal inclusions are already present [159], which may make it more difficult to observe dramatic reductions in storage material accumulation.

**Figure 5.8**

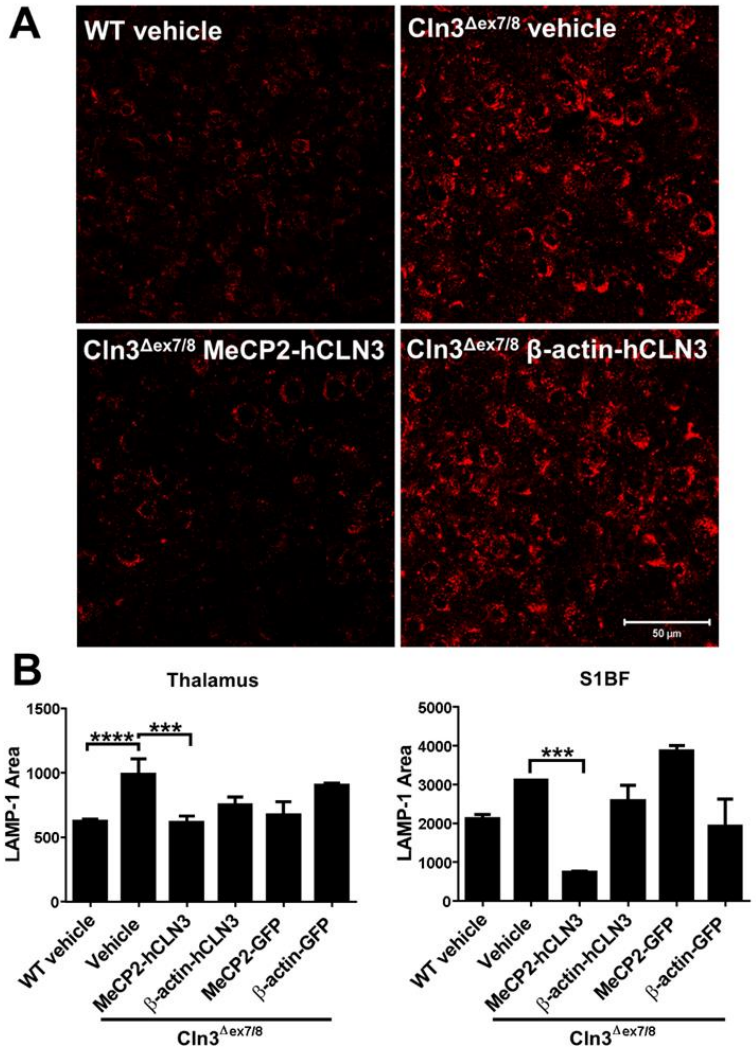


**Effect of systemic scAAV9-hCLN3 delivery on lysosomal pathology in the Cln3$^{\Delta ex7/8}$ brain.** One month-old mice Cln3$^{\Delta ex7/8}$ mice (n=4-5/group) received one i.v. injection of 2x10$^{12}$ vg of scAAV9/MeCP2-hCLN3, scAAV9/β-actin-hCLN3, or GFP constructs, with vehicle treated Cln3$^{\Delta ex7/8}$ and WT animals as controls, whereupon immunofluorescence staining for LAMP-1 was performed in the thalamus and somatosensory barrel field cortex (S1BF) with representative images of the S1BF shown in (A) and quantitative analysis in (B). Significant differences are denoted by asterisks (***, $p < 0.001$; and ****, $p < 0.0001$, using a mixed linear model).

**Figure 5.9**

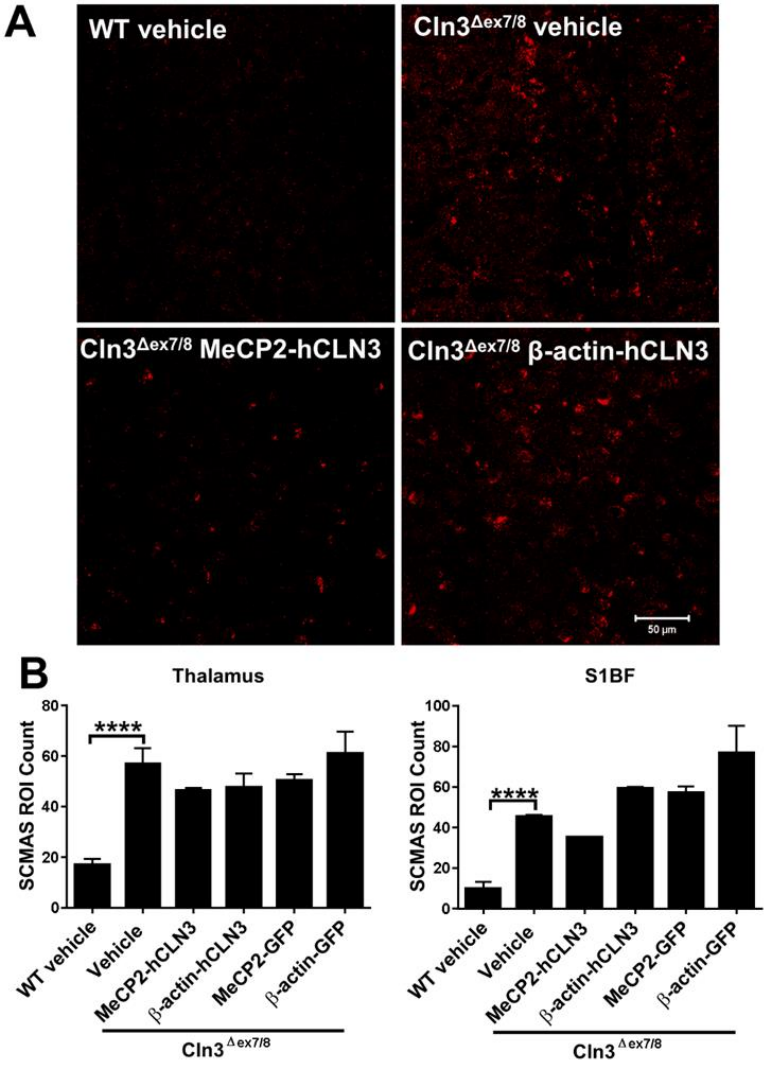


**Effect of systemic scAAV9-hCLN3 delivery on lysosomal inclusions in the Cln3$^{\Delta ex7/8}$ brain.** One month-old mice Cln3$^{\Delta ex7/8}$ mice (n=4-5/group) received one i.v. injection of 2x10$^{12}$ vg of scAAV9/MeCP2-hCLN3, scAAV9/β-actin-hCLN3, or GFP constructs, with vehicle treated Cln3$^{\Delta ex7/8}$ and WT animals as controls, whereupon immunofluorescence staining for SCMAS was performed in the thalamus and somatosensory barrel field cortex (S1BF) with representative images of the S1BF shown in (A) and quantitative analysis in (B). Significant differences are denoted by asterisks (****, $p < 0.0001$, using a mixed linear model).

**DISCUSSION**

Currently, no therapeutics exist for JNCL. Although lysosomal inclusions form throughout the body due to the ubiquitous expression of CLN3, the primary site of disease manifestation is the CNS [60]. Since neurons are the principle cell type lost during the disease, it was critical to devise a strategy to target this population at a relatively high frequency, since cross-correction is not possible based on the fact that CLN3 encodes for a transmembrane protein [87]. To this end, we utilized scAAV9 harboring the human CLN3 cDNA under the control of either the high or low expressing β-actin and MeCP2 promoters, respectively, to assess potential gene dosage effects on disease outcome. β-actin is ubiquitously expressed and its promoter drives high transgene expression [317]. In contrast, the MeCP2 promoter is tightly regulated, since overexpression by ~2-fold produces neurological complications [318, 319]. MeCP2 levels rise postnatally and continued expression is essential throughout adult life [320-322], which would ensure that the exogenous MeCP2 promoter used here to drive hCLN3 is transcriptionally active in juvenile and adult animals. Since the MeCP2 promoter is preferentially active in neurons [323], this also provides an attractive approach to correct intrinsic neuronal defects in JNCL. Indeed, a recent study utilizing the native MeCP2 promoter to drive wild type MeCP2 expression in a mouse model of Rett syndrome reported widespread neuronal transduction in the hippocampus, cortex, and cerebellum following systemic i.v. injection of adult animals, which rescued behavioral and cellular deficits [193]. In our study, we selected MeCP2 instead of the CLN3 promoter to drive low transgene expression, since the regulatory elements of CLN3 are not well-defined.

This study is the first to utilize systemic scAAV9 delivery to drive CLN3 expression in the CNS and importantly, only a single i.v. injection of scAAV9/MeCP2-hCLN3 was required to improve motor function, glial activation, and lysosomal pathology. In addition,

i.v. injection led to widespread transgene expression in the brain, spinal cord, and eye. scAAV9 did not negatively affect liver function as determined by blood chemistry analysis and all mice receiving scAAV9 constructs demonstrated equivalent weight gain. None of the scAAV9 constructs elicited signs of peripheral inflammation and there was no gross evidence of tumor formation in the liver at either 5 or 13 months post-injection (data not shown). Hepatocellular carcinoma has been reported in some mouse studies with specific AAV serotypes [324-326]; however, this is typically observed when virus is administered to neonatal mice [327, 328], which differs from our study where scAAV9 was used in juvenile animals. Collectively, these findings demonstrate the safety and tolerability of scAAV9/hCLN3, which are important attributes when considering the potential translation of this gene delivery approach.

scAAV9 has been well characterized within the CNS following systemic i.v. injection [204, 311, 329-331]. Specifically, the AAV9 capsid allows the virus to cross the BBB, resulting in stable CNS transgene expression. Prior reports have demonstrated that the age at which animals are injected can influence virus biodistribution and cell type targeting. For example, i.v. injection of P1 mice with a scAAV9/β-actin-GFP construct led to a large population of transgene$^+$ neurons and astrocytes [204]. In contrast, i.v. injections of mice that were P30 or older with scAAV9/β-actin-GFP primarily resulted in astrocyte targeting with few transgene$^+$ neurons. Besides mouse age, the promoter used to drive transgene expression can also have a major impact. For example, i.v. injection of a scAAV9/MeCP2-MeCP2 construct in a mouse model of Rett syndrome led to robust transgene expression in neurons, despite the fact that animals did not receive the virus until adulthood (i.e. 2-3 months of age) [193]. Therefore, other mechanisms are at play besides age at injection, indicating that cell-type promoter preference may also influence transgene levels. In our studies, the scAA9/MeCP2-GFP construct led to significantly more transgene$^+$ neurons than scAA9/β-actin-GFP, suggesting a promoter preference

for MeCP2 in neurons. This is also supported by studies showing that the MeCP2 promoter is preferentially expressed in neurons as compared to glia [318, 319]. Since both the MeCP2 and β-actin constructs utilized the same viral capsid (AAV9), these differences likely result from promoter preferences in each cell population.

In terms of disease outcomes, only the scAAV9/MeCP2-hCLN3 construct was capable of improving motor function, attenuating glial activation, and reducing lysosomal pathology, all hallmarks of JNCL [32, 67]. However, it remains to be determined whether the beneficial effects of scAAV9/MeCP2-hCLN3 resulted from lower transgene levels or preferential expression in neurons. Because we did not observe any adverse effects with scAAV9/β-actin-hCLN3 that drives a 3- to 8-fold increase in hCLN3 depending on the brain region, this suggests that the beneficial effects of scAAV9/MeCP2-hCLN3 are likely due to preferential transgene expression in neurons. However, additional studies are needed to definitively address this possibility, including the generation of neuronal- and astrocyte-targeted hCLN3 constructs (i.e. synapsin-hCLN3 and GFAP-hCLN3, respectively). We are currently pursuing the longevity of scAAV9/MeCP2-hCLN3 gene transfer effects with larger cohorts of animals in conjunction with cell type selective targeting to neurons or astrocytes, such that coincident data can be collected with accelerating rotarod and histopathology (the former of which requires large group sizes of $\geq$ 8). Preliminary analysis was performed with the limited numbers of $Cln3^{\Delta ex7/8}$ mice that were sacrificed at 13 months post-injection in the current study, including unbiased stereology to estimate neurons in the VPM/VPL thalamic nuclei. Although a prior study reported thalamic neuron loss in $Cln3^{\Delta ex7/8}$ mice on a mixed 129Sv/Ev/CD1 background at 12 months [33], this reduction was modest and we did not observe any differences in neuronal counts in the current study between vehicle treated WT and $Cln3^{\Delta ex7/8}$ animals on a C57BL/6 background, which is known to harbor milder disease phenotypes. The fact that we could not demonstrate evidence of neuronal loss in $Cln3^{\Delta ex7/8}$ mice

precluded our ability to assess the effects of CLN3 gene delivery on promoting neuronal survival. Nevertheless, we found that neuron counts in the thalamus were similar between WT animals and $Cln3^{\Delta ex7/8}$ mice receiving either the MeCP2 or β-actin hCLN3 constructs at 13 months post-injection (data not shown). This indicates that CLN3 gene delivery did not exert any deleterious effects on neurons, which is an important indicator of safety. Likewise, although our results demonstrated that elevated hCLN3 expression driven by the β-actin promoter did not improve disease outcome, there was no evidence of toxicity, since scAAV9/β-actin-hCLN3 did not worsen motor performance, glial activation, lysosomal pathology, or blood chemistry values in $Cln3^{\Delta ex7/8}$ mice. Collectively, these results indicate that unlike prior *in vitro* studies, elevated hCLN3 expression *in vivo* is not deleterious, as determined by the readouts examined here. This is also supported by a study with rhAAV.10/β-actin-CLN3 where direct intracranial injection was not associated with adverse effects even though hCLN3 mRNA expression was elevated 12 to 100-fold [219].

A major hallmark of JNCL is lysosomal storage material accumulation and although this heterogeneous material, primarily composed of SCMAS, has not been directly implicated in neuronal death [316], inclusion quantification is still widely used to assess lysosomal function and disease progression. Only scAAV9/MeCP2-hCLN3 led to reductions in SCMAS accumulation in $Cln3^{\Delta ex7/8}$ mice, although this did not reach statistical significance. Another marker of lysosomal dysfunction is increased LAMP-1 expression and similar to SCMAS, only scAAV9/MeCP2-hCLN3 was capable of significantly reducing LAMP-1 in the $Cln3^{\Delta ex7/8}$ brain to WT levels. This finding was substantial given the fact that virus administration was delayed until 1 month of age, when significant lysosomal pathology had already manifested [159].

Like many other LSDs, JNCL mouse models are typified by early glial activation (i.e. 1-3 months of age) that coincides with regions of modest neuronal loss that occurs much later in disease (i.e. 12-18 months; Pontikis et al., 2005; Burkovetskaya, 2014). While initial glial activation may represent a neuroprotective attempt, this clearly is not achieved and chronic inflammation can create a neurotoxic environment [34]. Indeed, our prior work revealed that $Cln3^{\Delta ex7/8}$ microglia are primed to release exaggerated levels of numerous proinflammatory cytokines/chemokines [123]. Here we report that only the scAAV9/MeCP2-hCLN3 construct was able to reduce glial activation, which coincided with improvements in motor function. By extension, this suggests that either 1) reactive microglia and/or astrocytes contribute to CNS dysfunction in early disease; or 2) preferential transgene expression in neurons driven by the MeCP2 promoter improves neuronal homeostasis, such that surrounding glia do not sense neuronal danger signals and, as such, are less activated. These possibilities currently remain speculative and require additional studies using cell type-specific scAAV9 constructs. There is a long standing question of what occurs first, inflammation induced by reactive glia, or neurons releasing danger signals to induce glial activation and inflammation [172]. In other LSDs, such as Gaucher disease, inflammation is elicited by either neurons or astrocytes but not from microglia [332, 333]. In our studies, the scAAV9/β-actin-hCLN3 construct predominantly drove transgene expression in astrocytes; however, it had no effect on glial activation. Furthermore, relatively fewer $transgene^{+}$ astrocytes and no microglia were observed following scAAV9/MeCP2-hCLN3 injection. This implies that glia sense signals from diseased neurons, since most glia were still CLN3-deficient, yet their activation status was significantly reduced. This suggests that neurons are a primary driver of disease progression, although a confounding role from activated glia cannot be disregarded at this time. The importance of cell intrinsic CLN3 loss in neurons is also

supported by the finding that although the percentages of transgene$^{+}$ cells were roughly similar with both viruses (Fig 2A), the MeCP2 construct resulted in significantly more transgene$^{+}$ neurons compared to β-actin and was associated with therapeutic efficacy. This is likely attributed to preferential promoter activity in neurons, since both promoter constructs were delivered by the same viral capsid (AAV9).

In summary, a highly regulated, neuron-targeted promoter (MeCP2) restored motor function and decreased glial activation and lysosomal pathology in the Cln3$^{\Delta ex7/8}$ brain. Our study is the first to show that systemic gene delivery with scAAV9 can be used to improve a lysosomal transmembrane mutation. This represents a critical first step towards a viable therapeutic for JNCL.

# Chapter 6: General discussion and future directions.

JNCL is the most common pediatric neurodegenerative disease with an incidence of 2-4 in every 100,000 live births [60-62]. The disease is caused by mutations in CLN3, resulting in loss of a protein expression and impaired lysosomal function [60, 233]. Children with CLN3 disease typically develop normally until symptoms present around 7-10 years of age, which are primarily neurological and include vision loss, seizures, and motor and cognitive decline [73-77]. While the CLN3 mutation is present in all cell types throughout the body, the CNS and neurons in particular are the most affected [71, 72, 158, 159, 334]. The exact function of CLN3 is currently unknown and there is no cure for JNCL, only palliative management. Therefore, is it imperative to investigate core pathways that are disrupted in JNCL to identify novel therapeutic targets to prolong patient survival.

Previous studies have found that activated astrocytes and microglia precede and predict regions of future neurodegeneration in the thalamus, S1BF, and hippocampus [32, 33, 102]. Our laboratory found that $Cln3^{\Delta ex7/8}$ astrocytes have significantly reduced expression of the glutamate transporter GLAST and glutamine synthetase in multiple brains regions [159]. These astrocytic proteins are critical for regulating glutamate-glutamine cycling and ensuring low extracellular glutamate concentrations are maintained [124-126]. Loss of these regulatory proteins supports the hypothesis that neuronal death is caused by excitotoxicity [104, 166, 167]. Recently, electrophysiology studies conducted in our laboratory found that neurons are hyperactive in 1-4-month-old $Cln3^{\Delta ex7/8}$ mice, which can lead to increases in glutamate release progressing to neuronal excitotoxicity [158]. Therefore, it was hypothesized that the CLN3 mutation causes abnormalities in astrocyte function to regulate the glutamate-glutamine cycle in JNCL.

Astrocytes influence neuronal activity and communicate with surrounding glia to interpret extracellular signals by $Ca^{2+}$ fluctuations [246, 247]. When neurons release

glutamate, astrocyte transporters become active and increase intracellular $Ca^{2+}$ levels to promote glutamate transporter expression at the plasma membrane, increase mitochondrial activity, and regulate neuronal firing. Astrocytes also send activity-dependent $Ca^{2+}$ signals to surrounding astrocytes via hemichannels and gap junctions effectively establishing a complex signaling syncytium [250-254]. To determine if astrocyte $Ca^{2+}$ signaling networks were disrupted in the context of CLN3 disease, live cell imaging was used to record primary $Cln3^{\Delta ex7/8}$ astrocyte responses to glutamate. It was found that $Cln3^{\Delta ex7/8}$ astrocytes had significantly lower basal spontaneous $Ca^{2+}$ oscillations as well as significantly lower $Ca^{2+}$ responses when stimulated with high concentrations of extracellular glutamate. This phenotype was also found when astrocytes were pre-treated with pro-inflammatory cytokines to mimic an inflammatory milieu that cells might encounter in the JNCL brain. These results indicate that CLN3 mutation causes a disruption in astrocyte $Ca^{2+}$ signaling networks. Astrocytes interpret extracellular signals and relay information through $Ca^{2+}$ to promote homeostasis; therefore, the fact that $Cln3^{\Delta ex7/8}$ astrocytes have significantly lower spontaneous $Ca^{2+}$ oscillations under resting conditions suggests that they are incapable of monitoring the extracellular milieu. Low basal $Ca^{2+}$ coupled with an inability to respond to glutamate stimulation implies that $Cln3^{\Delta ex7/8}$ astrocytes do not properly regulate synaptic activity allowing for continuous neuronal firing and increased glutamate release setting the stage for future neurodegeneration.

Glutamate regulation is an energy demanding process whereby astrocytes rely heavily on continuous metabolic support for energy [140, 141]. Previous studies have found that mitochondria in a $Cln3^{\Delta ex7/8}$ cerebellar neuron line have altered morphology, increased mitochondrial oxidative stress, and disrupted mitochondrial membrane depolarization, yet no studies have yet investigated astrocyte mitochondrial function in

real-time [89, 91, 256-258]. Utilizing a Seahorse mitochondrial bioassay, we found that $Cln3^{\Delta ex7/8}$ astrocytes displayed significant defects in mitochondrial respiration. In particular, $Cln3^{\Delta ex7/8}$ astrocytes had significantly lower basal respiration and ATP production under resting conditions. Mitochondrial disruption became even more apparent when $Cln3^{\Delta ex7/8}$ astrocytes were treated with either pro-inflammatory cytokines or C6 ceramide and neuronal lysate used to simulate DAMPs found in the JNCL brain. This phenotype was independent of mitochondrial number per cell, since $Cln3^{\Delta ex7/8}$ astrocytes had significantly more mitochondria then WT cells, possibly due to disrupted mitophagy that has been reported in JNCL models. The loss of mitochondrial respiration in $Cln3^{\Delta ex7/8}$ astrocytes can be attributed, in part, to reduced $Ca^{2+}$ signaling, as mitochondria rely heavily on intracellular $Ca^{2+}$ concentrations. Mitochondrial respiration supplies large quantities of ATP for multiple cellular processes, including glutamate transport and metabolism. During times of heightened neuronal activity, astrocyte energy demands significantly increase. We have demonstrated that $Cln3^{\Delta ex7/8}$ astrocytes have significantly lower ATP production, suggesting that the cells do not have sufficient energy required for optimal glutamate transporter function. This would disrupt the glutamate concentration gradient, effectively increasing extracellular glutamate concentrations. During times of stress, astrocytes switch to a more glycolytic profile to compensate for increasing energy demands [136]. We found no significant differences in glycolytic rates between $Cln3^{\Delta ex7/8}$ and WT astrocytes, indicating that $Cln3^{\Delta ex7/8}$ cells were not able to compensate for reductions in mitochondrial respiration. Disrupted mitochondria not only effect the glutamate-glutamine regulation pathway but a multitude of other cellular processes, such as protein synthesis, $Ca^{2+}$ regulation, and apoptotic processes, which may negatively impact the overall health of $Cln3^{\Delta ex7/8}$ astrocytes [335]. The mitochondrial defect in $Cln3^{\Delta ex7/8}$ cells could also be attributed to loss of lysosomal function. One of the main components of the lysosomal inclusions in JNCL is

mitochondrial ATP synthase subunit c, which implies a loss or disruption in mitochondrial turnover [336]. This would effectively propagate a negative feedback loop between lysosomal dysfunction and mitochondrial energy production.

While it is becoming increasingly apparent that $Cln3^{\Delta ex7/8}$ astrocytes contribute to glutamate dysregulation in JNCL, this is not an exclusively cell-autonomous process. It is hypothesized that neurodegeneration in JNCL is caused by excitotoxicity [104, 158]. This is based on studies reporting a loss of GABAergic inhibitory neurons and increased levels of glutamate in $Cln3^{-/-}$ animals. However, no studies have directly examined the response of Cln3 neurons to glutamate. Our study found that primary $Cln3^{\Delta ex7/8}$ neurons were hyper-responsive to 25nM glutamate, which mimics levels normally released in the synaptic cleft after physiological neuronal firing. $Cln3^{\Delta ex7/8}$ neurons responded with significantly higher intracellular $Ca^{2+}$ concentrations and while WT neurons also responded to glutamate stimulation, $Ca^{2+}$ levels rapidly retuned to baseline, whereas intracellular $Ca^{2+}$ remained elevated in $Cln3^{\Delta ex7/8}$ neurons for the duration of the experiment. This is an indication of excitotoxicity. Based on these results, we propose the following mechanism for neurodegeneration caused by excitotoxicity in JNCL. First the loss of CLN3 protein initiates lysosomal dysfunction in neurons, leading to the progressive accumulation of inclusions [159]. Unlike other NCL forms, the onset of disease symptoms in JNCL is protracted, suggesting compensatory mechanisms are in place until a certain pathological threshold is reached. At that time, neurons begin to become hyperreactive and overly sensitive to glutamate stimulation [159]. This leads to a continuous activation cycle that becomes unchecked due to the loss of GABAergic inhibitory neurons, which, in turn, causes a gradual rise in extracellular glutamate concentrations [33]. Astrocytes are the primary cell responsible for regulating glutamate release and clearance to prevent excitotoxicity. Astrocytes interpret the conditions in the

extracellular milieu and signal to surrounding cells through $Ca^{2+}$ signaling. CLN3 mutation disrupts astrocyte $Ca^{2+}$ signaling under homeostatic conditions, indicating that the cells are refractory to communication or interpreting extracellular signals. When exposed to extracellular glutamate, the response of $Cln3^{\Delta ex7/8}$ astrocytes is significantly blunted, as revealed by low intracellular $Ca^{2+}$ concentrations, suggesting that the cells are unable to properly respond to neuronal activity, which can cause a rise in extracellular glutamate. Increased extracellular glutamate disrupts concentration gradients and has been found to reduce astrocyte glutamate transporter expression [277]. Previous work from our laboratory has found that $Cln3^{\Delta ex7/8}$ mice have significantly lower expression of the glutamate transporter GLAST and glutamine synthetase [159]. The loss of these two key glutamate regulatory proteins suggests that $Cln3^{\Delta ex7/8}$ astrocytes cannot compensate or clear elevations in extracellular glutamate, leading to glutamate accumulation in the tripartite synapse. Astrocytes require energy to maintain homeostatic processes and energy demands further increase during times of heightened neuronal activity [140, 141]. However, $Cln3^{\Delta ex7/8}$ astrocytes have significantly lower mitochondrial basal respiration and ATP production during both resting and disease-like conditions. This indicates that $Cln3^{\Delta ex7/8}$ astrocytes do not have the necessary energy-generating pathways to properly regulate glutamate-glutamine cycling, neuronal activity, or other homeostatic processes, which, in turn, leads to a loss of glial support. At this point, both $Cln3^{\Delta ex7/8}$ neurons and astrocytes are likely undergoing stress that can trigger neuroinflammatory pathways to perpetuate disease progressing, leading to further glial activation and neurodegeneration.

As previously stated, there is currently no cure for JNCL. Since the exact function of the CLN3 protein is unknown, researchers must rely on targeting disrupted cellular pathways to develop new therapeutics. Developing a drug that is capable of affecting a

broad range of pathological mechanisms as well as cell types would be an ideal therapeutic for JNCL. PDE4 inhibitors have been found to be beneficial in multiple neurodegenerative diseases, such as AD, PD, and traumatic brain injury [185, 186, 190, 286]. These inhibitors have been found to reduce neuroinflammation, improve neuronal health and function, as well as augment glutamate transporter expression, all of which are pathways disrupted in JNCL [185, 186, 286]. PDE4 inhibitors function through regulating intracellular cAMP levels. Previous reports have ascertained that cAMP reductions impact neurobehavioral and cognitive functions during normal aging [182, 183]. Low intracellular cAMP levels are known to be closely correlated with inflammatory activation and signaling pathways [282, 283]. Our study is the first to report that cAMP levels are significantly reduced in the thalamus and trending towards lower levels in the hippocampus and visual cortex of $Cln3^{\Delta ex7/8}$ mice at 7 months of age. This phenotype becomes progressively worse with time and by 12 months $Cln3^{\Delta ex7/8}$ mice have decreased cAMP concentrations in all 3 brain regions. This finding was confirmed by immunohistochemical staining. No significant differences in cAMP levels were identified in the somatosensory barrel field cortex (S1BF), indicating that cAMP disruption is region-dependent. Based on these data we tested the efficacy of three distinct PDE4 inhibitors, including rolipram (first generation), FDA-approved roflumilast (second generation) and PF-06266047 (PF, a third-generation drug obtained from Pfizer) in $Cln3^{\Delta ex7/8}$ mice. Animals were treated with each compound beginning at 1 month of age, which correlates with the onset of disease pathology. Multiple concentrations were utilized for each drug based on half-life and clearance to determine the optimal effective dose. To determine if PDE4 inhibitors had a positive effect on motor dysfunction in $Cln3^{\Delta ex7/8}$ mice, animals were tested on the accelerating rotarod to measure fine motor coordination. Each of the PDE4 inhibitors significantly improved motor coordination in $Cln3^{\Delta ex7/8}$ mice at different dosages. What was striking about this study was that rolipram

and PF improved motor activity as early as 1 month post-treatment, which was either maintained or progressively improved throughout the study. These findings suggest that PDE4 inhibitors act rapidly to improve neuronal function as well as slow disease progression. Roflumilast did not provide benefits until 3 months post-treatment, which is most likely due to its low BBB permeability [221]. Roflumilast is an FDA-approved pharmaceutical used to reduce the risk of inflammatory exacerbations in chronic obstructive pulmonary disease (COPD) and has been shown to be well-tolerated following a single dose in children with mild to moderate asthma [301]. Our studies found that all three PDE4 inhibitors did not cause any disruption to liver, kidney, or pancreatic function throughout the 6 month treatment course; however, weight loss was evident, which has been reported for this drug class. These findings offer the possibility that roflumilast can be repurposed for the treatment of JNCL patients, whereas PF has yet to undergo clinical trials for FDA-approval, which would take years.

One of the pathways modulated by PDE4 inhibitors is the glutamatergic pathway. As previously noted, glutamate transporter expression is reduced, which coincides with increased glutamate levels in the CNS of JNCL mouse models [104, 158, 159]. A 6 month treatment period with roflumilast and PF significantly increased GLAST expression in the S1BF and thalamus of $Cln3^{\Delta ex7/8}$ mice. Concurrently, PF treatment significantly increased cAMP levels in the thalamus, visual cortex, and hippocampus. cAMP is known to promote neuronal homeostasis and regulate synaptic functions. It is that that raising cAMP levels has a synergistic effect on $Cln3^{\Delta ex7/8}$ neuron-astrocyte cross-talk by normalizing neuronal activity and increasing glutamate transporter expression to prevent excitotoxicity. This, in turn, would lead to improved neuronal health. Another indication that PDE4 inhibitors improved neuronal fitness was the finding that lysosomal pathology, which is primarily found in neurons, was significantly reduced

in Cln3$^{\Delta ex7/8}$ mice treated with PDE4 inhibitors. While the mechanism of action for this finding is unknown, improving overall neuronal health might reduce lysosomal stress and slow lysosomal dysfunction.

By improving neuronal function, PDE4 inhibitors may establish a symbiotic environment with surrounding glial cells in Cln3$^{\Delta ex7/8}$ animals. Previously our laboratory has found activated astrocytes and microglia at later time points of disease and Cln3$^{\Delta ex7/8}$ microglia display a pro-inflammatory profile *ex vivo*. After roflumilast and PF treatment, microglial and astrocyte activation was significantly reduced in Cln3$^{\Delta ex7/8}$ mice as measured by CD68 and GFAP expression. These results indicate that increasing cAMP levels and improving neuronal health leads to reduced gliosis in the JNCL brain. By improving overall neuronal heath and limiting glial activation, PDE4 inhibitors have the ability to slow JNCL progression.

Finally, it is important to note that PF and roflumilast significantly improved motor coordination in Cln3$^{\Delta ex7/8}$ mice even when treatment was delayed until 3 months of age. At this time point, Cln3$^{\Delta ex7/8}$ mice have more severe disease pathology, including significant motor deficits, increased lysosomal dysfunction, and glial activation. Both PDE4 inhibitors improved motor coordination after just a single month of treatment and Cln3$^{\Delta ex7/8}$ mice continued to improve out to 12 months of age. While we did not evaluate neuron survival at this interval, we speculate that PDE4 inhibitors prevented neurodegeneration due to the fact that rotarod performance was similar between Cln3$^{\Delta ex7/8}$ mice receiving PDE4 inhibitors and WT animals. These results suggest that PDE4 inhibitors can have a beneficial effect after disease pathology has developed. Many children with JNCL are often misdiagnosed in the beginning and by the time a proper diagnosis is made disease pathology has already begun to have detrimental effects on patients' health. Therefore, PDE4 inhibitors appear to represent an excellent

potential therapeutic for JNCL because several are currently FDA-approved and commercially available, have shown efficacy in clinical trials of neurodegenerative diseases, and are able to significantly improve numerous pathological attributes in $Cln3^{\Delta ex7/8}$ mice, which closely recapitulate CLN3 disease in humans.

While PDE4 inhibitors were successful in improving motor coordination and disease pathology, this is not a sustainable long-term approach, since they will not correct the underlying mutation. In this case the disease would continue to progress, albeit it at a slower rate. Therefore, we investigated the use of gene therapy as a more permanent therapeutic for JNCL. Because CLN3 is a transmembrane protein, cross correction is not possible, which requires a larger number of transduced cells for gene therapy to be beneficial. Therefore, we devised a strategy to utilize scAVV9 harboring hCLN3 driven by either the MeCP2 promoter (low expression level targeting neurons) or chicken β-actin promoter (high expression level targeting astrocytes) [193]. Separate scAAV9 constructs were generated with each promoter driving GFP to assess the identity of transfected cells. A dual hCLN3-GFP construct could not be generated, since the gene size exceeded the packaging capacity of scAAV9. This study was designed to test two hypotheses; first, to determine the efficacy of gene therapy to replace a transmembrane protein and second, to identify the appropriate CLN3 expression level required for cellular homeostasis. Previous gene therapy studies for NCLs have administered viruses via stereotaxic intracranial injections, which does not allow viral dissemination throughout the brain and provides obstacles for patient administration [219]. Therefore, we injected a single dose of scAAV9-hCLN3 or scAAV9-GFP systemically via retro-orbital injections into 1 month-old $CLN3^{\Delta ex7/8}$ mice to model the age of when children are diagnosed with JNCL. This approach is not only less invasive but also promotes transduction in the periphery, since cardiac defects manifest in CLN3

patients later in the disease process. Throughout the entirety of the study, mice exhibited no signs of toxicity, indicating that scAAV9 had no adverse side effects, which have been reported with retroviral therapies. Viral distribution was assessed at 5 months post-injection, where transduction was widespread in several brain regions and also occurred in the spinal cord and eye, indicating that scAAV9 successfully crossed the BBB after intravenous injection. Viral-GFP expression was still found 1 year after injection in a small cohort of mice demonstrating scAAV9 stability in post-mitotic cells. This is important to highlight because it represents a more long-term clinical approach requiring a single non-invasive injection and a single treatment.

There is a long-standing hypothesis in the JNCL field that CLN3 protein expression must be maintained at low levels [95, 99, 216]. This theory is based on experiments demonstrating low levels of CLN3 mRNA expression throughout development and that CLN3 over expression is toxic to yeast. However, to date, no studies have been performed to directly investigate this question. To determine appropriate CLN3 expression levels, two different promoters were tested, namely, MeCP2 that is tightly regulated and maintained at low levels throughout life, and chicken β-active that is ubiquitously expressed and drives high transgene expression. Western blot analysis and RT-qPCR found that the β-actin promoter resulted in up to a 8-fold increase in hCLN3 mRNA expression compared to the MeCP2 promoter. Not only was there a difference in hCLN3 mRNA expression with the two promoters but also a cell-type specific promoter preference. Specifically, scAAV9/MeCP2-GFP preferentially transduced neurons, whereas scAAV9/β-actin-GFP primarily targeted astrocytes. After 12 months post-injection, unbiased stereology was performed to determine if hCLN3 gene therapy was able to prevent neurodegeneration reported in other JNCL mouse models. However, there were no differences in neuronal counts between WT and

CLN3$^{\Delta ex7/8}$ vehicle treated mice, which made it impossible to discern any effects of scAAV9/MeCP-hCLN3 or scAAV9/β-actin-hCLN3 on CLN3$^{\Delta ex7/8}$ treated animals. This can possibly be attributed to the C57BL/6 genetic background of the CLN3$^{\Delta ex7/8}$ mice which have a milder disease phenotype compared to mice on the 129Sv/Ev/CD1 background. However, these studies did establish that CLN3 overexpression from the chicken β-actin promoter did not cause any neurotoxicity.

Once it was established that scAAV9 successfully transduced the CNS with high efficacy, effects on disease pathology were examined. Only CLN3$^{\Delta ex7/8}$ mice receiving scAAV9/MeCP-hCLN3 had improved motor function beginning at 1 month post-injection and continuing for up to 5 months (the latest time point examined), whereas scAAV9/β-actin-hCLN3 had little to no effect. These results suggest that either low expression levels of CLN3 are required to maintain cellular homeostasis and/and restoring CLN3 activity in neurons (with MeCP2) is more therapeutically beneficial than targeting astrocytes (with β-actin). Interestingly, only scAAV9/MeCP-hCLN3 reduced microglial activation in the thalamus and S1BF. While not direct evidence, this supports the theory that microglia activation is triggered by distressed signals from Cln3$^{\Delta ex7/8}$ neurons, since microglia were not transduced by scAAV9. Conversely, scAAV9/β-actin-hCLN3 had no effect on reducing microglial activation and in the case of the thalamus reactive microglia were more prominant than vehicle treated Cln3$^{\Delta ex7/8}$ mice. Coincident with microglia activation, only scAAV9/MeCP-hCLN3 reduced astrocyte activation in the thalamus and S1BF. One possible explanation for the, inability of scAAV9/β-actin-hCLN3, a primarily astrocyte targeted vector, to reduce astrocyte activation is that surrounding Cln3$^{\Delta ex7/8}$ neurons were non-transduced and remained dysfunctional. Even though WT CLN3 was restored in many Cln3$^{\Delta ex7/8}$ astrocytes with scAAV9/β-actin-hCLN3, the cells are still unable to cope with neuronal defects, further supporting the idea that neurons and not

inflammation or glial reactivity plays a larger role in disease pathology. Finally, lysosomal pathology was assessed by monitoring two commonly used makers, namely LAMP-1 and mitochondrial ATP synthase subunit C (SCMAS), a primary component of lysosomal aggregates in JNCL. Similar to previous results, only scAAV9/MeCP-hCLN3 reduced LAMP-1 expression and SCMAS inclusions. This finding was significant, since virus was administered at a time point when significant lysosomal dysfunction and inclusion burdens have already manifested in $Cln3^{\Delta ex7/8}$ mice (i.e. 1 month of age). These results suggest that scAAV9/MeCP-hCLN3 is capable of improving lysosomal function and preventing further inclusion development. Collectively, this data indicate that gene therapy may be a viable long-term therapeutic option for JNCL.

**Future directions and outstanding questions**

The work presented in this dissertation has provided new insights into the role of astrocyte and neuron dysfunction in JNCL as well as identified novel therapeutic strategies that have the potential to slow disease progression and prolong survival for JNCL patients. However, there are still many unanswered questions. The first of which is centered on early neuronal dysfunction that potentially creates a toxic extracellular milieu and induction of neuroinflammatory pathways. The CLN3 mutation is present in all cell types throughout the body, yet neurons are the most dramatically affected [71, 72, 158, 159, 334]. As previously discussed, we found that $Cln3^{\Delta ex7/8}$ neurons are hypersensitive to glutamate stimulation *in vitro* and are hyperactive in the visual cortex and hippocampus of $Cln3^{\Delta ex7/8}$ mice between 1-4 months of age *in vivo*. To date, there have been no studies that have directly shown how the loss of lysosomal function leads to hyperactive neurons. Therefore, it is vital to elucidate these pathways to gain a better understanding of events that trigger neurodegeneration in JNCL. Another interesting question is why JNCL disease progression is more protracted compared to INCL and

LNCL [79]. The delay in JNCL symptom manifestation suggests the existence of compensatory mechanisms that prevent cellular demise until a threshold of pathology is achieved. It is unknown what this mechanism(s) might be but if determined this could be a therapeutic target to promote compensatory mechanisms and slow disease progression. With regard to new therapeutic development, it would be informative to determine which cell type plays a dominant role in disease progression. This can be achieved with scAAV9 engineered with cell type-specific promoters, such as synaptophysin for neurons and GFAP for astrocytes. It would also be interesting to delve deeper into $Cln3^{\Delta ex7/8}$ neuron pathology by placing hCLN3 expression under the control of GABAergic or glutamatergic promoters to examine the role excitatory versus inhibitory neurons play in disease progression. Since the identification of CLN3 as the causative mutation for JNCL in 1995, many important discoveries have been made in this field in an effort to improve the quality of life and survival of children afflicted with JNCL, with the hope of one day finding a cure for this fatal LSD.

## References


1. de Duve, D., *The peroxisome: a new cytoplasmic organelle.* Proc R Soc Lond B Biol Sci, 1969. **173**(1030): p. 71-83.
2. Vitner, E.B., A.H. Futerman, and N. Platt, *Innate immune responses in the brain of sphingolipid lysosomal storage diseases.* Biol Chem, 2015. **396**(6-7): p. 659-67.
3. Meikle, P.J., et al., *Prevalence of lysosomal storage disorders.* JAMA, 1999. **281**(3): p. 249-54.
4. Wolf, D.A., et al., *Gene therapy for neurologic manifestations of mucopolysaccharidoses.* Expert Opin Drug Deliv, 2015. **12**(2): p. 283-96.
5. Alroy, J., C. Garganta, and G. Wiederschain, *Secondary biochemical and morphological consequences in lysosomal storage diseases.* Biochemistry (Mosc), 2014. **79**(7): p. 619-36.
6. Baudry, M., et al., *Postnatal development of inflammation in a murine model of Niemann-Pick type C disease: immunohistochemical observations of microglia and astroglia.* Exp Neurol, 2003. **184**(2): p. 887-903.
7. Kollmann, K., et al., *Cell biology and function of neuronal ceroid lipofuscinosis-related proteins.* Biochim Biophys Acta, 2013. **1832**(11): p. 1866-81.
8. Cotman, S.L. and J.F. Staropoli, *The juvenile Batten disease protein, CLN3, and its role in regulating anterograde and retrograde post-Golgi trafficking.* Clin Lipidol, 2012. **7**(1): p. 79-91.
9. Pearce, D.A., et al., *Action of BTN1, the yeast orthologue of the gene mutated in Batten disease.* Nat Genet, 1999. **22**(1): p. 55-8.
10. Tuxworth, R.I., et al., *The Batten disease gene CLN3 is required for the response to oxidative stress.* Hum Mol Genet, 2011. **20**(10): p. 2037-47.
11. Persaud-Sawin, D.A., A. VanDongen, and R.M. Boustany, *Motifs within the CLN3 protein: modulation of cell growth rates and apoptosis.* Hum Mol Genet, 2002. **11**(18): p. 2129-42.
12. Huang, X., et al., *A Drosophila model of the Niemann-Pick type C lysosome storage disease: dnpc1a is required for molting and sterol homeostasis.* Development, 2005. **132**(22): p. 5115-24.
13. Park, I.H., et al., *Disease-specific induced pluripotent stem cells.* Cell, 2008. **134**(5): p. 877-86.
14. Appelqvist, H., et al., *The lysosome: from waste bag to potential therapeutic target.* J Mol Cell Biol, 2013. **5**(4): p. 214-26.
15. Boya, P., *Lysosomal function and dysfunction: mechanism and disease.* Antioxid Redox Signal, 2012. **17**(5): p. 766-74.
16. Cooper, G., *Lyosome*, in *The Cell: A Molecular Approach.* 2000, Sinauer Associates: Sunderland (MA).
17. Luzio, J.P., P.R. Pryor, and N.A. Bright, *Lysosomes: fusion and function.* Nat Rev Mol Cell Biol, 2007. **8**(8): p. 622-32.
18. Saftig, P. and J. Klumperman, *Lysosome biogenesis and lysosomal membrane proteins: trafficking meets function.* Nat Rev Mol Cell Biol, 2009. **10**(9): p. 623-35.
19. Eskelinen, E.L., Y. Tanaka, and P. Saftig, *At the acidic edge: emerging functions for lysosomal membrane proteins.* Trends Cell Biol, 2003. **13**(3): p. 137-45.
20. Huynh, K.K., et al., *LAMP proteins are required for fusion of lysosomes with phagosomes.* EMBO J, 2007. **26**(2): p. 313-24.

21. Korolchuk, V.I., et al., *Lysosomal positioning coordinates cellular nutrient responses.* Nat Cell Biol, 2011. **13**(4): p. 453-60.
22. Turk, B. and V. Turk, *Lysosomes as "suicide bags" in cell death: myth or reality?* J Biol Chem, 2009. **284**(33): p. 21783-7.
23. Boya, P. and G. Kroemer, *Lysosomal membrane permeabilization in cell death.* Oncogene, 2008. **27**(50): p. 6434-51.
24. Roberg, K. and K. Ollinger, *Oxidative stress causes relocation of the lysosomal enzyme cathepsin D with ensuing apoptosis in neonatal rat cardiomyocytes.* Am J Pathol, 1998. **152**(5): p. 1151-6.
25. Chen, Y., et al., *Endothelial Nlrp3 inflammasome activation associated with lysosomal destabilization during coronary arteritis.* Biochim Biophys Acta, 2015. **1853**(2): p. 396-408.
26. Heid, M.E., et al., *Mitochondrial reactive oxygen species induces NLRP3-dependent lysosomal damage and inflammasome activation.* J Immunol, 2013. **191**(10): p. 5230-8.
27. Platt, F.M., B. Boland, and A.C. van der Spoel, *The cell biology of disease: lysosomal storage disorders: the cellular impact of lysosomal dysfunction.* J Cell Biol, 2012. **199**(5): p. 723-34.
28. Ballabio, A. and V. Gieselmann, *Lysosomal disorders: from storage to cellular damage.* Biochim Biophys Acta, 2009. **1793**(4): p. 684-96.
29. Futerman, A.H. and G. van Meer, *The cell biology of lysosomal storage disorders.* Nat Rev Mol Cell Biol, 2004. **5**(7): p. 554-65.
30. Farooqui, A.A., *Lipid mediators in the neural cell nucleus: their metabolism, signaling, and association with neurological disorders.* Neuroscientist, 2009. **15**(4): p. 392-407.
31. Cooper, G., *Structure of the Plasma Membrane*, in *The Cell: A Molecular Approach*, R.E.H. Geoffrey M. Cooper, Editor. 2000, Sinauer Associates: Sunderland (MA).
32. Pontikis, C.C., et al., *Late onset neurodegeneration in the Cln3-/- mouse model of juvenile neuronal ceroid lipofuscinosis is preceded by low level glial activation.* Brain Res, 2004. **1023**(2): p. 231-42.
33. Pontikis, C.C., et al., *Thalamocortical neuron loss and localized astrocytosis in the Cln3Deltaex7/8 knock-in mouse model of Batten disease.* Neurobiol Dis, 2005. **20**(3): p. 823-36.
34. Fernandes-Alnemri, T., et al., *AIM2 activates the inflammasome and cell death in response to cytoplasmic DNA.* Nature, 2009. **458**(7237): p. 509-13.
35. Lyman, M., et al., *Neuroinflammation: the role and consequences.* Neurosci Res, 2014. **79**: p. 1-12.
36. Lee, K.M. and A.G. MacLean, *New advances on glial activation in health and disease.* World J Virol, 2015. **4**(2): p. 42-55.
37. Gadani, S.P., et al., *Dealing with Danger in the CNS: The Response of the Immune System to Injury.* Neuron, 2015. **87**(1): p. 47-62.
38. Bergsbaken, T., S.L. Fink, and B.T. Cookson, *Pyroptosis: host cell death and inflammation.* Nat Rev Microbiol, 2009. **7**(2): p. 99-109.
39. Heneka, M.T., et al., *Neuroinflammation in Alzheimer's disease.* Lancet Neurol, 2015. **14**(4): p. 388-405.
40. Nixon, G.F., *Sphingolipids in inflammation: pathological implications and potential therapeutic targets.* Br J Pharmacol, 2009. **158**(4): p. 982-93.
41. Mencarelli, C. and P. Martinez-Martinez, *Ceramide function in the brain: when a slight tilt is enough.* Cell Mol Life Sci, 2013. **70**(2): p. 181-203.

42. Puranam, K., et al., *Upregulation of Bcl-2 and elevation of ceramide in Batten disease.* Neuropediatrics, 1997. **28**(1): p. 37-41.
43. Brunkhorst, R., R. Vutukuri, and W. Pfeilschifter, *Fingolimod for the treatment of neurological diseases-state of play and future perspectives.* Front Cell Neurosci, 2014. **8**: p. 283.
44. Davies, L., K. Fassbender, and S. Walter, *Sphingolipids in neuroinflammation.* Handb Exp Pharmacol, 2013(216): p. 421-30.
45. Ogawa, Y., et al., *FcRgamma-dependent immune activation initiates astrogliosis during the asymptomatic phase of Sandhoff disease model mice.* Sci Rep, 2017. **7**: p. 40518.
46. Hong, Y.B., E.Y. Kim, and S.C. Jung, *Upregulation of proinflammatory cytokines in the fetal brain of the Gaucher mouse.* J Korean Med Sci, 2006. **21**(4): p. 733-8.
47. Farfel-Becker, T., et al., *Spatial and temporal correlation between neuron loss and neuroinflammation in a mouse model of neuronopathic Gaucher disease.* Hum Mol Genet, 2011. **20**(7): p. 1375-86.
48. Pereira, V.G., et al., *Evidence of lysosomal membrane permeabilization in mucopolysaccharidosis type I: rupture of calcium and proton homeostasis.* J Cell Physiol, 2010. **223**(2): p. 335-42.
49. Tschopp, J. and K. Schroder, *NLRP3 inflammasome activation: The convergence of multiple signalling pathways on ROS production?* Nat Rev Immunol, 2010. **10**(3): p. 210-5.
50. Boustany, R.M., *Lysosomal storage diseases--the horizon expands.* Nat Rev Neurol, 2013. **9**(10): p. 583-98.
51. Vitner, E.B., F.M. Platt, and A.H. Futerman, *Common and uncommon pathogenic cascades in lysosomal storage diseases.* J Biol Chem, 2010. **285**(27): p. 20423-7.
52. Zundorf, G. and G. Reiser, *Calcium dysregulation and homeostasis of neural calcium in the molecular mechanisms of neurodegenerative diseases provide multiple targets for neuroprotection.* Antioxid Redox Signal, 2011. **14**(7): p. 1275-88.
53. Sama, D.M. and C.M. Norris, *Calcium dysregulation and neuroinflammation: discrete and integrated mechanisms for age-related synaptic dysfunction.* Ageing Res Rev, 2013. **12**(4): p. 982-95.
54. Bronson, R.T., et al., *Motor neuron degeneration of mice is a model of neuronal ceroid lipofuscinosis (Batten's disease).* Ann Neurol, 1993. **33**(4): p. 381-5.
55. Doyle, K.M., et al., *Unfolded proteins and endoplasmic reticulum stress in neurodegenerative disorders.* J Cell Mol Med, 2011. **15**(10): p. 2025-39.
56. Vitner, E.B. and A.H. Futerman, *Neuronal forms of Gaucher disease.* Handb Exp Pharmacol, 2013(216): p. 405-19.
57. Salminen, A., et al., *ER stress in Alzheimer's disease: a novel neuronal trigger for inflammation and Alzheimer's pathology.* J Neuroinflammation, 2009. **6**: p. 41.
58. Pahl, H.L. and P.A. Baeuerle, *The ER-overload response: activation of NF-kappa B.* Trends Biochem Sci, 1997. **22**(2): p. 63-7.
59. Meares, G.P., et al., *PERK-dependent activation of JAK1 and STAT3 contributes to endoplasmic reticulum stress-induced inflammation.* Mol Cell Biol, 2014. **34**(20): p. 3911-25.
60. *Isolation of a novel gene underlying Batten disease, CLN3. The International Batten Disease Consortium.* Cell, 1995. **82**(6): p. 949-57.
61. Jalanko, A. and T. Braulke, *Neuronal ceroid lipofuscinoses.* Biochim Biophys Acta, 2009. **1793**(4): p. 697-709.

62. Schultz, M.L., et al., *Clarifying lysosomal storage diseases.* Trends Neurosci, 2011. **34**(8): p. 401-10.
63. Santorelli, F.M., et al., *Molecular epidemiology of childhood neuronal ceroid-lipofuscinosis in Italy.* Orphanet J Rare Dis, 2013. **8**: p. 19.
64. Kousi, M., A.E. Lehesjoki, and S.E. Mole, *Update of the mutation spectrum and clinical correlations of over 360 mutations in eight genes that underlie the neuronal ceroid lipofuscinoses.* Hum Mutat, 2012. **33**(1): p. 42-63.
65. Warrier, V., M. Vieira, and S.E. Mole, *Genetic basis and phenotypic correlations of the neuronal ceroid lipofusinoses.* Biochim Biophys Acta, 2013. **1832**(11): p. 1827-30.
66. Cooper, J.D., *Progress towards understanding the neurobiology of Batten disease or neuronal ceroid lipofuscinosis.* Curr Opin Neurol, 2003. **16**(2): p. 121-8.
67. Finn, R., A.D. Kovacs, and D.A. Pearce, *Altered sensitivity of cerebellar granule cells to glutamate receptor overactivation in the Cln3(Deltaex7/8)-knock-in mouse model of juvenile neuronal ceroid lipofuscinosis.* Neurochem Int, 2011. **58**(6): p. 648-55.
68. Mitchison, H.M., M.J. Lim, and J.D. Cooper, *Selectivity and types of cell death in the neuronal ceroid lipofuscinoses.* Brain Pathol, 2004. **14**(1): p. 86-96.
69. Anderson, G.W., H.H. Goebel, and A. Simonati, *Human pathology in NCL.* Biochim Biophys Acta, 2013. **1832**(11): p. 1807-26.
70. Dolisca, S.B., et al., *Batten disease: clinical aspects, molecular mechanisms, translational science, and future directions.* J Child Neurol, 2013. **28**(9): p. 1074-100.
71. Haltia, M., *The neuronal ceroid-lipofuscinoses.* J Neuropathol Exp Neurol, 2003. **62**(1): p. 1-13.
72. Williams, R.E., et al., *Diagnosis of the neuronal ceroid lipofuscinoses: an update.* Biochim Biophys Acta, 2006. **1762**(10): p. 865-72.
73. Bennett, M.J. and D. Rakheja, *The neuronal ceroid-lipofuscinoses.* Dev Disabil Res Rev, 2013. **17**(3): p. 254-9.
74. Aberg, L., et al., *Decreased striatal dopamine transporter density in JNCL patients with parkinsonian symptoms.* Neurology, 2000. **54**(5): p. 1069-74.
75. Wisniewski, K.E., I. Rapin, and J. Heaney-Kieras, *Clinico-pathological variability in the childhood neuronal ceroid-lipofuscinoses and new observations on glycoprotein abnormalities.* Am J Med Genet Suppl, 1988. **5**: p. 27-46.
76. Nita, D.A., S.E. Mole, and B.A. Minassian, *Neuronal ceroid lipofuscinoses.* Epileptic Disord, 2016. **18**(S2): p. 73-88.
77. Autti, T., et al., *MRI of neuronal ceroid lipofuscinosis. I. Cranial MRI of 30 patients with juvenile neuronal ceroid lipofuscinosis.* Neuroradiology, 1996. **38**(5): p. 476-82.
78. Tokola, A.M., et al., *Hippocampal volumes in juvenile neuronal ceroid lipofuscinosis: a longitudinal magnetic resonance imaging study.* Pediatr Neurol, 2014. **50**(2): p. 158-63.
79. Santavuori, P., et al., *Neuronal ceroid lipofuscinoses in childhood.* Suppl Clin Neurophysiol, 2000. **53**: p. 443-51.
80. Carcel-Trullols, J., A.D. Kovacs, and D.A. Pearce, *Cell biology of the NCL proteins: What they do and don't do.* Biochim Biophys Acta, 2015. **1852**(10 Pt B): p. 2242-55.
81. Chan, C.H., H.M. Mitchison, and D.A. Pearce, *Transcript and in silico analysis of CLN3 in juvenile neuronal ceroid lipofuscinosis and associated mouse models.* Hum Mol Genet, 2008. **17**(21): p. 3332-9.
82. Palmer, D.N., et al., *Mitochondrial ATP synthase subunit c storage in the ceroid-lipofuscinoses (Batten disease).* Am J Med Genet, 1992. **42**(4): p. 561-7.

83. Conradi, N.G., et al., *First-trimester diagnosis of juvenile neuronal ceroid lipofuscinosis by demonstration of fingerprint inclusions in chorionic villi.* Prenat Diagn, 1989. **9**(4): p. 283-7.
84. Santavuori, P., S.L. Vanhanen, and T. Autti, *Clinical and neuroradiological diagnostic aspects of neuronal ceroid lipofuscinoses disorders.* Eur J Paediatr Neurol, 2001. **5 Suppl A**: p. 157-61.
85. Ezaki, J., et al., *Characterization of Cln3p, the gene product responsible for juvenile neuronal ceroid lipofuscinosis, as a lysosomal integral membrane glycoprotein.* J Neurochem, 2003. **87**(5): p. 1296-308.
86. Kyttala, A., et al., *Functional biology of the neuronal ceroid lipofuscinoses (NCL) proteins.* Biochim Biophys Acta, 2006. **1762**(10): p. 920-33.
87. Nugent, T., S.E. Mole, and D.T. Jones, *The transmembrane topology of Batten disease protein CLN3 determined by consensus computational prediction constrained by experimental data.* FEBS Lett, 2008. **582**(7): p. 1019-24.
88. Cooper, J.D., M.A. Tarczyluk, and H.R. Nelvagal, *Towards a new understanding of NCL pathogenesis.* Biochim Biophys Acta, 2015. **1852**(10 Pt B): p. 2256-61.
89. Chandrachud, U., et al., *Unbiased Cell-based Screening in a Neuronal Cell Model of Batten Disease Highlights an Interaction between Ca2+ Homeostasis, Autophagy, and CLN3 Protein Function.* J Biol Chem, 2015. **290**(23): p. 14361-80.
90. Chang, J.W., et al., *Neuronal vulnerability of CLN3 deletion to calcium-induced cytotoxicity is mediated by calsenilin.* Hum Mol Genet, 2007. **16**(3): p. 317-26.
91. Fossale, E., et al., *Membrane trafficking and mitochondrial abnormalities precede subunit c deposition in a cerebellar cell model of juvenile neuronal ceroid lipofuscinosis.* BMC Neurosci, 2004. **5**: p. 57.
92. Ramirez-Montealegre, D. and D.A. Pearce, *Defective lysosomal arginine transport in juvenile Batten disease.* Hum Mol Genet, 2005. **14**(23): p. 3759-73.
93. Botstein, D. and G.R. Fink, *Yeast: an experimental organism for 21st Century biology.* Genetics, 2011. **189**(3): p. 695-704.
94. Gachet, Y., et al., *btn1, the Schizosaccharomyces pombe homologue of the human Batten disease gene CLN3, regulates vacuole homeostasis.* J Cell Sci, 2005. **118**(Pt 23): p. 5525-36.
95. Pearce, D.A. and F. Sherman, *A yeast model for the study of Batten disease.* Proc Natl Acad Sci U S A, 1998. **95**(12): p. 6915-8.
96. Codlin, S., R.L. Haines, and S.E. Mole, *btn1 affects endocytosis, polarization of sterol-rich membrane domains and polarized growth in Schizosaccharomyces pombe.* Traffic, 2008. **9**(6): p. 936-50.
97. Kim, Y., D. Ramirez-Montealegre, and D.A. Pearce, *A role in vacuolar arginine transport for yeast Btn1p and for human CLN3, the protein defective in Batten disease.* Proc Natl Acad Sci U S A, 2003. **100**(26): p. 15458-62.
98. Pears, M.R., et al., *Deletion of btn1, an orthologue of CLN3, increases glycolysis and perturbs amino acid metabolism in the fission yeast model of Batten disease.* Mol Biosyst, 2010. **6**(6): p. 1093-102.
99. Vitiello, S.P., et al., *Interaction between Sdo1p and Btn1p in the Saccharomyces cerevisiae model for Batten disease.* Hum Mol Genet, 2010. **19**(5): p. 931-42.
100. Cotman, S.L., et al., *Cln3(Deltaex7/8) knock-in mice with the common JNCL mutation exhibit progressive neurologic disease that begins before birth.* Hum Mol Genet, 2002. **11**(22): p. 2709-21.

101. Mitchison, H.M., et al., *Targeted disruption of the Cln3 gene provides a mouse model for Batten disease. The Batten Mouse Model Consortium [corrected].* Neurobiol Dis, 1999. **6**(5): p. 321-34.
102. Staropoli, J.F., et al., *Large-scale phenotyping of an accurate genetic mouse model of JNCL identifies novel early pathology outside the central nervous system.* PLoS One, 2012. **7**(6): p. e38310.
103. Kovacs, A.D. and D.A. Pearce, *Finding the most appropriate mouse model of juvenile CLN3 (Batten) disease for therapeutic studies: the importance of genetic background and gender.* Dis Model Mech, 2015. **8**(4): p. 351-61.
104. Pears, M.R., et al., *High resolution 1H NMR-based metabolomics indicates a neurotransmitter cycling deficit in cerebral tissue from a mouse model of Batten disease.* J Biol Chem, 2005. **280**(52): p. 42508-14.
105. Seigel, G.M., et al., *Retinal pathology and function in a Cln3 knockout mouse model of juvenile Neuronal Ceroid Lipofuscinosis (batten disease).* Mol Cell Neurosci, 2002. **19**(4): p. 515-27.
106. Osorio, N.S., et al., *Neurodevelopmental delay in the Cln3Deltaex7/8 mouse model for Batten disease.* Genes Brain Behav, 2009. **8**(3): p. 337-45.
107. Rock, R.B., et al., *Role of microglia in central nervous system infections.* Clin Microbiol Rev, 2004. **17**(4): p. 942-64, table of contents.
108. Schafer, D.P., et al., *Microglia sculpt postnatal neural circuits in an activity and complement-dependent manner.* Neuron, 2012. **74**(4): p. 691-705.
109. Stevens, B., et al., *The classical complement cascade mediates CNS synapse elimination.* Cell, 2007. **131**(6): p. 1164-78.
110. Thundyil, J. and K.L. Lim, *DAMPs and Neurodegeneration.* Ageing Res Rev, 2014.
111. Hanke, M.L. and T. Kielian, *Toll-like receptors in health and disease in the brain: mechanisms and therapeutic potential.* Clin Sci (Lond), 2011. **121**(9): p. 367-87.
112. Amor, S., et al., *Inflammation in neurodegenerative diseases--an update.* Immunology, 2014. **142**(2): p. 151-66.
113. Perry, V.H., J.A. Nicoll, and C. Holmes, *Microglia in neurodegenerative disease.* Nat Rev Neurol, 2010. **6**(4): p. 193-201.
114. Suzumura, A., *Neuron-microglia interaction in neuroinflammation.* Curr Protein Pept Sci, 2013. **14**(1): p. 16-20.
115. ElAli, A. and S. Rivest, *Microglia Ontology and Signaling.* Front Cell Dev Biol, 2016. **4**: p. 72.
116. Kuno, R., et al., *Autocrine activation of microglia by tumor necrosis factor-alpha.* J Neuroimmunol, 2005. **162**(1-2): p. 89-96.
117. Vezzani, A. and B. Viviani, *Neuromodulatory properties of inflammatory cytokines and their impact on neuronal excitability.* Neuropharmacology, 2015. **96**(Pt A): p. 70-82.
118. Morris, G.P., et al., *Microglia: a new frontier for synaptic plasticity, learning and memory, and neurodegenerative disease research.* Neurobiol Learn Mem, 2013. **105**: p. 40-53.
119. Spittau, B., *Aging Microglia-Phenotypes, Functions and Implications for Age-Related Neurodegenerative Diseases.* Front Aging Neurosci, 2017. **9**: p. 194.
120. Tyynela, J., et al., *Hippocampal pathology in the human neuronal ceroid-lipofuscinoses: distinct patterns of storage deposition, neurodegeneration and glial activation.* Brain Pathol, 2004. **14**(4): p. 349-57.

121. Hanamsagar, R., V. Torres, and T. Kielian, *Inflammasome activation and IL-1beta/IL-18 processing are influenced by distinct pathways in microglia.* J Neurochem, 2011. **119**(4): p. 736-48.
122. von Bernhardi, R., L. Eugenin-von Bernhardi, and J. Eugenin, *Microglial cell dysregulation in brain aging and neurodegeneration.* Front Aging Neurosci, 2015. **7**: p. 124.
123. Xiong, J. and T. Kielian, *Microglia in juvenile neuronal ceroid lipofuscinosis are primed toward a pro-inflammatory phenotype.* J Neurochem, 2013. **127**(2): p. 245-58.
124. Haydon, P.G. and M. Nedergaard, *How do astrocytes participate in neural plasticity?* Cold Spring Harb Perspect Biol, 2015. **7**(3): p. a020438.
125. Verkhratsky, A., M. Nedergaard, and L. Hertz, *Why are astrocytes important?* Neurochem Res, 2015. **40**(2): p. 389-401.
126. Verkhratsky, A. and V. Parpura, *Astrogliopathology in neurological, neurodevelopmental and psychiatric disorders.* Neurobiol Dis, 2015.
127. Clarke, L.E. and B.A. Barres, *Emerging roles of astrocytes in neural circuit development.* Nat Rev Neurosci, 2013. **14**(5): p. 311-21.
128. Nedergaard, M., B. Ransom, and S.A. Goldman, *New roles for astrocytes: redefining the functional architecture of the brain.* Trends Neurosci, 2003. **26**(10): p. 523-30.
129. Belanger, M., I. Allaman, and P.J. Magistretti, *Brain energy metabolism: focus on astrocyte-neuron metabolic cooperation.* Cell Metab, 2011. **14**(6): p. 724-38.
130. Nielsen, S., et al., *Specialized membrane domains for water transport in glial cells: high-resolution immunogold cytochemistry of aquaporin-4 in rat brain.* J Neurosci, 1997. **17**(1): p. 171-80.
131. Takano, T., et al., *Astrocyte-mediated control of cerebral blood flow.* Nat Neurosci, 2006. **9**(2): p. 260-7.
132. Zielke, H.R., C.L. Zielke, and P.J. Baab, *Direct measurement of oxidative metabolism in the living brain by microdialysis: a review.* J Neurochem, 2009. **109 Suppl 1**: p. 24-9.
133. Pellerin, L. and P.J. Magistretti, *Glutamate uptake into astrocytes stimulates aerobic glycolysis: a mechanism coupling neuronal activity to glucose utilization.* Proc Natl Acad Sci U S A, 1994. **91**(22): p. 10625-9.
134. Allen, N.J., *Astrocyte regulation of synaptic behavior.* Annu Rev Cell Dev Biol, 2014. **30**: p. 439-63.
135. Halassa, M.M., T. Fellin, and P.G. Haydon, *The tripartite synapse: roles for gliotransmission in health and disease.* Trends Mol Med, 2007. **13**(2): p. 54-63.
136. Danbolt, N.C., *Glutamate uptake.* Prog Neurobiol, 2001. **65**(1): p. 1-105.
137. Fonnum, F., *Glutamate: a neurotransmitter in mammalian brain.* J Neurochem, 1984. **42**(1): p. 1-11.
138. Sofroniew, M.V. and H.V. Vinters, *Astrocytes: biology and pathology.* Acta Neuropathol, 2010. **119**(1): p. 7-35.
139. Beart, P.M. and R.D. O'Shea, *Transporters for L-glutamate: an update on their molecular pharmacology and pathological involvement.* Br J Pharmacol, 2007. **150**(1): p. 5-17.
140. Attwell, D. and S.B. Laughlin, *An energy budget for signaling in the grey matter of the brain.* J Cereb Blood Flow Metab, 2001. **21**(10): p. 1133-45.
141. McKenna, M.C., *Glutamate pays its own way in astrocytes.* Front Endocrinol (Lausanne), 2013. **4**: p. 191.
142. McKenna, M.C., *The glutamate-glutamine cycle is not stoichiometric: fates of glutamate in brain.* J Neurosci Res, 2007. **85**(15): p. 3347-58.
143. Blot, A., et al., *Functional expression of two system A glutamine transporter isoforms in rat auditory brainstem neurons.* Neuroscience, 2009. **164**(3): p. 998-1008.

144. Solbu, T.T., et al., *SAT1, A Glutamine Transporter, is Preferentially Expressed in GABAergic Neurons.* Front Neuroanat, 2010. **4**: p. 1.
145. Dienel, G.A., *Astrocytic energetics during excitatory neurotransmission: What are contributions of glutamate oxidation and glycolysis?* Neurochem Int, 2013. **63**(4): p. 244-58.
146. Assous, M., et al., *Progressive Parkinsonism by acute dysfunction of excitatory amino acid transporters in the rat substantia nigra.* Neurobiol Dis, 2014. **65**: p. 69-81.
147. Kulijewicz-Nawrot, M., et al., *Astrocytes and glutamate homoeostasis in Alzheimer's disease: a decrease in glutamine synthetase, but not in glutamate transporter-1, in the prefrontal cortex.* ASN Neuro, 2013. **5**(4): p. 273-82.
148. van der Hel, W.S., et al., *Reduced glutamine synthetase in hippocampal areas with neuron loss in temporal lobe epilepsy.* Neurology, 2005. **64**(2): p. 326-33.
149. Dong, Y. and E.N. Benveniste, *Immune function of astrocytes.* Glia, 2001. **36**(2): p. 180-90.
150. Farina, C., F. Aloisi, and E. Meinl, *Astrocytes are active players in cerebral innate immunity.* Trends Immunol, 2007. **28**(3): p. 138-45.
151. Nagai, M., et al., *Astrocytes expressing ALS-linked mutated SOD1 release factors selectively toxic to motor neurons.* Nat Neurosci, 2007. **10**(5): p. 615-22.
152. Radford, R.A., et al., *The established and emerging roles of astrocytes and microglia in amyotrophic lateral sclerosis and frontotemporal dementia.* Front Cell Neurosci, 2015. **9**: p. 414.
153. Robel, S. and H. Sontheimer, *Glia as drivers of abnormal neuronal activity.* Nat Neurosci, 2016. **19**(1): p. 28-33.
154. Robel, S., et al., *Conditional deletion of beta1-integrin in astroglia causes partial reactive gliosis.* Glia, 2009. **57**(15): p. 1630-47.
155. DiRosario, J., et al., *Innate and adaptive immune activation in the brain of MPS IIIB mouse model.* J Neurosci Res, 2009. **87**(4): p. 978-90.
156. Karpuk, N., et al., *Neuroinflammation leads to region-dependent alterations in astrocyte gap junction communication and hemichannel activity.* J Neurosci, 2011. **31**(2): p. 414-25.
157. Orellana, J.A., et al., *Amyloid beta-induced death in neurons involves glial and neuronal hemichannels.* J Neurosci, 2011. **31**(13): p. 4962-77.
158. Burkovetskaya, M., N. Karpuk, and T. Kielian, *Age-dependent alterations in neuronal activity in the hippocampus and visual cortex in a mouse model of Juvenile Neuronal Ceroid Lipofuscinosis (CLN3).* Neurobiol Dis, 2017. **100**: p. 19-29.
159. Burkovetskaya, M., Karpuk, N, Xiong, J, Bosch M, Boska, M, Takeuchi, H, Suzumur,A, and Kielian, T, *Evidence for aberrant astrocyte hemichannel activity in Juvenile Neuronal Ceroid Lipofuscinosis (JNCL).* PLoS One, 2014.
160. Bosch, M. and T. Kielian, *Hemichannels in neurodegenerative diseases: is there a link to pathology?* Front Cell Neurosci, 2014. **8**: p. 242.
161. Herculano-Houzel, S., *The human brain in numbers: a linearly scaled-up primate brain.* Front Hum Neurosci, 2009. **3**: p. 31.
162. Lodish H, B.A., Zipursky SL, et al., *Overview of Neuron Structure and Function*, in *Molecular Cell Biology*. 2000, W. H. Freeman: New York.
163. Disorders., F.o.N.a.N.S., *Glutamate-Related Biomarkers in Drug Development for Disorders of the Nervous System: Workshop Summary.* 2011.
164. Goebel, H.H. and K.E. Wisniewski, *Current state of clinical and morphological features in human NCL.* Brain Pathol, 2004. **14**(1): p. 61-9.

165. Wilkinson, F.L., et al., *Neuropathology in mouse models of mucopolysaccharidosis type I, IIIA and IIIB.* PLoS One, 2012. **7**(4): p. e35787.
166. Chattopadhyay, S., et al., *An autoantibody inhibitory to glutamic acid decarboxylase in the neurodegenerative disorder Batten disease.* Hum Mol Genet, 2002. **11**(12): p. 1421-31.
167. Mitoma, H., M. Manto, and C.S. Hampe, *Pathogenic Roles of Glutamic Acid Decarboxylase 65 Autoantibodies in Cerebellar Ataxias.* J Immunol Res, 2017. **2017**: p. 2913297.
168. Kielar, C., et al., *Molecular correlates of axonal and synaptic pathology in mouse models of Batten disease.* Hum Mol Genet, 2009. **18**(21): p. 4066-80.
169. Archer, L.D., et al., *Mucopolysaccharide diseases: a complex interplay between neuroinflammation, microglial activation and adaptive immunity.* J Inherit Metab Dis, 2014. **37**(1): p. 1-12.
170. Williams, I.M., et al., *Improved neuroprotection using miglustat, curcumin and ibuprofen as a triple combination therapy in Niemann-Pick disease type C1 mice.* Neurobiol Dis, 2014. **67**: p. 9-17.
171. Wraith, J.E., *The mucopolysaccharidoses: a clinical review and guide to management.* Arch Dis Child, 1995. **72**(3): p. 263-7.
172. Bosch, M.E. and T. Kielian, *Neuroinflammatory paradigms in lysosomal storage diseases.* Front Neurosci, 2015. **9**: p. 417.
173. David, K.M., et al., *Mycophenolate mofetil vs. azathioprine is associated with decreased acute rejection, late acute rejection, and risk for cardiovascular death in renal transplant recipients with pre-transplant diabetes.* Clin Transplant, 2005. **19**(2): p. 279-85.
174. Duncan, M.D. and D.S. Wilkes, *Transplant-related immunosuppression: a review of immunosuppression and pulmonary infections.* Proc Am Thorac Soc, 2005. **2**(5): p. 449-55.
175. FDA. *CellCept (Mycophenolate Mofetil)*. 2001; Available from: https://www.accessdata.fda.gov/drugsatfda_docs/nda/2000/50-722S007_CellCept.cfm.
176. Seehafer, S.S., et al., *Immunosuppression alters disease severity in juvenile Batten disease mice.* J Neuroimmunol, 2011. **230**(1-2): p. 169-72.
177. Augustine, E., *Cellcept for Treatment of Juvenile Neuronal Ceroid Lipofuscinosis (JUMP)*, U.o. Rochester, Editor. 2011.
178. Bennett, L.L. and D. Mohan, *Gaucher disease and its treatment options.* Ann Pharmacother, 2013. **47**(9): p. 1182-93.
179. Conti, M. and J. Beavo, *Biochemistry and physiology of cyclic nucleotide phosphodiesterases: essential components in cyclic nucleotide signaling.* Annu Rev Biochem, 2007. **76**: p. 481-511.
180. Azevedo, M.F., et al., *Clinical and molecular genetics of the phosphodiesterases (PDEs).* Endocr Rev, 2014. **35**(2): p. 195-233.
181. Sette, C. and M. Conti, *Phosphorylation and activation of a cAMP-specific phosphodiesterase by the cAMP-dependent protein kinase. Involvement of serine 54 in the enzyme activation.* J Biol Chem, 1996. **271**(28): p. 16526-34.
182. Davis, R.L., et al., *The cyclic AMP system and Drosophila learning.* Mol Cell Biochem, 1995. **149-150**: p. 271-8.
183. Kandel, E.R., *The molecular biology of memory: cAMP, PKA, CRE, CREB-1, CREB-2, and CPEB.* Mol Brain, 2012. **5**: p. 14.
184. Lee, D., *Global and local missions of cAMP signaling in neural plasticity, learning, and memory.* Front Pharmacol, 2015. **6**: p. 161.

185. Atkins, C.M., et al., *Modulation of the cAMP signaling pathway after traumatic brain injury.* Exp Neurol, 2007. **208**(1): p. 145-58.
186. Nikulina, E., et al., *The phosphodiesterase inhibitor rolipram delivered after a spinal cord lesion promotes axonal regeneration and functional recovery.* Proc Natl Acad Sci U S A, 2004. **101**(23): p. 8786-90.
187. Oliva, A.A., Jr., et al., *Phosphodiesterase isoform-specific expression induced by traumatic brain injury.* J Neurochem, 2012. **123**(6): p. 1019-29.
188. Beavo, J.A., M. Conti, and R.J. Heaslip, *Multiple cyclic nucleotide phosphodiesterases.* Mol Pharmacol, 1994. **46**(3): p. 399-405.
189. Conti, M. and S.L. Jin, *The molecular biology of cyclic nucleotide phosphodiesterases.* Prog Nucleic Acid Res Mol Biol, 1999. **63**: p. 1-38.
190. Gong, B., et al., *Persistent improvement in synaptic and cognitive functions in an Alzheimer mouse model after rolipram treatment.* J Clin Invest, 2004. **114**(11): p. 1624-34.
191. (NIA), N.I.o.A., *NCT00017940.* Gene Therapy for Alzheimer's Disease Clinical Trial, 2001.
192. Gadalla, K.K., et al., *Improved survival and reduced phenotypic severity following AAV9/MECP2 gene transfer to neonatal and juvenile male Mecp2 knockout mice.* Mol Ther, 2013. **21**(1): p. 18-30.
193. Garg, S.K., et al., *Systemic delivery of MeCP2 rescues behavioral and cellular deficits in female mouse models of Rett syndrome.* J Neurosci, 2013. **33**(34): p. 13612-20.
194. Meyer, K., et al., *Improving single injection CSF delivery of AAV9-mediated gene therapy for SMA: a dose-response study in mice and nonhuman primates.* Mol Ther, 2015. **23**(3): p. 477-87.
195. Rastall, D.P. and A. Amalfitano, *Recent advances in gene therapy for lysosomal storage disorders.* Appl Clin Genet, 2015. **8**: p. 157-69.
196. Choi, K.H., *Viral polymerases.* Adv Exp Med Biol, 2012. **726**: p. 267-304.
197. Sands, M.S. and B.L. Davidson, *Gene therapy for lysosomal storage diseases.* Mol Ther, 2006. **13**(5): p. 839-49.
198. Elsner, C. and J. Bohne, *The retroviral vector family: something for everyone.* Virus Genes, 2017.
199. Trabalza, A., et al., *Enhanced central nervous system transduction with lentiviral vectors pseudotyped with RVG/HIV-1gp41 chimeric envelope glycoproteins.* J Virol, 2014. **88**(5): p. 2877-90.
200. Henckaerts, E. and R.M. Linden, *Adeno-associated virus: a key to the human genome?* Future Virol, 2010. **5**(5): p. 555-574.
201. Naso, M.F., et al., *Adeno-Associated Virus (AAV) as a Vector for Gene Therapy.* BioDrugs, 2017.
202. Nathwani, A.C., et al., *Adenovirus-associated virus vector-mediated gene transfer in hemophilia B.* N Engl J Med, 2011. **365**(25): p. 2357-65.
203. Cearley, C.N. and J.H. Wolfe, *Transduction characteristics of adeno-associated virus vectors expressing cap serotypes 7, 8, 9, and Rh10 in the mouse brain.* Mol Ther, 2006. **13**(3): p. 528-37.
204. Foust, K.D., et al., *Intravascular AAV9 preferentially targets neonatal neurons and adult astrocytes.* Nat Biotechnol, 2009. **27**(1): p. 59-65.
205. Gao, G., et al., *Clades of Adeno-associated viruses are widely disseminated in human tissues.* J Virol, 2004. **78**(12): p. 6381-8.
206. Akache, B., et al., *The 37/67-kilodalton laminin receptor is a receptor for adeno-associated virus serotypes 8, 2, 3, and 9.* J Virol, 2006. **80**(19): p. 9831-6.

207. Daya, S. and K.I. Berns, *Gene therapy using adeno-associated virus vectors.* Clin Microbiol Rev, 2008. **21**(4): p. 583-93.
208. Wang, J., et al., *Existence of transient functional double-stranded DNA intermediates during recombinant AAV transduction.* Proc Natl Acad Sci U S A, 2007. **104**(32): p. 13104-9.
209. McCarty, D.M., *Self-complementary AAV vectors; advances and applications.* Mol Ther, 2008. **16**(10): p. 1648-56.
210. Saraiva, J., R.J. Nobre, and L. Pereira de Almeida, *Gene therapy for the CNS using AAVs: The impact of systemic delivery by AAV9.* J Control Release, 2016. **241**: p. 94-109.
211. Kondo, M.Y., et al., *Analysis of catalytic properties of tripeptidyl peptidase I (TTP-I), a serine carboxyl lysosomal protease, and its detection in tissue extracts using selective FRET peptide substrate.* Peptides, 2016. **76**: p. 80-6.
212. Wang, R., et al., *Identification of palmitoyl protein thioesterase 1 in human THP1 monocytes and macrophages and characterization of unique biochemical activities for this enzyme.* Biochemistry, 2013. **52**(43): p. 7559-74.
213. Passini, M.A., et al., *Intracranial delivery of CLN2 reduces brain pathology in a mouse model of classical late infantile neuronal ceroid lipofuscinosis.* J Neurosci, 2006. **26**(5): p. 1334-42.
214. Haskell, R.E., et al., *Viral-mediated delivery of the late-infantile neuronal ceroid lipofuscinosis gene, TPP-I to the mouse central nervous system.* Gene Ther, 2003. **10**(1): p. 34-42.
215. Michalewski, M.P., et al., *Evidence for phosphorylation of CLN3 protein associated with Batten disease.* Biochem Biophys Res Commun, 1998. **253**(2): p. 458-62.
216. Eliason, S.L., et al., *A knock-in reporter model of Batten disease.* J Neurosci, 2007. **27**(37): p. 9826-34.
217. Hocquemiller, M., et al., *Adeno-Associated Virus-Based Gene Therapy for CNS Diseases.* Hum Gene Ther, 2016. **27**(7): p. 478-96.
218. Calcedo, R., et al., *Worldwide epidemiology of neutralizing antibodies to adeno-associated viruses.* J Infect Dis, 2009. **199**(3): p. 381-90.
219. Sondhi, D., et al., *Partial correction of the CNS lysosomal storage defect in a mouse model of juvenile neuronal ceroid lipofuscinosis by neonatal CNS administration of an adeno-associated virus serotype rh.10 vector expressing the human CLN3 gene.* Hum Gene Ther, 2014. **25**(3): p. 223-39.
220. Krause, W. and G. Kuhne, *Pharmacokinetics of rolipram in the rhesus and cynomolgus monkeys, the rat and the rabbit. Studies on species differences.* Xenobiotica, 1988. **18**(5): p. 561-71.
221. Hatzelmann, A., et al., *The preclinical pharmacology of roflumilast--a selective, oral phosphodiesterase 4 inhibitor in development for chronic obstructive pulmonary disease.* Pulm Pharmacol Ther, 2010. **23**(4): p. 235-56.
222. Rabe, K.F., *Update on roflumilast, a phosphodiesterase 4 inhibitor for the treatment of chronic obstructive pulmonary disease.* Br J Pharmacol, 2011. **163**(1): p. 53-67.
223. Hedde, J., et al., *The phosphodiesterase-4 inhibitor, ABI-4, attenuates the increases in brain cytokines and translocator protein binding caused by lipopolysaccharide.* Schizophrenia Bulletin, 2015. **41**(Supplement 1): p. S1-S341.
224. Landis, S.C., et al., *A call for transparent reporting to optimize the predictive value of preclinical research.* Nature, 2012. **490**(7419): p. 187-91.
225. Geifman, N. and E. Rubin, *The mouse age phenome knowledgebase and disease-specific inter-species age mapping.* PLoS One, 2013. **8**(12): p. e81114.

226. Lee, J.H., et al., *Rhes suppression enhances disease phenotypes in Huntington's disease mice.* J Huntingtons Dis, 2014. **3**(1): p. 65-71.
227. Burkovetskaya, M., et al., *Evidence for aberrant astrocyte hemichannel activity in Juvenile Neuronal Ceroid Lipofuscinosis (JNCL).* PLoS One, 2014. **9**(4): p. e95023.
228. Adachi, M., E.W. Keefer, and F.S. Jones, *A segment of the Mecp2 promoter is sufficient to drive expression in neurons.* Hum Mol Genet, 2005. **14**(23): p. 3709-22.
229. Costes, S.V., et al., *Automatic and quantitative measurement of protein-protein colocalization in live cells.* Biophys J, 2004. **86**(6): p. 3993-4003.
230. Banovic, D., et al., *Drosophila neuroligin 1 promotes growth and postsynaptic differentiation at glutamatergic neuromuscular junctions.* Neuron, 2010. **66**(5): p. 724-38.
231. Vidal-Donet, J.M., et al., *Alterations in ROS activity and lysosomal pH account for distinct patterns of macroautophagy in LINCL and JNCL fibroblasts.* PLoS One, 2013. **8**(2): p. e55526.
232. Rakheja, D., S.B. Narayan, and M.J. Bennett, *Juvenile neuronal ceroid-lipofuscinosis (Batten disease): a brief review and update.* Curr Mol Med, 2007. **7**(6): p. 603-8.
233. Williams, R.E. and S.E. Mole, *New nomenclature and classification scheme for the neuronal ceroid lipofuscinoses.* Neurology, 2012. **79**(2): p. 183-91.
234. Getty, A.L. and D.A. Pearce, *Interactions of the proteins of neuronal ceroid lipofuscinosis: clues to function.* Cell Mol Life Sci, 2011. **68**(3): p. 453-74.
235. Orellana, J.A., et al., *ATP and glutamate released via astroglial connexin 43 hemichannels mediate neuronal death through activation of pannexin 1 hemichannels.* J Neurochem, 2011. **118**(5): p. 826-40.
236. Kovacs, A.D. and D.A. Pearce, *Attenuation of AMPA receptor activity improves motor skills in a mouse model of juvenile Batten disease.* Exp Neurol, 2008. **209**(1): p. 288-91.
237. Sitter, B., et al., *High-resolution magic angle spinning and 1H magnetic resonance spectroscopy reveal significantly altered neuronal metabolite profiles in CLN1 but not in CLN3.* J Neurosci Res, 2004. **77**(5): p. 762-9.
238. Anzai, Y., et al., *Protracted juvenile neuronal ceroid lipofuscinosis--an autopsy report and immunohistochemical analysis.* Brain Dev, 2006. **28**(7): p. 462-5.
239. Stobart, J.L. and C.M. Anderson, *Multifunctional role of astrocytes as gatekeepers of neuronal energy supply.* Front Cell Neurosci, 2013. **7**: p. 38.
240. Eid, T., et al., *Loss of glutamine synthetase in the human epileptogenic hippocampus: possible mechanism for raised extracellular glutamate in mesial temporal lobe epilepsy.* Lancet, 2004. **363**(9402): p. 28-37.
241. Vercellino, M., et al., *Altered glutamate reuptake in relapsing-remitting and secondary progressive multiple sclerosis cortex: correlation with microglia infiltration, demyelination, and neuronal and synaptic damage.* J Neuropathol Exp Neurol, 2007. **66**(8): p. 732-9.
242. Byun, K., et al., *Alteration of the glutamate and GABA transporters in the hippocampus of the Niemann-Pick disease, type C mouse using proteomic analysis.* Proteomics, 2006. **6**(4): p. 1230-6.
243. Eroglu, C. and B.A. Barres, *Regulation of synaptic connectivity by glia.* Nature, 2010. **468**(7321): p. 223-31.
244. Li, D., et al., *New tools for investigating astrocyte-to-neuron communication.* Front Cell Neurosci, 2013. **7**: p. 193.
245. Ullian, E.M., et al., *Control of synapse number by glia.* Science, 2001. **291**(5504): p. 657-61.

246. Bazargani, N. and D. Attwell, *Astrocyte calcium signaling: the third wave.* Nat Neurosci, 2016. **19**(2): p. 182-9.
247. Scemes, E. and C. Giaume, *Astrocyte calcium waves: what they are and what they do.* Glia, 2006. **54**(7): p. 716-25.
248. Manning, T.J., Jr. and H. Sontheimer, *Spontaneous intracellular calcium oscillations in cortical astrocytes from a patient with intractable childhood epilepsy (Rasmussen's encephalitis).* Glia, 1997. **21**(3): p. 332-7.
249. Seifert, G., K. Schilling, and C. Steinhauser, *Astrocyte dysfunction in neurological disorders: a molecular perspective.* Nat Rev Neurosci, 2006. **7**(3): p. 194-206.
250. Dani, J.W., A. Chernjavsky, and S.J. Smith, *Neuronal activity triggers calcium waves in hippocampal astrocyte networks.* Neuron, 1992. **8**(3): p. 429-40.
251. Volterra, A., N. Liaudet, and I. Savtchouk, *Astrocyte Ca(2)(+) signalling: an unexpected complexity.* Nat Rev Neurosci, 2014. **15**(5): p. 327-35.
252. Mashimo, M., et al., *Inositol 1,4,5-trisphosphate signaling maintains the activity of glutamate uptake in Bergmann glia.* Eur J Neurosci, 2010. **32**(10): p. 1668-77.
253. Stephen, T.L., S. Gupta-Agarwal, and J.T. Kittler, *Mitochondrial dynamics in astrocytes.* Biochem Soc Trans, 2014. **42**(5): p. 1302-10.
254. Wang, F., et al., *Astrocytes modulate neural network activity by Ca(2)+-dependent uptake of extracellular K+.* Sci Signal, 2012. **5**(218): p. ra26.
255. Allaman, I., M. Belanger, and P.J. Magistretti, *Methylglyoxal, the dark side of glycolysis.* Front Neurosci, 2015. **9**: p. 23.
256. Cao, Y., et al., *Distinct early molecular responses to mutations causing vLINCL and JNCL presage ATP synthase subunit C accumulation in cerebellar cells.* PLoS One, 2011. **6**(2): p. e17118.
257. Hong, M., et al., *Fibrates inhibit the apoptosis of Batten disease lymphoblast cells via autophagy recovery and regulation of mitochondrial membrane potential.* In Vitro Cell Dev Biol Anim, 2016. **52**(3): p. 349-55.
258. Kang, S., et al., *Batten disease is linked to altered expression of mitochondria-related metabolic molecules.* Neurochem Int, 2013. **62**(7): p. 931-5.
259. Cao, Y., et al., *Autophagy is disrupted in a knock-in mouse model of juvenile neuronal ceroid lipofuscinosis.* J Biol Chem, 2006. **281**(29): p. 20483-93.
260. Ward, C., et al., *Autophagy, lipophagy and lysosomal lipid storage disorders.* Biochim Biophys Acta, 2016. **1861**(4): p. 269-84.
261. Kanai, Y. and M.A. Hediger, *The glutamate and neutral amino acid transporter family: physiological and pharmacological implications.* Eur J Pharmacol, 2003. **479**(1-3): p. 237-47.
262. Kim, K., et al., *Role of excitatory amino acid transporter-2 (EAAT2) and glutamate in neurodegeneration: opportunities for developing novel therapeutics.* J Cell Physiol, 2011. **226**(10): p. 2484-93.
263. Kovacs, A.D., et al., *Age-dependent therapeutic effect of memantine in a mouse model of juvenile Batten disease.* Neuropharmacology, 2012. **63**(5): p. 769-75.
264. Cavus, I., et al., *Elevated basal glutamate and unchanged glutamine and GABA in refractory epilepsy: Microdialysis study of 79 patients at the yale epilepsy surgery program.* Ann Neurol, 2016. **80**(1): p. 35-45.
265. Dzubay, J.A. and C.E. Jahr, *The concentration of synaptically released glutamate outside of the climbing fiber-Purkinje cell synaptic cleft.* J Neurosci, 1999. **19**(13): p. 5265-74.
266. Herman, M.A. and C.E. Jahr, *Extracellular glutamate concentration in hippocampal slice.* J Neurosci, 2007. **27**(36): p. 9736-41.

267. Moussawi, K., et al., *Extracellular glutamate: functional compartments operate in different concentration ranges.* Front Syst Neurosci, 2011. **5**: p. 94.
268. Arundine, M. and M. Tymianski, *Molecular mechanisms of glutamate-dependent neurodegeneration in ischemia and traumatic brain injury.* Cell Mol Life Sci, 2004. **61**(6): p. 657-68.
269. Berdichevsky, E., et al., *Kainate, N-methylaspartate and other excitatory amino acids increase calcium influx into rat brain cortex cells in vitro.* Neurosci Lett, 1983. **36**(1): p. 75-80.
270. Mattson, M.P., *Calcium and neurodegeneration.* Aging Cell, 2007. **6**(3): p. 337-50.
271. Mole, S.E., H.M. Mitchison, and P.B. Munroe, *Molecular basis of the neuronal ceroid lipofuscinoses: mutations in CLN1, CLN2, CLN3, and CLN5.* Hum Mutat, 1999. **14**(3): p. 199-215.
272. Augustine, E.F., et al., *Standardized assessment of seizures in patients with juvenile neuronal ceroid lipofuscinosis.* Dev Med Child Neurol, 2015. **57**(4): p. 366-71.
273. Coulter, D.A. and T. Eid, *Astrocytic regulation of glutamate homeostasis in epilepsy.* Glia, 2012. **60**(8): p. 1215-26.
274. Rueda, C.B., et al., *Glutamate excitotoxicity and Ca2+-regulation of respiration: Role of the Ca2+ activated mitochondrial transporters (CaMCs).* Biochim Biophys Acta, 2016. **1857**(8): p. 1158-66.
275. Parpura, V., et al., *Glutamate-mediated astrocyte-neuron signalling.* Nature, 1994. **369**(6483): p. 744-7.
276. Munhoz, C.D., et al., *Stress-induced neuroinflammation: mechanisms and new pharmacological targets.* Braz J Med Biol Res, 2008. **41**(12): p. 1037-46.
277. Takaki, J., et al., *L-glutamate released from activated microglia downregulates astrocytic L-glutamate transporter expression in neuroinflammation: the 'collusion' hypothesis for increased extracellular L-glutamate concentration in neuroinflammation.* J Neuroinflammation, 2012. **9**: p. 275.
278. Vesce, S., et al., *Glutamate release from astrocytes in physiological conditions and in neurodegenerative disorders characterized by neuroinflammation.* Int Rev Neurobiol, 2007. **82**: p. 57-71.
279. Autti, T., et al., *Thalami and corona radiata in juvenile NCL (CLN3): a voxel-based morphometric study.* Eur J Neurol, 2007. **14**(4): p. 447-50.
280. Autti, T.H., et al., *JNCL patients show marked brain volume alterations on longitudinal MRI in adolescence.* J Neurol, 2008. **255**(8): p. 1226-30.
281. Brockmann, K., et al., *Localized proton magnetic resonance spectroscopy of cerebral metabolic disturbances in children with neuronal ceroid lipofuscinosis.* Neuropediatrics, 1996. **27**(5): p. 242-8.
282. Tawfik, V.L., et al., *Induction of astrocyte differentiation by propentofylline increases glutamate transporter expression in vitro: heterogeneity of the quiescent phenotype.* Glia, 2006. **54**(3): p. 193-203.
283. Mizuno, T., et al., *Neuroprotective role of phosphodiesterase inhibitor ibudilast on neuronal cell death induced by activated microglia.* Neuropharmacology, 2004. **46**(3): p. 404-11.
284. Nicol, X. and P. Gaspar, *Routes to cAMP: shaping neuronal connectivity with distinct adenylate cyclases.* Eur J Neurosci, 2014. **39**(11): p. 1742-51.
285. Francis, S.H., M.A. Blount, and J.D. Corbin, *Mammalian cyclic nucleotide phosphodiesterases: molecular mechanisms and physiological functions.* Physiol Rev, 2011. **91**(2): p. 651-90.

286. Sommer, N., et al., *Therapeutic potential of phosphodiesterase type 4 inhibition in chronic autoimmune demyelinating disease.* J Neuroimmunol, 1997. **79**(1): p. 54-61.
287. Pearse, D.D., et al., *cAMP and Schwann cells promote axonal growth and functional recovery after spinal cord injury.* Nat Med, 2004. **10**(6): p. 610-6.
288. Myeku, N., et al., *Tau-driven 26S proteasome impairment and cognitive dysfunction can be prevented early in disease by activating cAMP-PKA signaling.* Nat Med, 2016. **22**(1): p. 46-53.
289. Bosch, M.E., et al., *Self-Complementary AAV9 Gene Delivery Partially Corrects Pathology Associated with Juvenile Neuronal Ceroid Lipofuscinosis (CLN3).* J Neurosci, 2016. **36**(37): p. 9669-82.
290. Kovacs, A.D., et al., *Temporary inhibition of AMPA receptors induces a prolonged improvement of motor performance in a mouse model of juvenile Batten disease.* Neuropharmacology, 2011. **60**(2-3): p. 405-9.
291. Salek, R.M., et al., *A metabolomic comparison of mouse models of the Neuronal Ceroid Lipofuscinoses.* J Biomol NMR, 2011. **49**(3-4): p. 175-84.
292. Griswold, D.E., et al., *Effect of selective phosphodiesterase type IV inhibitor, rolipram, on fluid and cellular phases of inflammatory response.* Inflammation, 1993. **17**(3): p. 333-44.
293. Choi, C.H., et al., *Pharmacological reversal of synaptic plasticity deficits in the mouse model of fragile X syndrome by group II mGluR antagonist or lithium treatment.* Brain Res, 2011. **1380**: p. 106-19.
294. Tawfik, V.L., et al., *Propentofylline-induced astrocyte modulation leads to alterations in glial glutamate promoter activation following spinal nerve transection.* Neuroscience, 2008. **152**(4): p. 1086-92.
295. Meikle, P.J., et al., *Diagnosis of lysosomal storage disorders: evaluation of lysosome-associated membrane protein LAMP-1 as a diagnostic marker.* Clin Chem, 1997. **43**(8 Pt 1): p. 1325-35.
296. Usenovic, M., et al., *Deficiency of ATP13A2 leads to lysosomal dysfunction, alpha-synuclein accumulation, and neurotoxicity.* J Neurosci, 2012. **32**(12): p. 4240-6.
297. Ryazantsev, S., et al., *Lysosomal accumulation of SCMAS (subunit c of mitochondrial ATP synthase) in neurons of the mouse model of mucopolysaccharidosis III B.* Mol Genet Metab, 2007. **90**(4): p. 393-401.
298. Saftig, P., et al., *Mice deficient in lysosomal acid phosphatase develop lysosomal storage in the kidney and central nervous system.* J Biol Chem, 1997. **272**(30): p. 18628-35.
299. Rama Rao, K.V. and T. Kielian, *Neuron-astrocyte interactions in neurodegenerative diseases: Role of neuroinflammation.* Clin Exp Neuroimmunol, 2015. **6**(3): p. 245-263.
300. Menniti, F.S., W.S. Faraci, and C.J. Schmidt, *Phosphodiesterases in the CNS: targets for drug development.* Nat Rev Drug Discov, 2006. **5**(8): p. 660-70.
301. Neville, K.A., et al., *Single-dose pharmacokinetics of roflumilast in children and adolescents.* J Clin Pharmacol, 2008. **48**(8): p. 978-85.
302. Sato, T., et al., *Inhibitory effects of group II mGluR-related drugs on memory performance in mice.* Physiol Behav, 2004. **80**(5): p. 747-58.
303. Retamal, M.A., et al., *Cx43 hemichannels and gap junction channels in astrocytes are regulated oppositely by proinflammatory cytokines released from activated microglia.* J Neurosci, 2007. **27**(50): p. 13781-92.
304. Ostergaard, J.R., T.B. Rasmussen, and H. Molgaard, *Cardiac involvement in juvenile neuronal ceroid lipofuscinosis (Batten disease).* Neurology, 2011. **76**(14): p. 1245-51.

305. Omori, K. and J. Kotera, *Overview of PDEs and their regulation.* Circ Res, 2007. **100**(3): p. 309-27.
306. Castaneda, J.A. and D.A. Pearce, *Identification of alpha-fetoprotein as an autoantigen in juvenile Batten disease.* Neurobiol Dis, 2008. **29**(1): p. 92-102.
307. Westlake, V.J., et al., *Immunocytochemical studies in the ceroid-lipofuscinoses (Batten disease) using antibodies to subunit c of mitochondrial ATP synthase.* Am J Med Genet, 1995. **57**(2): p. 177-81.
308. Macauley, S.L., et al., *Synergistic effects of central nervous system-directed gene therapy and bone marrow transplantation in the murine model of infantile neuronal ceroid lipofuscinosis.* Ann Neurol, 2012. **71**(6): p. 797-804.
309. Duque, S., et al., *Intravenous administration of self-complementary AAV9 enables transgene delivery to adult motor neurons.* Mol Ther, 2009. **17**(7): p. 1187-96.
310. Acland, G.M., et al., *Long-term restoration of rod and cone vision by single dose rAAV-mediated gene transfer to the retina in a canine model of childhood blindness.* Mol Ther, 2005. **12**(6): p. 1072-82.
311. Foust, K.D., et al., *Therapeutic AAV9-mediated suppression of mutant SOD1 slows disease progression and extends survival in models of inherited ALS.* Mol Ther, 2013. **21**(12): p. 2148-59.
312. McCarty, D.M., P.E. Monahan, and R.J. Samulski, *Self-complementary recombinant adeno-associated virus (scAAV) vectors promote efficient transduction independently of DNA synthesis.* Gene Ther, 2001. **8**(16): p. 1248-54.
313. Aschauer, D.F., S. Kreuz, and S. Rumpel, *Analysis of transduction efficiency, tropism and axonal transport of AAV serotypes 1, 2, 5, 6, 8 and 9 in the mouse brain.* PLoS One, 2013. **8**(9): p. e76310.
314. Bemelmans, A.P., et al., *A single intravenous AAV9 injection mediates bilateral gene transfer to the adult mouse retina.* PLoS One, 2013. **8**(4): p. e61618.
315. Foust, K.D., et al., *Rescue of the spinal muscular atrophy phenotype in a mouse model by early postnatal delivery of SMN.* Nat Biotechnol, 2010. **28**(3): p. 271-4.
316. Palmer, D.N., et al., *NCL disease mechanisms.* Biochim Biophys Acta, 2013. **1832**(11): p. 1882-93.
317. Cheever, T.R., B. Li, and J.M. Ervasti, *Restricted morphological and behavioral abnormalities following ablation of beta-actin in the brain.* PLoS One, 2012. **7**(3): p. e32970.
318. Collins, A.L., et al., *Mild overexpression of MeCP2 causes a progressive neurological disorder in mice.* Hum Mol Genet, 2004. **13**(21): p. 2679-89.
319. Luikenhuis, S., et al., *Expression of MeCP2 in postmitotic neurons rescues Rett syndrome in mice.* Proc Natl Acad Sci U S A, 2004. **101**(16): p. 6033-8.
320. McGraw, C.M., R.C. Samaco, and H.Y. Zoghbi, *Adult neural function requires MeCP2.* Science, 2011. **333**(6039): p. 186.
321. Cheval, H., et al., *Postnatal inactivation reveals enhanced requirement for MeCP2 at distinct age windows.* Hum Mol Genet, 2012. **21**(17): p. 3806-14.
322. Nguyen, M.V., et al., *MeCP2 is critical for maintaining mature neuronal networks and global brain anatomy during late stages of postnatal brain development and in the mature adult brain.* J Neurosci, 2012. **32**(29): p. 10021-34.
323. Ballas, N., et al., *Non-cell autonomous influence of MeCP2-deficient glia on neuronal dendritic morphology.* Nat Neurosci, 2009. **12**(3): p. 311-7.
324. Chandler, R.J., et al., *Genotoxicity in Mice Following AAV Gene Delivery: A Safety Concern for Human Gene Therapy?* Mol Ther, 2016. **24**(2): p. 198-201.

325. Donsante, A., et al., *Observed incidence of tumorigenesis in long-term rodent studies of rAAV vectors.* Gene Ther, 2001. **8**(17): p. 1343-6.
326. Rosas, L.E., et al., *Patterns of scAAV vector insertion associated with oncogenic events in a mouse model for genotoxicity.* Mol Ther, 2012. **20**(11): p. 2098-110.
327. Chandler, R.J., et al., *Vector design influences hepatic genotoxicity after adeno-associated virus gene therapy.* J Clin Invest, 2015. **125**(2): p. 870-80.
328. Donsante, A., et al., *AAV vector integration sites in mouse hepatocellular carcinoma.* Science, 2007. **317**(5837): p. 477.
329. Duncan, F.J., et al., *Broad functional correction of molecular impairments by systemic delivery of scAAVrh74-hSGSH gene delivery in MPS IIIA mice.* Mol Ther, 2015. **23**(4): p. 638-47.
330. Kantor, B., et al., *Methods for gene transfer to the central nervous system.* Adv Genet, 2014. **87**: p. 125-97.
331. Murrey, D.A., et al., *Feasibility and Safety of Systemic rAAV9-hNAGLU Delivery for Treating MPS IIIB: Toxicology, Bio-distribution and Immunological Assessments in Primates.* Hum Gene Ther Clin Dev, 2014.
332. Enquist, I.B., et al., *Murine models of acute neuronopathic Gaucher disease.* Proc Natl Acad Sci U S A, 2007. **104**(44): p. 17483-8.
333. Vitner, E.B., et al., *Contribution of brain inflammation to neuronal cell death in neuronopathic forms of Gaucher's disease.* Brain, 2012. **135**(Pt 6): p. 1724-35.
334. Badaut, J., et al., *Induction of brain aquaporin 9 (AQP9) in catecholaminergic neurons in diabetic rats.* Brain Res, 2008. **1188**: p. 17-24.
335. Plotegher, N. and M.R. Duchen, *Mitochondrial Dysfunction and Neurodegeneration in Lysosomal Storage Disorders.* Trends Mol Med, 2017. **23**(2): p. 116-134.
336. Terman, A., et al., *Mitochondrial turnover and aging of long-lived postmitotic cells: the mitochondrial-lysosomal axis theory of aging.* Antioxid Redox Signal, 2010. **12**(4): p. 503-35.